A finite element model for the deck of plate-girder bridges including compressive membrane action, which predicts the ultimate collapse load

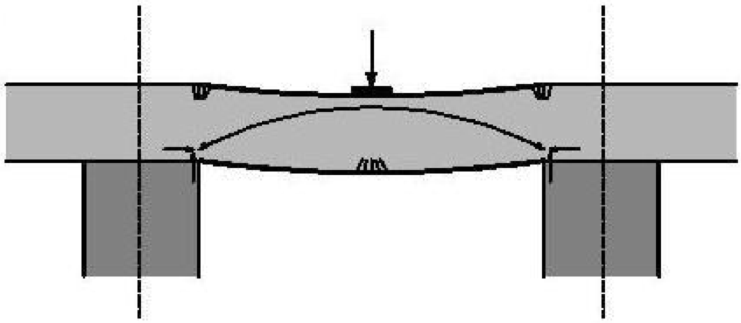

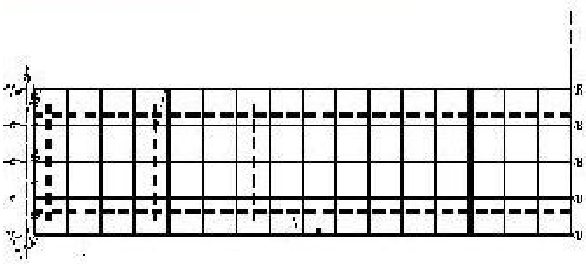

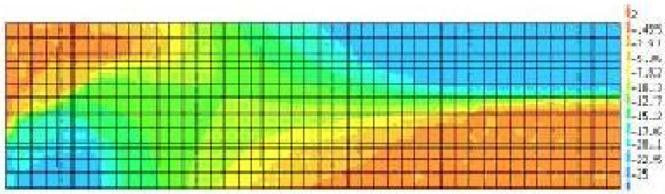

Gert Jan Bakker
Amsterdam, August 25, 2008

A finite element model for the deck of plate-girder bridges including compressive membrane action, which predicts the ultimate collapse load

Gert Jan Bakker
Section Concrete structures – Structural engineering
Faculty of Civil Engineering and Geosciences
Delft University of Technology

Keywords:
compressive membrane action, concrete slabs, bridge decks,
lateral restrained, numerical analysis, test comparisons, ultimate limit state,
bearing capacity

August 25, 2008

Preface

This research was carried out as Master thesis project at the section Concrete Structures at Delft University of Technology in co-operation with Witteveen + Bos. With this research I got a chance to compare difficult and long theory's on compressive membrane actions with a more workable solution, using a finite element program. This is the first step towards using compressive membrane action in design calculations and to use it for recalculating existing bridges. Including compressive membrane action into design calculations might lead to thinner and thus more economical bridge design and may prove that existing bridges do not need maintenance or replacement as yet.

I would like to thank all the members of my examination committee for sharing their knowledge with me, while I was writing this paper. I would also like to thank the company Witteveen + Bos for providing me a workspace and letting me make use of their facilities. I address special thank to Arjan Luttikholt, who helped me with the finite element modelling in DIANA.

Gert Jan Bakker
Amsterdam August 8, 2008

Examination committee:
Prof.dr.ir. J.C. Walraven, Delft University of Technology – Section concrete structures
Dr.ir. C. van der Veen, Delft University of Technology – Section concrete structures
Dr.ir. P.C.J. Hoogenboom, Delft University of Technology – Section structural mechanics
Ir. F.J. Kaalberg, Witteveen + Bos
Ir. L.J.M. Houben, Delft University of Technology

Delft University of Technology
Faculty of Civil Engineering and Geosciences
Section concrete structures – structural mechanics

Summary

With traffic getting denser in a fast rate, and trucks carrying heavier loads using less axles, the remaining lifetime of concrete decks in viaducts and bridges becomes uncertain. The load of the traffic gets closer and closer to the ultimate bearing capacity of these decks, calculated according to the Dutch code. However, no collisions have occurred yet.

Tests on both full scale and small scale reinforced concrete slabs showed that, if the edges of the slabs where laterally restrained, the bearing capacity was significantly higher than the slabs that did not have laterally restrained edges. After these tests, performed in the 1960's various people did research on this phenomenon. They generally came to the same conclusion: after cracking of the slabs a compressive force is introduced which enhances both the shear and bending capacity of the slabs. This phenomenon is called compressive membrane action.

The theories however consisted of long and difficult derivations, ending up in big and hard to read formulas, which are of no use in practice. Furthermore, different derivations where made for bending and punching failure, making things even more complex.

With the introduction of faster computers and especially better finite element programs, which can include non-linear material behaviour, it can be checked if models can be made which takes into account this compressive membrane action. These finite element programs are used more and more in practice. Consequently, laterally restrained structures can be designed in a more economical way. These models can also be used to demonstrate if certain repairs or replacement are really necessary, or that the structure has enough extra bearing capacity to postpone the maintenance.

In this paper it is tried to include this compression membrane action in a finite element analysis and the results are compared to a theory for both bending and punching shear that includes compressive membrane action. The results are also compared to experimental data, which is presented in various articles. The results of the finite element models look very promising, using a concrete strength of f_{cu} = 35 N/mm^2. For lower values of the concrete strength, the finite element models seem to give values that are to high, and for higher values, the finite element model seem to give values that are to low.

For bridge decks, which commonly have a concrete strength that is about 35 N/mm^2, the finite element model gives results that lie in an acceptable range based on experimental found data. The finite element program is used to predict the ultimate load of bridge decks of a ZIP girder system, which is commonly used in the Netherlands. It can be concluded that the enhancement factor for this type of deck has a value that lies around 1,5. The enhancement factor is here defined as the collapse load found by the finite element calculation divided by the lowest value of an analytical determined flexural and punching shear capacity calculation according to the Dutch code.

This indicates that laterally restrained bridge decks have more bearing capacity than follows from an analytical calculation.

Contents

List of symbols

a	radius of a slab	[mm]
c	distance to the neutral axis in the sagging yield moment	[mm]
c'	distance to the neutral axis in the hogging yield moment	[mm]
c_k	parameter related to the ratio of compressive and tensile strength of concrete	[-]
d	effective depth of the cross-section	[mm]
d'	difference between the height and the effective depth of the cross-section	[mm]
d_0	length over which the concentrated load is spread	[mm]
d_1	outer diameter of the punched cone	[mm]
h	height of the cross-section	[mm]
f_{cc}	uni-axial concrete compression strength	[N/mm^2]
f_{ct}	uni-axial concrete tensile strength	[N/mm^2]
f_{cu}	cube strength of concrete	[N/mm^2]
f_s,f_y	yield strength of reinforcement steel	[N/mm^2]
f_c	cylindrical concrete tensile strength	[N/mm^2]
f'_c	cylindrical concrete compression strength	[N/mm^2]
k_d	factor related to the height of the slab	[-]
m_u	resisting moment at the mid depth axis at the hogging moment per unit width	[Nmm/mm]
m'_u	resisting moment at the mid depth axis at the sagging moment per unit width	[Nmm/mm]
n_a	dimensionless membrane force in the mid depth of a slab	[-]
n_r	dimensionless radial membrane force working on the surface of the failure cone	[-]
n_u	membrane force at the mid depth axis at the hogging moment per unit width	[N/mm]
n'_u	membrane force at the mid depth axis at the sagging moment per unit width	[N/mm]
p	perimeter	[mm]
p	perimeter of cone that is punched out	[mm]
q	distributed load over a length	[N/mm]
q	reinforcement percentage in the code of New Zealand	[-]
r	radius	[mm]
r	function of the failure surface over the height	[mm]
t	outward lateral displacement at the restrained edge	[mm]
w_0	critical deflection, empirical determined as 0,5 h	[mm]
w_i	deflection at which membrane action starts, empirical determined as 0,03 h	[mm]

A	cross-sectional area	[mm^2]
A,B	constants	[m], [1/m]
A_{sh}	cross-sectional area of hoop steel per unit width	[mm^2/mm]
C	compression force at the sagging yield moment per unit width	[N/mm]
C'	compression force at the hogging yield moment per unit width	[N/mm]
D_A	the internal energy dissipation per unit area in the deforming zone	[N/mm]
E	modulus of elasticity	[N/mm^2]
F	concentrated load	[N]
I	impact factor in the code of New Zealand	[-]
L	length of the span	[mm]
M	moment	[Nmm]
N	intern force	[N]
N_{rs}	sum of the radial membrane forces	[N]
R	radius of the edge beam	[mm]
R_i	unfactored ultimate resistance in the New Zealand code	[N]
P	ultimate load in punching shear failure	[N]
P_a	analytical ultimate load	[N]
P_e	ultimate load from tests	[N]
P_p	predicted ultimate load	[N]

Q	load distributed over an area	[N/mm^2]
S	stiffness parameter of a laterally restrained slab	[N/mm]
T'	tensile force in the steel at the hogging yield line per unit width	[N/mm]
T	tensile force in the steel at the sagging yield line per unit width	[N/mm]
W	virtual work	[Nmm]
α	angle between yield surface and displacement rate vector	[rad]
β	factor ($0 < \beta < 0{,}5$)	[-]
β	angle between relative displacement and vertical axes	[rad]
β_1	ratio of the depth of the equivalent rectangular stress-block to the neutral axis depth	[-]
γ_0	overload factor in the code of New Zealand	[-]
γ_L	live load factor in the code of New Zealand	[-]
δ	deflection in the middle of the span	[mm]
ε	strain	[-]
φ	angular rotation	[rad]
τ	shear stress	[N/mm^2]
τ_1	shear stress at with transverse reinforcement is necessary	[N/mm^2]
τ_2	ultimate shear stress capacity	[N/mm^2]
ϕ	flexibility factor of laterally restrained slabs	[-]
ϕ	strength reduction factor in the code of New Zealand	[-]
ϕ_D	strength reduction factor in the code of New Zealand	[-]
χ_u	height of the compression zone of the concrete	[mm]
ω_0	reinforcement ratio	[-]
Δ_L	change in length	[mm]
θ	virtual rotation	[rad]

1. INTRODUCTION

Dutch bridges will not collapse yet[1.1]

De Volkskrant, 4 October 2007

Twelve steel bridges need urgent maintenance.
1.180 concrete bridges need further investigation.
Details will be presented next year.

Fatigued brides
AMSTERDAM Although metal fatigue and stresses in the concrete assaulted the Dutch bridges at a large scale, there is no reason to panic. `There is no immediate security threat`, so the ministry of ´verkeer en waterstaat´ ensures. Experts approve this statement. ‘I do not believe that bridges in the Netherlands will collapse any time soon` claims Leo Wagemans, academic civil engineering at Delft University.
According to a report that was presented yesterday by ´rijkswaterstaat´, 25 of the 274 steel bridges suffer from metal fatigue. In the case of twelve of these bridges, including the ´Brienenoordbrug´ and the ´Moerdijkbrug´, the problems are so serious that short-term adjustments have to be made. From the total of 2.020 concrete bridges, 1.180 have to be examined more closely.
It is clear that the lifetime of bridges in the Netherlands is less then is assumed in the design. Cracks in the steel appear sooner and lumps of concrete fall out.
The increased traffic intensity, environmental load and the heavier trucks are the cause of the shortening in lifetime. In the sixties and seventies a lifetime of at least sixty years was assumed. Now it comes true that after just 30 years restoration is required.
‘Not only has truck traffic doubled, furthermore there is almost no empty truck left on the Dutch roads’, thus Dick Schaafsma of ´Rijkswaterstaat´.
According to his colleague Frans Bijlaard from Delft- academic steel structures – it is not a matter of carelessly or ignorance. The good reputation of hydraulics in the Netherlands is not a point of discussion. ‘The Dutch ability to build bridges has not declined. Many of the problems involve the greater rolling resistance of trucks. Due to technological developments the loads that needed to be carried by two tires can now be carried by just one tire. This concentrated load results in savings of fuel, but also in larger damage of the pavement.’
Collapsing of bridges happens more then men would suspect; last week in Vietnam, in august in Minneapolis. In the United States five bridges have collapsed since 2000, due to heavy rainfall and a collision.

Bijlaard: 'Disasters due to a collision can also happen in the Netherlands. But the maintenance mode in the United States is drastically worse than in the Netherlands.' Schaafsma: `Problems at the bridge in Minneapolis were already known. But nothing was done about it. This does not happen in the Netherlands.'
In May wear was detected at the ´Hollandse Brug´ at the A6 near Muiden and the bridge is now closed for all truck traffic. Meanwhile ´rijkswaterstaat´ has inspected 2.020 concrete bridges and viaducts and 274 steel bridges in the road infrastructure, which were build before 1975. Of the engineering structures 1.180 need further examination. The remaining lifetime of those bridges might be shorter then the lifetime of the original design.
At 25 of the steel bridges the problems are more urgent. Since necessary reparations have been made, no traffic restrictions are needed according to the ministry. 'On the mid-long period this is not enough. To guarantee the traffic flow, the bridges need to be reinforced or replaced in the next 5 years', according the ministry.
In the summer of 2008, a detailed report with all the needed adjustments will be presented. Then the total costs of the renovation project will also be known. The renovation of the ´Moerdijkbrug´ itself will cost 38 million Euro."

The above article shows that bridges and viaducts build before 1975 are a point of discussion in the Netherlands. The question is whether these structures really do need repairs or have to be replaced. Another option is to check whether the structure is actually stronger then the calculations show in the originally design. Varies studies have been performed to study the effect of compressive membrane forces in laterally restrained concrete slabs. The conclusions of those studies are in general the same: compressive membrane action enhances the ultimate load of laterally restrained slabs. However, none of these studies present a calculation model that is usable in practice. Because of this the effect of compressive membrane forces is neglected in current calculations. This report describes the development of a finite element model, which takes into account these compressive membrane forces.

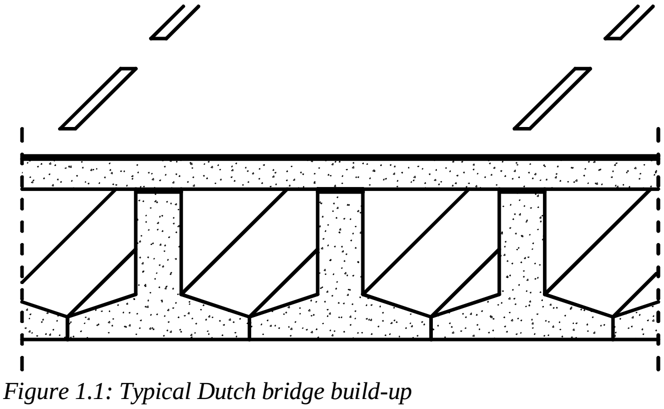

Figure 1.1: Typical Dutch bridge build-up

A large part of the structures discussed in the above article are build up of inverted T-beams with a compression layer of concrete on top (see figure 1.1). The starting point for this study will be this type of structure.

The traffic becomes denser in a fast rate. To get an indication how much the traffic load has increased since 1975 a comparison is made between the bridge load model used before 1975 (according to the VOSB 1963) and the bridge load model that is used nowadays (according to the NEN-EN 1991-2).

From figure 1.2 it can be concluded that the total load has not increased very much, but the loads get more concentrated. This means that the structural integrity as the structure as a whole will probably be not an issue, but locale failure (for example in the decks) might become governing. This local failure due to higher axle forces will also be taken into account in the finite element model. Another difference between the codes is the calculation of cyclic loading. In the VOSB 1963 no attention is paid to this type of loading, while in the NEN-EN 1991-2 this method is extensively described.

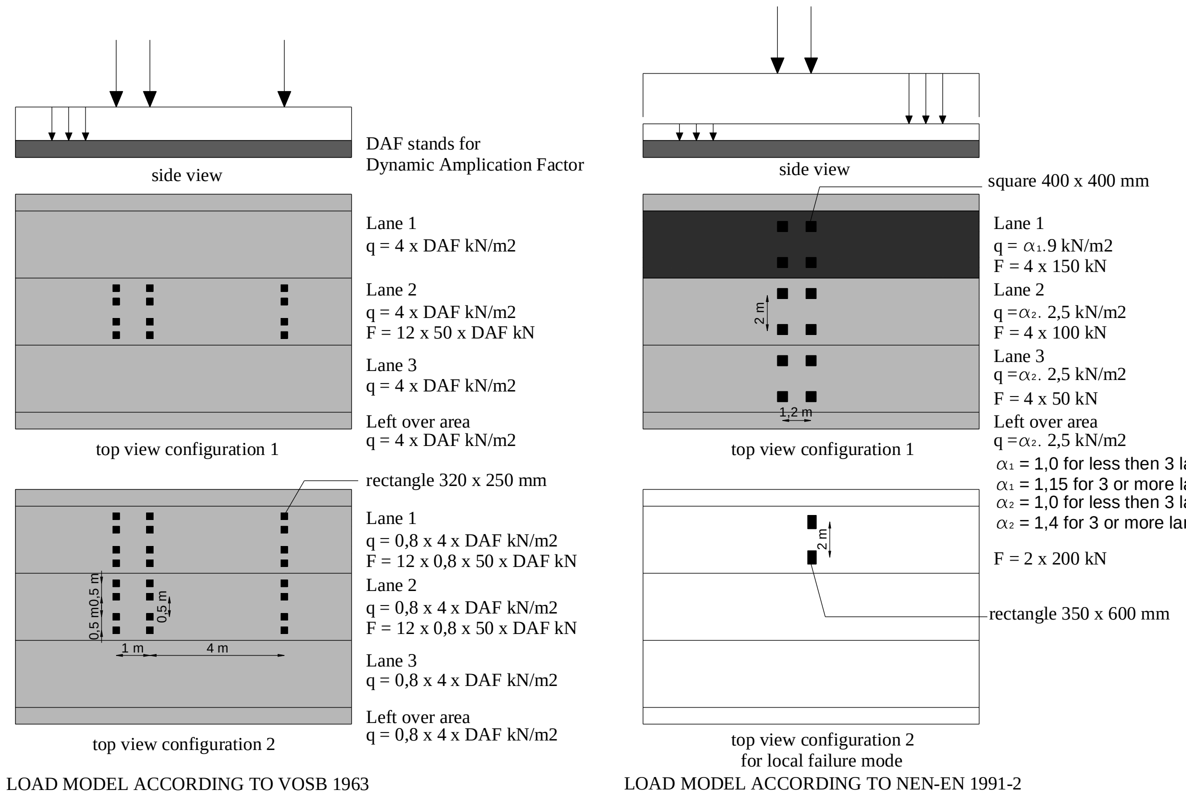

Figure 1.2: Traffic load of VOSB 1963 compared to the NEN-EN 1991-2 traffic load

1.1. The goal of this study

The goal of this study is to develop a numerical finite element model that is able to calculate the ultimate bearing capacity of one-way continuous concrete bridge decks, taking into account compressive membrane action. This model takes into account two modes of failure. The first is due to global failure in bending, the second due to local punching failure of the deck by concentrated axle loads. This model can be used to define the enhancement due to compressive membrane action in existing and new one-way concrete bridge deck structures.

1.2. The structure of this study

This study will be build up of three parts:

Part I: The theory
This part involves

- the theory on compressive membrane action in both bending and punching failure
- the comparison between analytical and the above mentioned theoretical solutions
- the comparison between test results presented in various articles and the above mentioned theoretical solutions

Part II: The numerical development of the finite element model
This part involves

- the creation of a numerical finite element model
- the comparison between the analytical and finite element results
- the comparison with some test results presented in various articles and the finite element results
- if necessary adjustments are made to the model

Part III: A practical example
This part will involve

- the application of the in part II found model on a practical bridge deck
- an estimation of the enhancement factor for these kind of structures

The study will finish with conclusions and recommendations.

Part I: The theory of compressive membrane action

2. THEORY OF COMPRESSIVE MEMBRANE ACTION

Compressive membrane action forms when two conditions are met. First the horizontal translation has to be (partly) restrained. The greater the restraint, the greater the compressive membrane force will be. Secondly the net tensile strain along a longitudinal fibre must be non-zero when there is no horizontal restraint [2.1]. Figure 2.1 shows a concrete one-way slab, which is in the cracking state. Due to the cracking, the slab wants to elongate, but the rigid lateral restrained supports prevent this from happening, so a compressive membrane force is introduced.

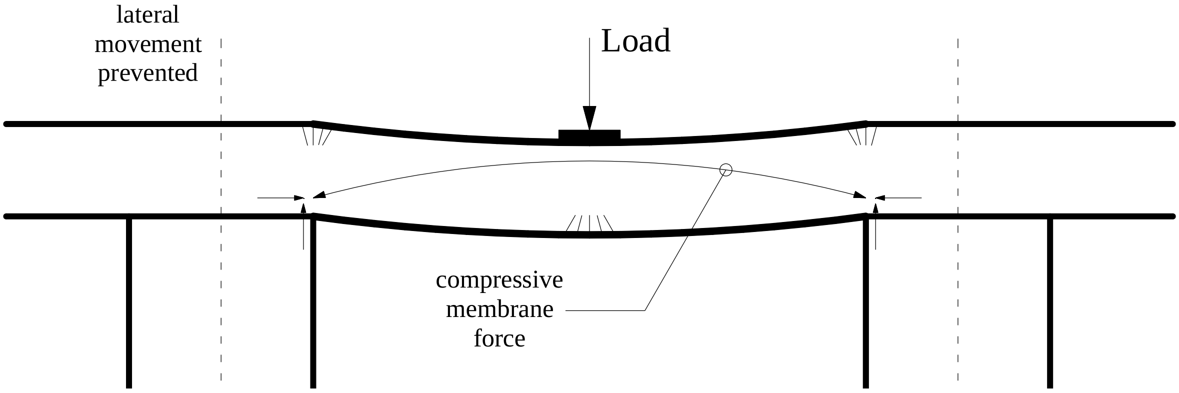

Figure 2.1: Compressive membrane action in a latterly restrained slab

The enhancement of the collapse load by compressive membrane action can be clearly seen in a load-deflection diagram, as shown in Figure 2.2 [2.5].

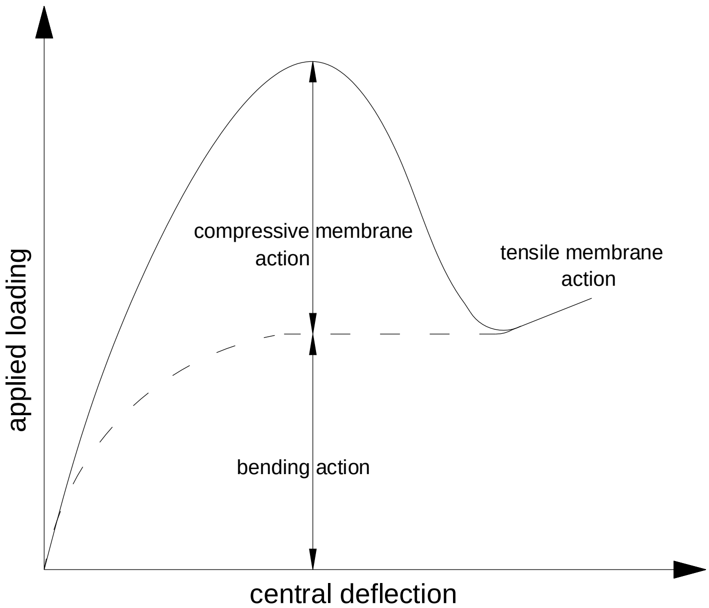

Figure 2.2: Load-deflection graph for a structure with compressive membrane action

2.1. Enhancement of the bending strength by compressive membrane forces

The calculation method used here is derived by Park [2.2]. The theory has its starting point as shown in Figure 2.3. In this figure *t* is the outward lateral movement.

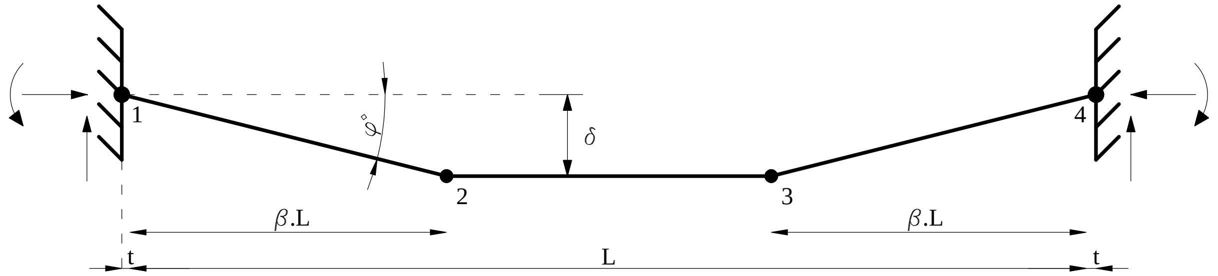

Figure 2.3: Starting point for Park's compressive membrane theory

Assumptions in his model are

- the tension steel in the plastic hinges is yielding
- the concrete in the plastic hinges has reached its compressive strength
- the tensile strength of concrete is neglected
- the rotations and strains are small
- the top reinforcement is the same on both sides
- the bottom reinforcement is constant over the length of the strip
- the top and bottom reinforcement may differ
- the 3 parts, 1-2, 2-3 and 3-4 of the beam remain straight
- the axial strain, ε (sum of the elastic, creep and shrinkage axial strain) has a constant value over the length
- shear forces are neglected, since their net contribution in virtual work equations is zero

The shortening of the middle part due to the strain is $\Delta L_{2-3} = \varepsilon(1-2\beta)L$. So points 2 and 3 will move $0{,}5\varepsilon(1-2\beta)L$ to the middle of the system. The distance from point 2 to the boundary now becomes $\beta L + 0{,}5\varepsilon(1-2\beta)L + t$. The parts 1-2 and 3-4 will shorten to the length $(1-\varepsilon)\beta L$. These values are shown in figure 2.3.

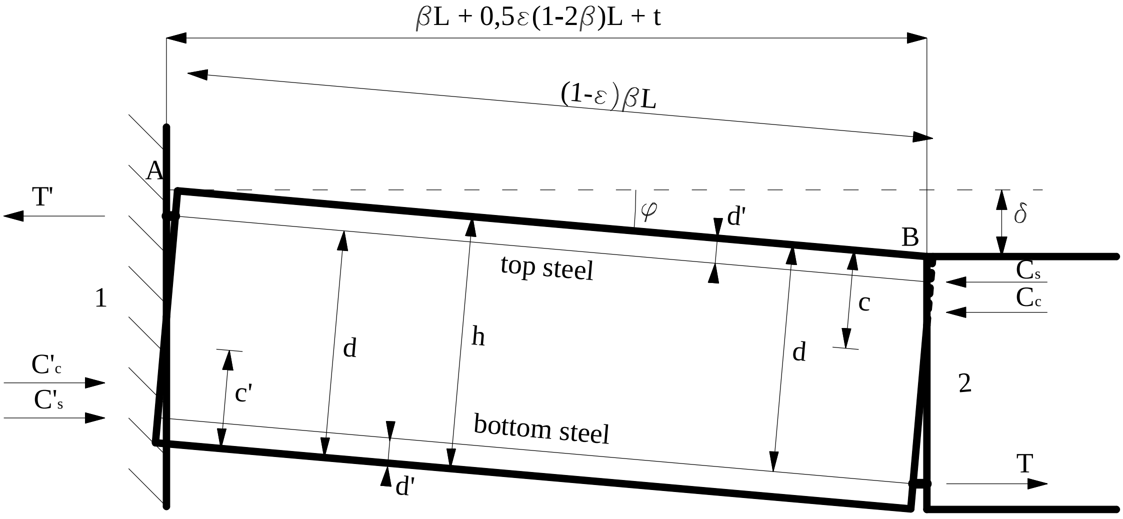

Figure 2.4: Section 1-2 in the deformed state

The distance between the points A and B can be calculated with the geometry of the deformations in two different ways, and so the next equation is derived:

$$dist_{A\to B} = \frac{(\beta L + 0{,}5\varepsilon(1-2\beta)L + t)}{\cos\varphi} = (h - c')\tan\varphi + (1-\varepsilon)\beta L - c\tan\varphi \qquad (1)$$

$$\frac{(\beta L + 0{,}5\varepsilon(1-2\beta)L + t)}{\cos\varphi} - (1-\varepsilon)\beta L = \left(h - c - c'\right)\frac{\sin\varphi}{\cos\varphi}$$

$$\frac{\beta L - \beta L\cos\varphi + \varepsilon\beta L\cos\varphi + 0{,}5\varepsilon(1-2\beta)L + t}{\sin\varphi} = h - c - c'$$

$$\sin^2 x = \frac{1-\cos 2x}{2} \rightarrow \beta L - \beta L\cos\varphi = 2\beta L\sin^2\frac{\varphi}{2}$$

$$h - c - c' = \frac{2\beta L\sin^2\frac{\varphi}{2} + \varepsilon\beta L\cos\varphi + 0{,}5\varepsilon(1-2\beta)L + t}{\sin\varphi}$$

Since φ and ε are small some simplifications can be used in this equation:

$$\sin\varphi = 2\sin\frac{\varphi}{2} = \frac{\delta}{\beta L}$$

$$\cos\varphi = 1$$

$$h - c - c' = \frac{\delta}{2} + \frac{\varepsilon(\beta L)^2}{\delta} + \frac{0{,}5\varepsilon\beta L^2}{\delta} - \frac{\varepsilon(\beta L)^2}{\delta} + \frac{t\beta L}{\delta}$$

$$c + c' = h - \frac{\delta}{2} - \frac{\beta L^2}{2\delta}\left(\varepsilon + \frac{2t}{L}\right) \tag{2}$$

The second equation is formed using horizontal force equilibrium:

$$C'_s + C'_c - T' = C_s + C_c - T \tag{3}$$

$$C'_c = 0{,}85 f_c^{'} \beta_1 c'$$

$$C_c = 0{,}85 f_c^{'} \beta_1 c$$

$$f_c^{'} = \text{concrete cylinder strength}$$

$$\beta_1 = 0{,}85 \text{ if } f_c^{'} \leq 30\frac{N}{mm^2}$$

β_1 reduces linear with 0,05 for every increase of $f_c^{'}$ by $7\frac{N}{mm^2}$ until a minium of 0,65

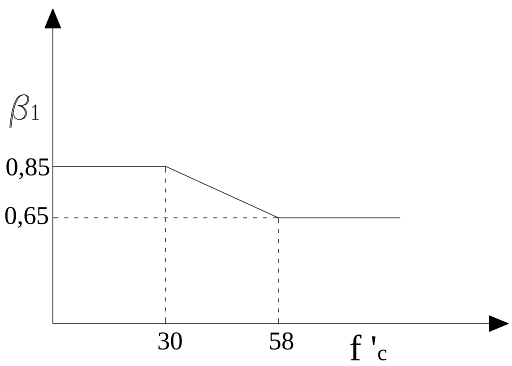

Figure 2.5: β_1 as a function of f'_c

With this information equation (3) forms into:

$$c'-c = \frac{T'-T-C_s^{'}+C_s}{0{,}85\beta_1 f_c^{'}} \tag{4}$$

Solving equation (2) and (4) simultaneously give the following solutions:

$$c' = \frac{h}{2} - \frac{\delta}{4} - \frac{\beta L^2}{4\delta}\left(\varepsilon + \frac{2t}{L}\right) + \frac{T'-T-C_s^{'}+C_s}{1{,}7 f_c^{'}\beta_1} \tag{5}$$

$$c = \frac{h}{2} - \frac{\delta}{4} - \frac{\beta L^2}{4\delta}\left(\varepsilon + \frac{2t}{L}\right) - \frac{T'-T-C_s^{'}+C_s}{1{,}7 f_c^{'}\beta_1} \tag{6}$$

In figure 2.6 it can be seen how the forces C_s, C_c and T work on the slab, and which stresses they generate for a field moment. A similar figure can be made for the support moment.

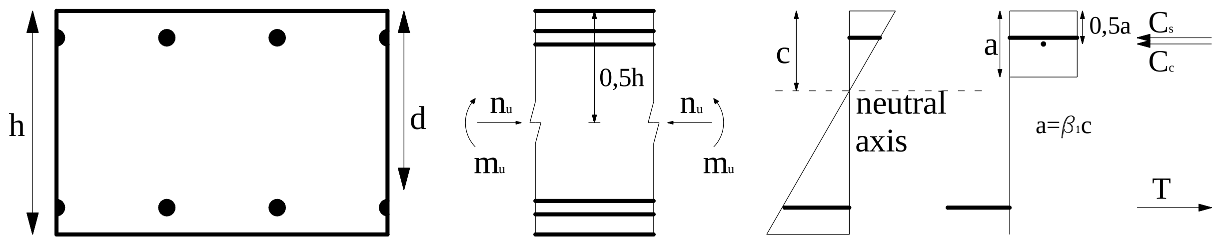

Figure 2.6: Forces and moments acting in the middle of the span of the slab

With this figure, the quantities n_s and m_s can be calculated.

$$n_u = C_c + C_s - T = 0{,}85 f_c^{'}\beta_1 c + C_s - T \tag{7}$$

$$m_u = 0{,}85 f_c^{'}\beta_1 c(0{,}5h - 0{,}5\beta_1 c) + C_s(0{,}5h - d') + T(d - 0{,}5h) \tag{8}$$

$$n_u^{'} = n_u \text{ (equilibrium)} \tag{9}$$

$$m_u^{'} = 0{,}85 f_c^{'}\beta_1 c'(0{,}5h - 0{,}5\beta_1 c') + C_s^{'}(0{,}5h - d') + T'(d - 0{,}5h) \tag{10}$$

The sum of the moments of the stress resultants at the yield section about an axis at mid depth at one end in the strip is given by the formula:

$$m_u^{'} + m_u - n_u\delta \tag{11}$$

The shear forces are neglected in this equation, since their net contribution to a virtual work analysis will be zero.

Substituting equations (5) to (10) in equation (11) gives the next formula:

$$m_u^{'} + m_u - n_u\delta = 0{,}85 f_c^{'}\beta_1 h \left[\begin{array}{l} \frac{h}{2}\left(1-\frac{\beta_1}{2}\right)+\frac{\delta}{4}(\beta_1-3)+\frac{\beta L^2}{4\delta}(\beta_1-1)\left(\varepsilon+\frac{2t}{L}\right) \\ +\frac{\delta^2}{8h}\left(2-\frac{\beta_1}{2}\right)+\frac{\beta L^2}{4h}\left(1-\frac{\beta_1}{2}\right)\left(\varepsilon+\frac{2t}{L}\right)-\frac{\beta_1\beta^2 L^4}{16h\delta^2}\left(\varepsilon+\frac{2t}{L}\right)^2 \end{array} \right]$$
$$-\frac{1}{3{,}4 f_c^{'}}\left(T'-T-C_s^{'}+C_s\right)^2+\left(C_s^{'}+C_s\right)\left(\frac{h}{2}-d'-\frac{\delta}{2}\right)+(T'+T)\left(d-\frac{h}{2}+\frac{\delta}{2}\right)$$

When a virtual rotation θ is given to a plastic hinge in the system, the virtual work done in that hinge is:

$$\left(m_u^{'} + m_u - n_u\delta\right)\theta$$

When the virtual work done by the load on a structure is known, a load-deflection relationship can be derived.
A few notes when using this formula:

- the model assumes that plastic hinges form immediately, this is of course not the case
- the first part of the curve will thus be inaccurate
- for large deflections, not the compressive but the tensile membrane action (catenary action) will be governing (see Figure 2.2)
- this formula can thus not be used for large deflections
- this formula gives good results for moderate deflections, when plastic hinges start to form

To get a feeling for the influence of the different input parameters, graphs are made. On the left side, the enhancement of the ultimate load provided by Park's theory, and on the right side the predicted load by Park is shown. For each set one of the input values is varied, while the other values are kept constant. For the basic input values, see the excel sheet in appendix A. Mind that these graphs hold for bending action only.

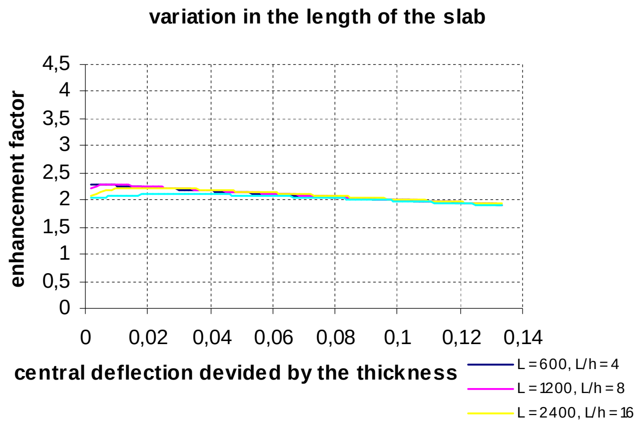

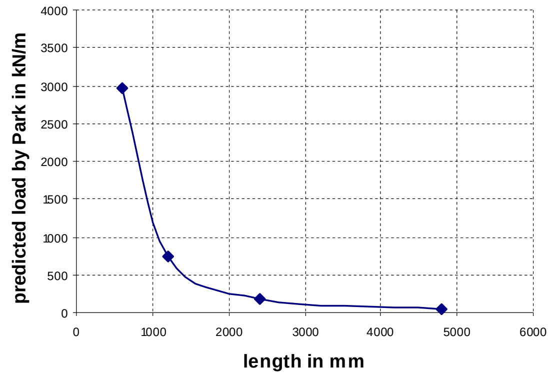

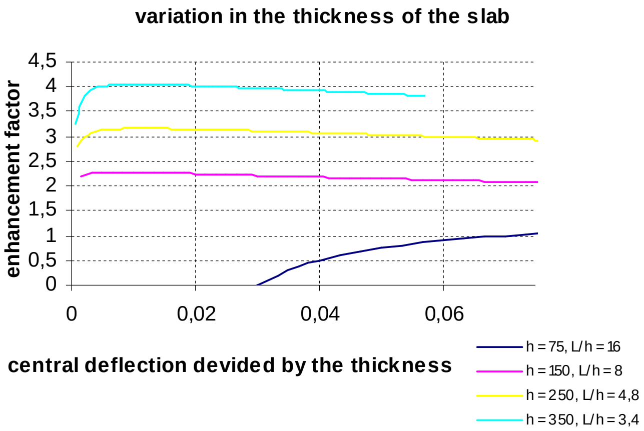
variation in the thickness of the slab
enhancement factor
central deflection devided by the thickness
h = 75, L/h = 16
h = 150, L/h = 8
h = 250, L/h = 4,8
h = 350, L/h = 3,4

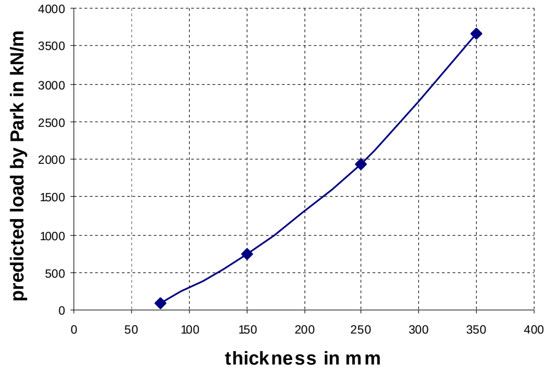
predicted load by Park in kN/m
thickness in mm

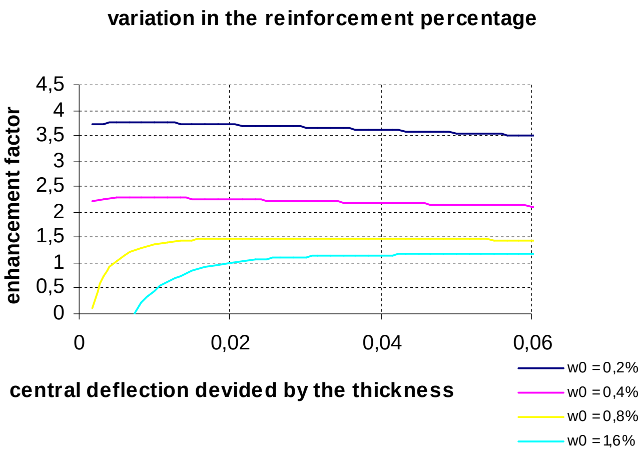
variation in the reinforcement percentage
enhancement factor
central deflection devided by the thickness
w0 = 0,2%
w0 = 0,4%
w0 = 0,8%
w0 = 1,6%

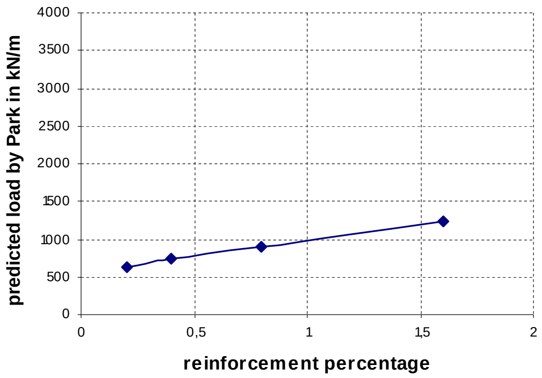
predicted load by Park in kN/m
reinforcement percentage

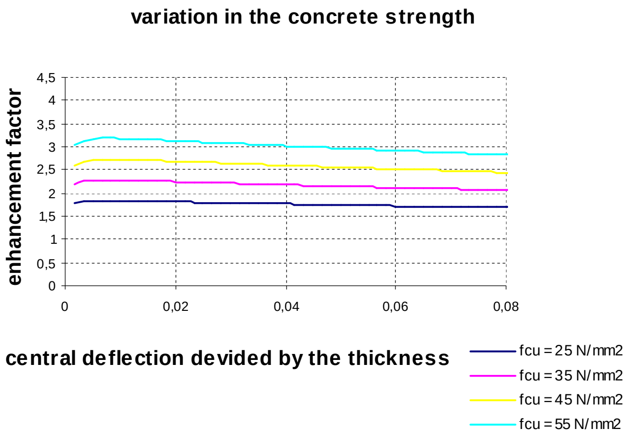
variation in the concrete strength
enhancement factor
central deflection devided by the thickness
fcu = 25 N/mm2
fcu = 35 N/mm2
fcu = 45 N/mm2
fcu = 55 N/mm2

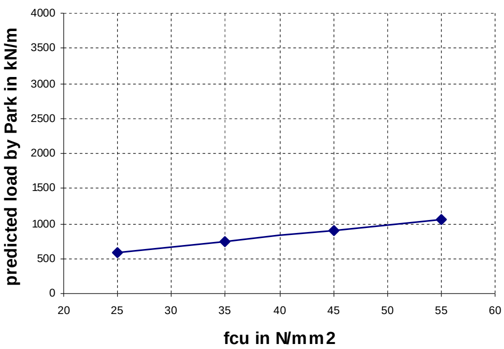
predicted load by Park in kN/m
fcu in N/mm2

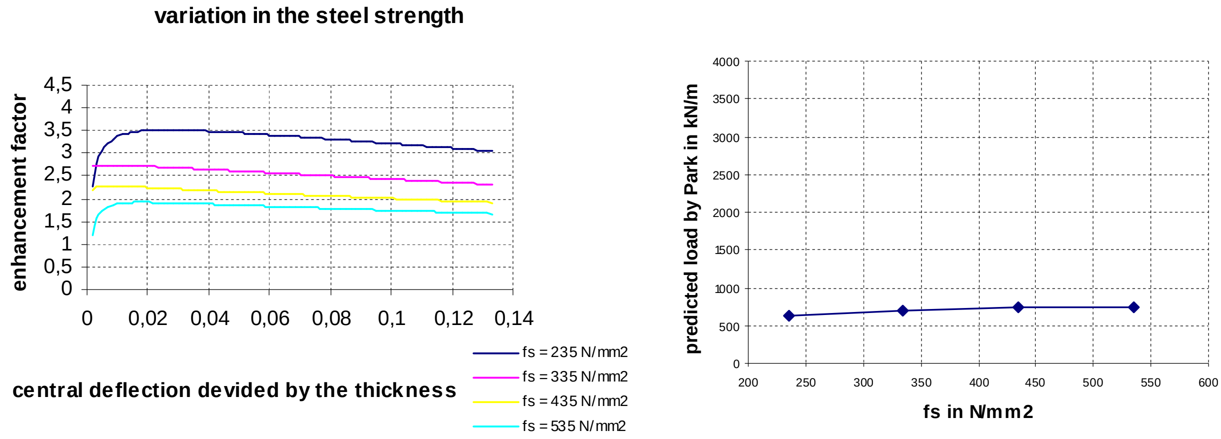

Figure 2.7: Enhancement factors (left) and absolute values (right) for Park's theory

From the graphs, the following conclusions can be made:

- the length of the slab is only of influence for short spans, the influence on the enhancement factor is rather small
- the thickness of the slabs has great influence on both the enhancement factor and the ultimate load
- the higher the reinforcement ratio, the lower the enhancement factor
- the higher the yield strength of the steel, the lower the enhancement factor
- for higher concrete strengths, the enhancement factor and the ultimate load will increase both

2.2. Enhancement of the punching shear strength by compressive membrane action

The enhancement of punching shear failure is discussed in an article published by the American Concrete Institute [2.3] and the international journal of mechanical sciences[2.4]. The theory used in this study will follow this method. Assumptions made in this model are:

- the failure mechanism consists of a solid cone-like plug
- the compressive membrane force has a constant value
- the behaviour is rigid plastic
- the energy in hoop expansion outside the plug is neglected

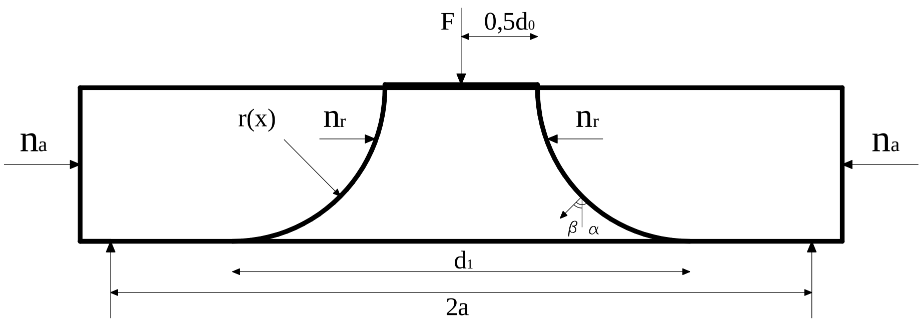

Figure 2.8: Punching shear failure model

The authors did some tests, but instead of making horizontal restrained clamped edges, they used hoop reinforcement to create a similar effect.

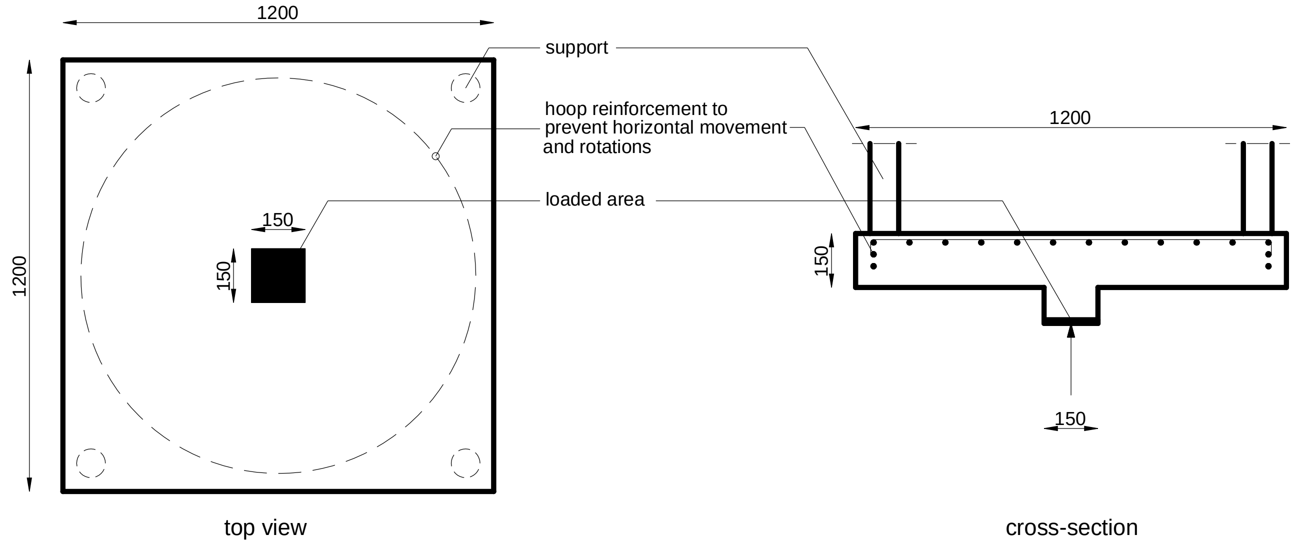

Figure 2.9: Schematic overview of the test set-up

An upper-bound solution is given by the virtual work theory:

$$W_{extern} = F\delta \cos\beta$$

$$W_{intern} = \int_0^h D_A 2\pi\sqrt{1+r'^2}\,dx + N_{rs}\delta \sin\beta$$

$$N_{rs} = f_{cc}\int_0^h n_r 2\pi r dx$$

$$n_r = n_a + \frac{w_0}{2h}\left(1-\frac{r}{a}\right)$$

$$n_a = -\left(ke^{\left(\frac{-w_0}{h\phi}\right)} - \frac{1}{2}\left(n_0 + \frac{1}{2} + \frac{\phi}{2}\right) + \frac{w_0}{4h}\right)$$

$$k = \left(\frac{n_0}{2} + \frac{1}{4} + \frac{\phi}{4} - \frac{w_i}{4h}\right)e^{\left(\frac{w_i}{h\phi}\right)}$$

$$n_0 = \frac{N_0}{hf_{cc}}$$

N_{rs} is the sum of the radial compressive membrane forces working on the failure surface of the cone. The value for n_a is derived by using the flow theory.

$$N_0 = 0{,}5hf_c - A_{sh} f_s$$
$$\phi = \frac{af_{cc}}{2hS}$$
$$\frac{1}{S} = \frac{aR}{0{,}8E_c A_c + E_s A_s} + \frac{a}{0{,}5E_c (x+h)}$$
$$a = 0{,}5L$$
$$R = 0{,}5L$$
$$x = 1{,}76 w_0 \frac{f_s}{f_{cu}}$$
$$w_i = 0{,}03h \ \textit{(deflection at which membrane action starts, emperical determined)}$$
$$w_0 = 0{,}5h \ \textit{(critical deflection, empirical determined)}$$

D_A is the internal energy dissipation per unit area in the deforming zone and is given by the following formula:

$$D_A = \delta f_{ct}\left(1 + \frac{c_k{}^2}{4}\cot^2\alpha\right)\sin\alpha$$
$$c_k = \sqrt{1 + \frac{f_{cc}}{f_{ct}}} - 1$$

Substituting all the above equations in the virtual work equation gives the following solution:

$$P = 2\pi f_{ct}\int_0^h r\left[r' + \tan\beta + \frac{c_k{}^2}{4}\frac{(1 - r'\tan\beta)^2}{r' + \tan\beta}\right]dx + 2\pi f_{cc}\int_0^h \left[n_a + \frac{w_0}{2h}\left(1 - \frac{r}{a}\right)\right] r\,dx \tan\beta$$

Minimising the first integral gives an equation that does not contain x and Euler's equation has the first integral. With two boundary conditions this integral can be solved.

$$F(r,r') = r\left[r' + \tan\beta + \frac{c_k{}^2}{4}\frac{(1-r'\tan\beta)^2}{r'+\tan\beta}\right]$$

$$\frac{\partial F}{\partial r} - \frac{d}{dx}\left(\frac{\partial F}{\partial r'}\right) = 0$$

$$F - r'\frac{\partial F}{\partial r'} = C$$

$$r(0) = \frac{d_0}{2}; r(h) = \frac{d_1}{2}$$

$$r = Ae^{Bx} - \frac{\tan\beta}{B}$$

$$\frac{d_0}{2} = A - \frac{\tan\beta}{B}$$

$$\frac{d_1}{2} = \left(\frac{d_0}{2} + \frac{\tan\beta}{B}\right)e^{Bh} - \frac{\tan\beta}{B}$$

When β is given, the constants A and B can be determined and the failure load P becomes:

$$P = 2\pi f_{ct}\left[\frac{A^2}{2}\left(e^{2Bh}-1\right) - \frac{2A}{B}\left(e^{Bh}-1\right)\tan\beta + \frac{h}{B}\tan^2\beta\right]$$
$$+\pi f_{ct}\frac{c_k{}^2}{2}\left[\frac{h}{B} + \frac{2A}{B}\left(e^{Bh}-1\right)\tan\beta + \frac{A^2}{2}\left(e^{2Bh}-1\right)\tan^2\beta\right] + N_{rs}\tan\beta$$

$$N_{rs} = 2\pi f_{cc}\left(n_a + \frac{w_0}{2h}\right)\left[\frac{A}{B}\left(e^{2Bh}-1\right) - \frac{h}{B}\tan\beta\right]$$
$$-\pi f_{cc}\frac{w_0}{ah}\left[\frac{A^2}{2B}\left(e^{2Bh}-1\right) - \frac{2A}{B^2}\left(e^{Bh}-1\right)\tan\beta + \frac{h}{B^2}\tan^2\beta\right]$$

For a minimum, the derivative $\frac{\partial P}{\partial \beta}$ must be zero

$$\frac{\partial P}{\partial \beta} = \pi f_{ct}\frac{c_k{}^2}{2}\left[\frac{2A}{B}\left(e^{Bh}-1\right) + A^2\left(e^{2Bh}-1\right)\tan\beta\right] - \pi f_{ct}\left[\frac{2A}{B}\left(e^{Bh}-1\right) - \frac{2h}{B}\tan\beta\right]$$
$$-2\pi f_{cc}\left(na + \frac{w_0}{2h}\right)\frac{h}{B}\tan\beta + \pi f_{cc}\frac{w_0}{ah}\left[\frac{2A}{B^2}\left(e^{Bh}-1\right) - \frac{2h}{B^2}\tan\beta\right]\tan\beta + N_{rs} = 0$$

To calculate the ultimate load for punching shear failure, the following method can be used:

- calculate d_1 for a simply supported plate with $\left(\frac{d_1}{d_0}\right)^{d_1} = e^{c_k h}$
- choose d_1 as a smaller value as just calculated
- assume a value for β
- calculate $\frac{\partial P}{\partial \beta}$
- adjust β until $\frac{\partial P}{\partial \beta} \approx 0$
- calculate P
- reduce d_1 and repeat the above steps till a minimum is found for P

According to the article by Salim and Sebastian, realistic values are gained for $\frac{f_{cc}}{f_{ct}} = 400$. This factor is used in the calculation model in the maple sheet, see appendix B. Mind that this factor should not be used to determine c_k, for which the standard value for f_{ct} should be used.

This analytical model is presented in a maple sheet, see appendix B.

To get a better understanding of the influence of the different input values, graphs are made. The basic values are shown in the maple sheet in appendix B, and for each graph one of the input values is varied. Mind that these graphs only hold for failure in pure punch.

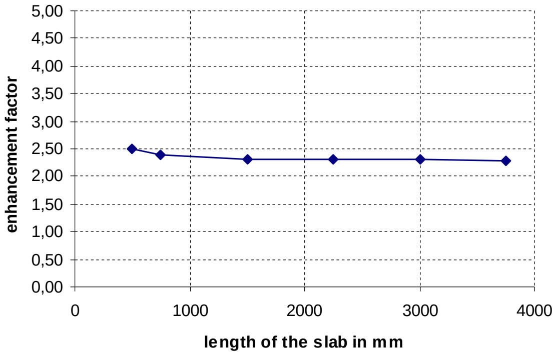

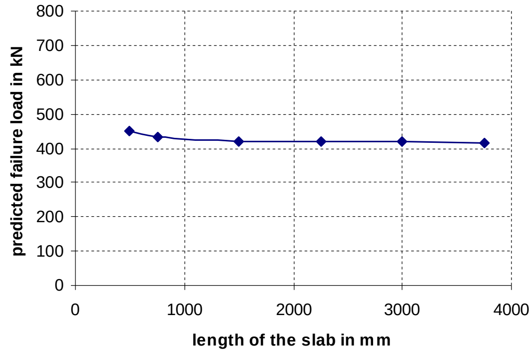

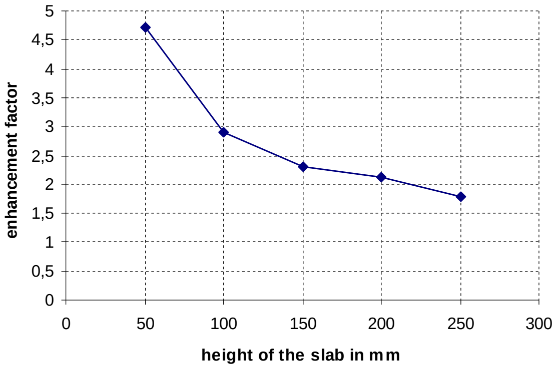

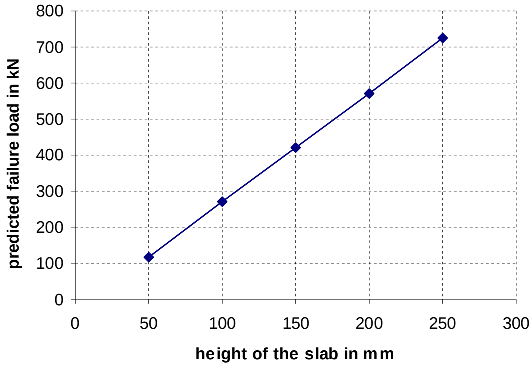

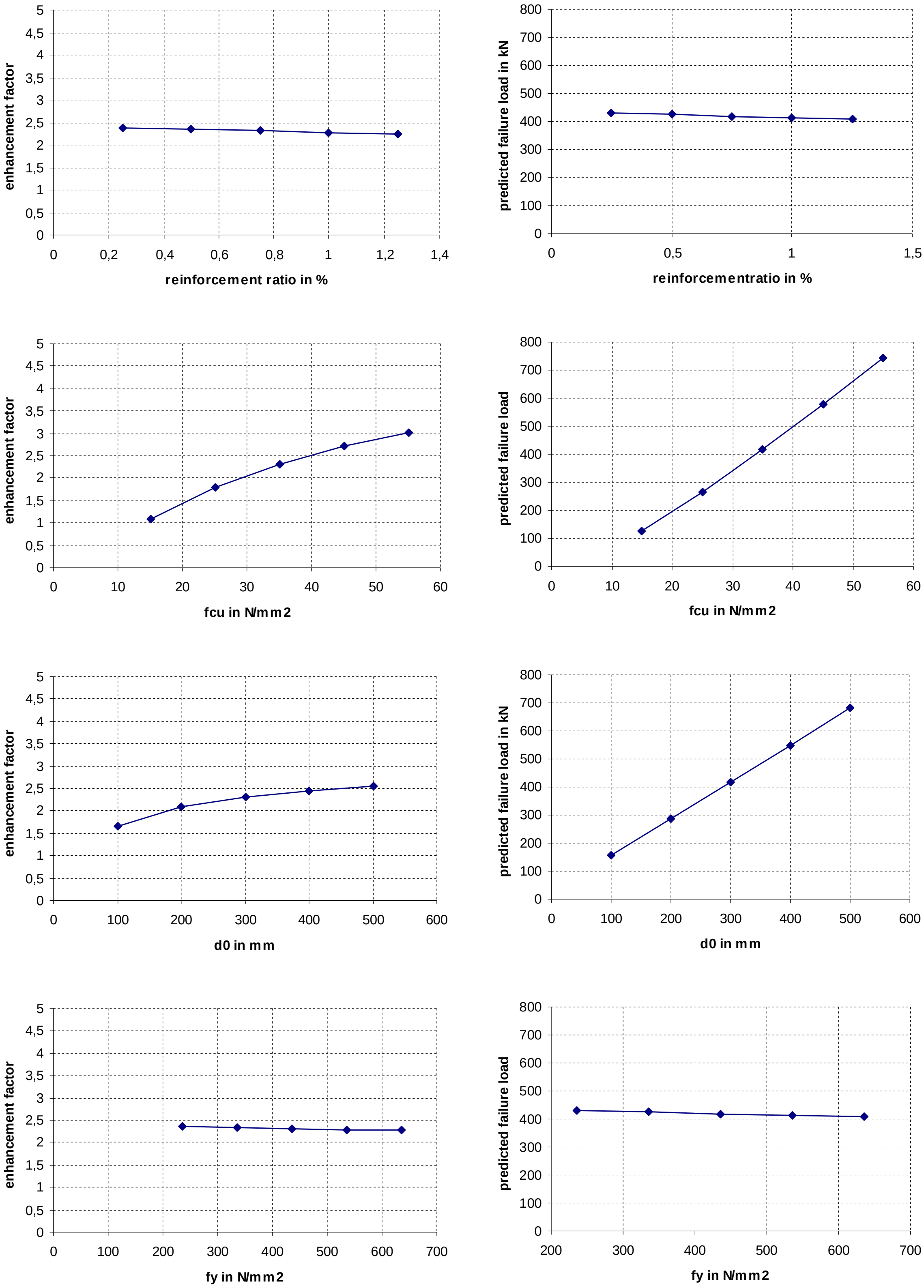

Figure 2.10 Enhancement factors (left) and absolute values (right) for the Punching failure theory

Looking at he graphs, the following can be concluded:

- the length of the slab, the reinforcement ratio and the reinforcement yield strength do not have much influence on both the enhancement factor and the total ultimate load
- the height has the largest influence on both the enhancement factor and the ultimate load
- the higher the slab, the smaller the enhancement factor becomes
- the concrete strength and the length of the loaded area have a positive influence on both the enhancement factor and the ultimate load

2.3. Comparison between bending and punching failure

To get an understanding if failure in bending or failure in punching occurs, the found results will be compared to each other. The enhancement factors of the previous sections cannot be used. To compare the results, two new enhancement factors will be used.

For bending:

$$if \quad q_{analytic,bending} \leq \frac{F_{punch,code}}{L} \rightarrow \frac{q_{Park}}{q_{analytic,bending}}$$

$$if \quad q_{analytic,bending} > \frac{F_{punch,code}}{L} \rightarrow \frac{q_{park}.L}{F_{punch,code}}$$

For punch:

$$if \quad q_{analytic,bending} \leq \frac{F_{punch,code}}{L} \rightarrow \frac{F_{punch,predicted}}{q_{analytic,bending}.L}$$

$$if \quad q_{analytic,bending} > \frac{F_{punch,code}}{L} \rightarrow \frac{F_{punch,predicted}}{F_{punch,code}}$$

In other words, the predicted values by the theory presented in chapter 2 are divided by the lowest value of the analytic bending and punch failure load.

The starting point or calculations is shown below. For each graph, one of the values is varied.

L	1500	mm
b	1000	mm
h	150	mm
d0	300	mm
fck	35	N/mm2
fs	435	N/mm2
wo	0,37	%

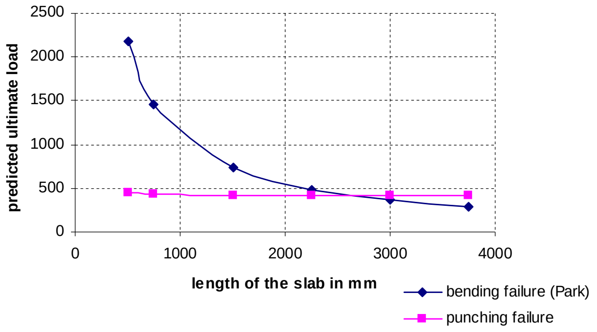
predicted ultimate load
2500
2000
1500
1000
500
0
0
1000
2000
3000
4000
length of the slab in mm
bending failure (Park)
punching failure

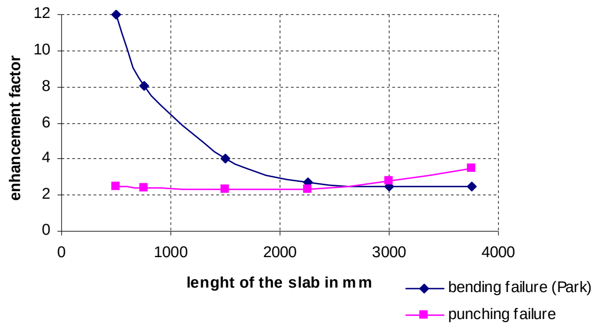
enhancement factor
12
10
8
6
4
2
0
0
1000
2000
3000
4000
lenght of the slab in mm
bending failure (Park)
punching failure

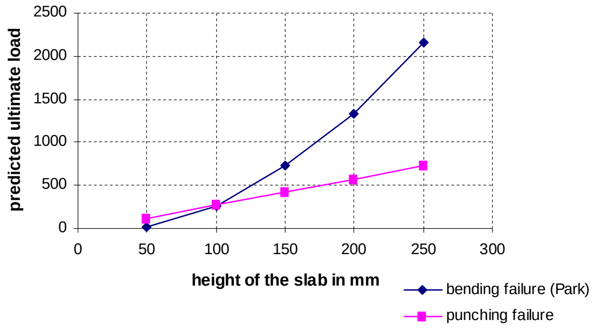
predicted ultimate load
2500
2000
1500
1000
500
0
0
50
100
150
200
250
300
height of the slab in mm
bending failure (Park)
punching failure

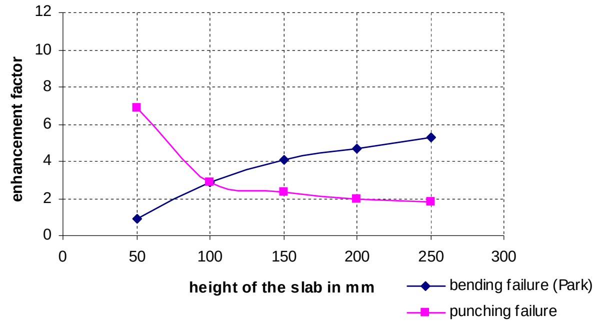
enhancement factor
12
10
8
6
4
2
0
0
50
100
150
200
250
300
height of the slab in mm
bending failure (Park)
punching failure

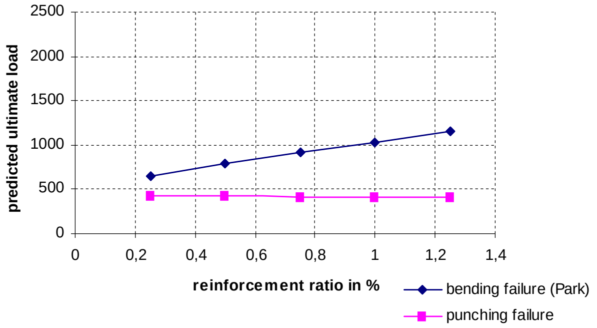
predicted ultimate load
2500
2000
1500
1000
500
0
0
0,2
0,4
0,6
0,8
1
1,2
1,4
reinforcement ratio in %
bending failure (Park)
punching failure

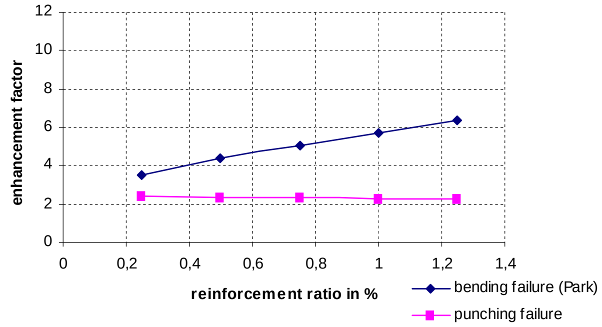
enhancement factor
12
10
8
6
4
2
0
0
0,2
0,4
0,6
0,8
1
1,2
1,4
reinforcement ratio in %
bending failure (Park)
punching failure

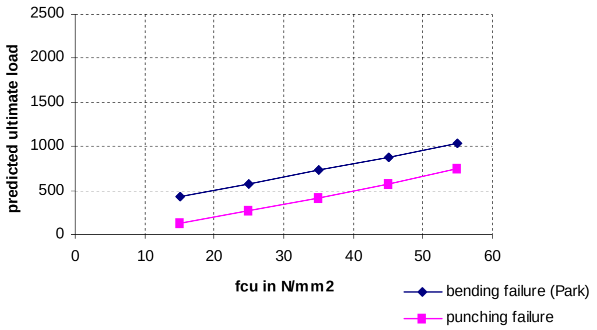
predicted ultimate load
2500
2000
1500
1000
500
0
0
10
20
30
40
50
60
fcu in N/mm2
bending failure (Park)
punching failure

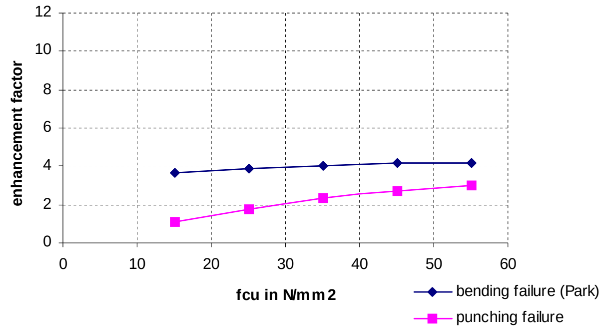
enhancement factor
12
10
8
6
4
2
0
0
10
20
30
40
50
60
fcu in N/mm2
bending failure (Park)
punching failure

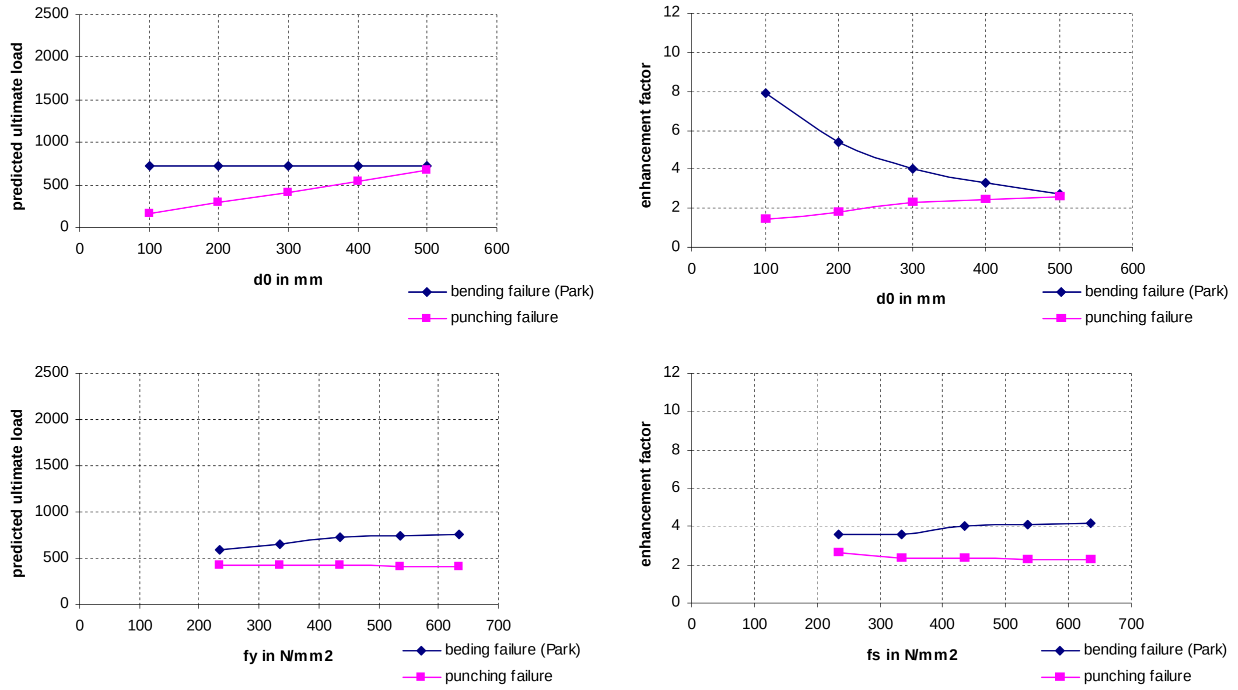

Figure 2.11: Enhancement factors (left) and absolute values (right) for both Park's and the punching failure theory

Conclusions that can be drawn from these graphs are:

- for a low slenderness, punch is governing
- if punch is governing, the flexural reinforcement is not a factor of influence
- the steel strength is not much of an influence factor

3. ANALYTIC SOLUTIONS

A number of trivial structural cases are discussed and compared to the calculations methods used in standard calculations nowadays. Before the comparison can be done these calculation methods will be briefly discussed.

3.1. Standard calculations methods used

Both the ultimate load in bending and in punch will be described.

3.1.1. Ultimate bearing capacity in bending

The method to determine the ultimate load will be the virtual work theory [3.1]. This theory makes use of the fact that the work done internal and external needs to be in equilibrium. This means that the work done by the displacements of the loads (external work), needs to be equal to the work done by the rotation of the plastic hinges (internal work):

$$W_{internal} = W_{external}$$

How this works for beam-like elements will be illustrated by a simple example, see figure 3.1.

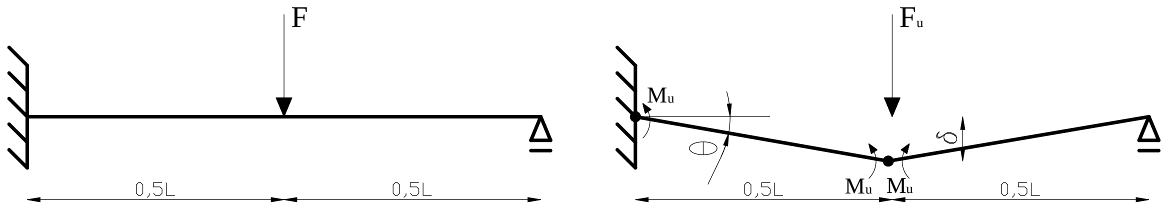

Figure 3.1Simple model with its failure mode

At least 2 plastic hinges need to be introduced to create a failure mechanism. It is assumed that the deformations remain small, so the displacement Δ can be written as the angle times the length of the rotated part. The virtual work equation now becomes:

$$W_{external} = F_u \delta = 0{,}5 L F_u \theta$$
$$W_{internal} = M_u \theta + M_u \theta + M_u \theta = 3 M_u \theta$$
$$W_{external} = W_{internal} \rightarrow 0{,}5 L F_u \theta = 3 M_u \theta$$
$$F_u = \frac{6 M_u}{L}$$

If the ultimate moment of the cross-section is known, than the ultimate load F_u can be easily calculated. For reinforced concrete, the ultimate moment can be calculated with the help of figure 3.2[3.2].

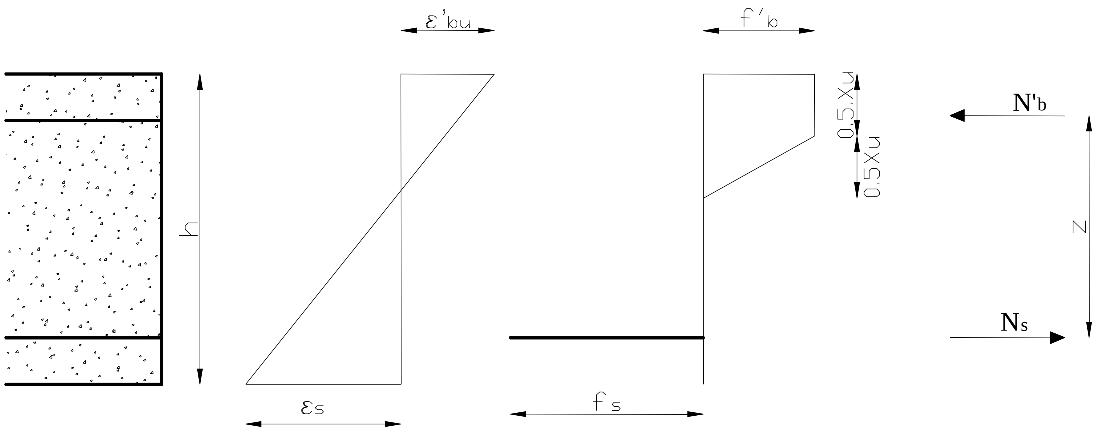

Figure 3.2: Stress and strain distribution in a concrete cross-section, to determine the moment capacity

The ultimate moment for the cross section can now be calculated:

$$N_s = N'_b \ \textit{(equlibrium)}$$

$$N_s = A_s f_s$$

$$N'_b = \frac{3}{4}\chi_u f'_c b$$

$$\chi_u = \frac{4A_s f_s}{3f'_c b}$$

$$z = d - 0{,}39\chi_u$$

$$M_u = N_s z = A_s f_s\left(d - 0{,}39\frac{4A_s f_s}{3f'_c b}\right)$$

With M_u known, the ultimate load of system can be calculated.

3.1.2. Ultimate concentrated load

For the maximum concentrated load, the punching model described by Sagel and van Dongen [3.2] will be used.

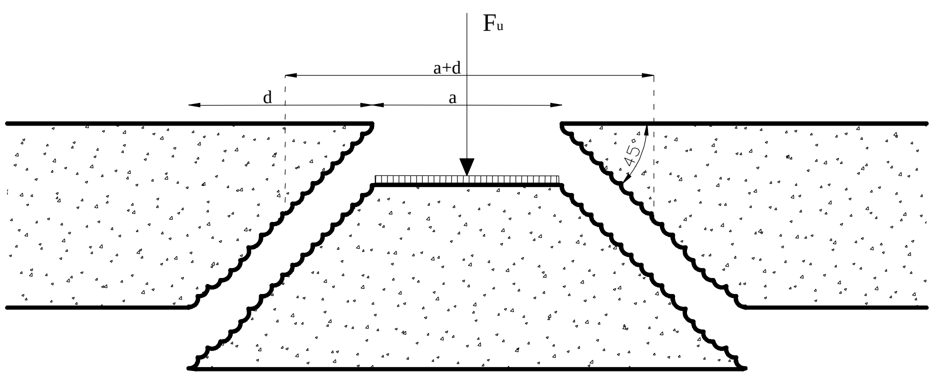

Figure 3.3: Punching shear failure for a concentrated load

The height of the load that induces this failure mechanism can be calculated as follows:

$$F_a = \tau_1 p d$$
$$p = \pi(a+d)$$
$$\pi a = 4a_1 \rightarrow a = \frac{4a_1}{\pi}$$
$$\tau_1 = 0{,}8 f_c k_d \sqrt[3]{\varpi_0} \geq 0{,}8 f_c$$
$$\tau_1 \leq \tau_2$$
$$k_d = 1{,}5 - 0{,}6d \geq 1$$
$$\varpi_0 = \sqrt{\varpi_{0x}\varpi_{0y}} \leq 2\%$$

In the formulae for k_d, d is in meters.

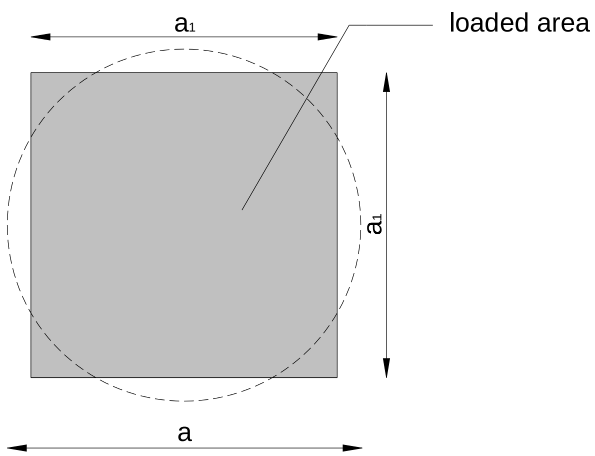

Figure 3.4: Difference between a and a_1

When there is a normal force acting on the structure, τ_1 may even be increased by τ_n:

$$\tau_n = 0{,}15.\sigma_{bmd}$$
$$\tau_{1,increased} = \tau_1 + \tau_n$$

4. COMPARISONS BETWEEN THE ANALYTICAL SOLUTIONS AND TEST RESULTS

To check whether the analytical models give an accurate solution, they will be compared to different test results, which can be found in various articles.

4.1. The bending model

To calculate the solution by Park, a excel sheet is made (see Appendix A). In this sheet, the theory is used as described in chapter 2.1. To calculate C_s and C'_s the strain in the compression reinforcement has to be known. The strain however depends on the concrete compression strain and the distance to the neutral axis. These values are variable as can be seen in the figure below.

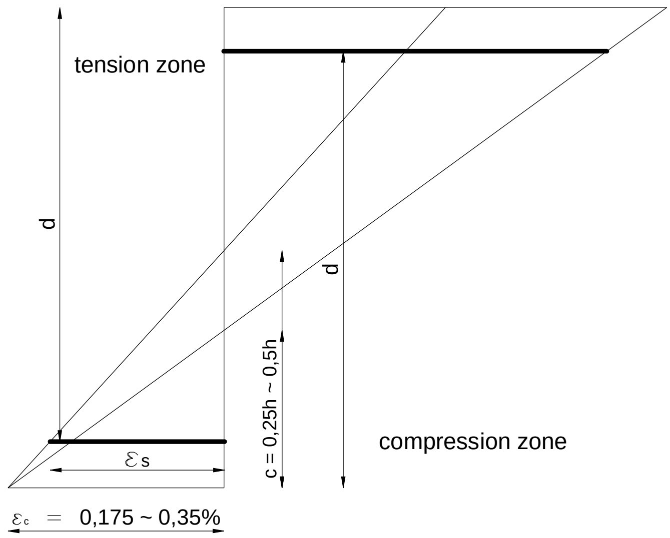

Figure 4.1: The strain distribution for different neutral axis depths

To get an estimation of the steel strain in the compression steel, the average of the above shown values will be used. The value C_s thus becomes

$$\frac{\varepsilon_c}{0{,}375h} = \frac{\varepsilon_s}{d - 0{,}625h}$$

$$\varepsilon_s = 0{,}002625\frac{(d - 0{,}625h)}{0{,}375h}$$

$$C_s = \frac{A_s E_s \varepsilon_s}{b} = 0{,}002625.\frac{A_s E_c (d - 0{,}625h)}{0{,}375bh}$$

Park presents the following graph in his work [2.2], which shows the difference between an experimental result and his analytical solution.

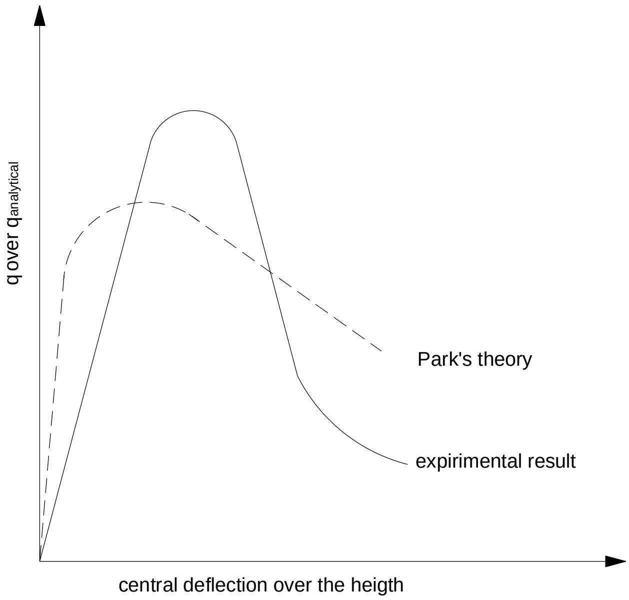

Figure 4.2: Difference between Park's theory and a test specimen

As can be seen, Park's theory gives a somewhat lower ultimate load then the actual specimen. This graph is roughly the same for all test results. It is thus expected that the value of Park's model will lie in between the analytical virtual work solution and the ultimate strength of the tested specimens.

4.1.1. Test results from L. K. Guice and E. J. Rhomberg

The article [4.1] presents test results for a 1-way clamped slab. A sketch with the dimensions of the experiment is showed below.

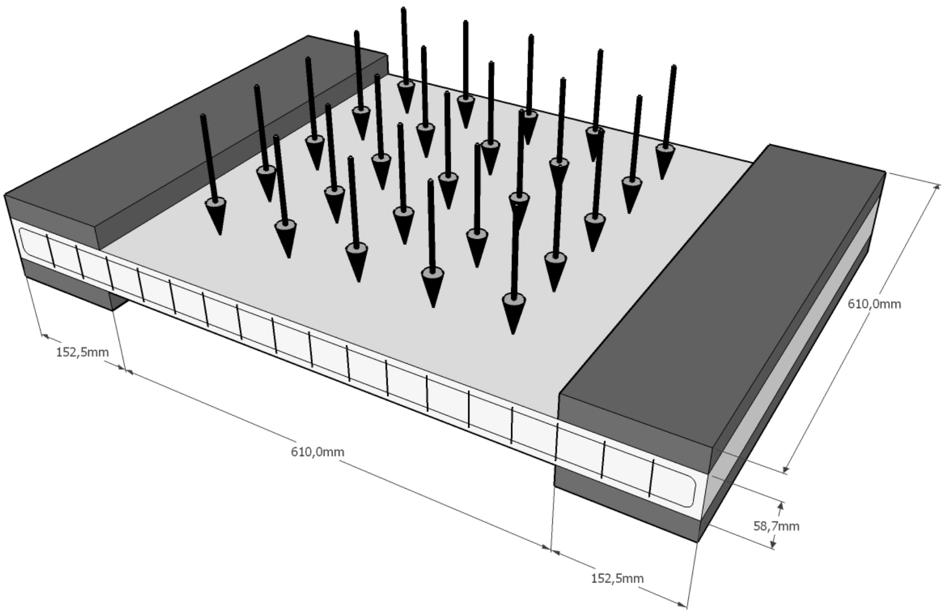

Figure 4.3: Dimensions of the test specimens

A table, which compares the virtual work results, the experimental results and results from the bending theory presented in chapter 2.1, is presented in Table 4.1.

	Slab	fcu N/mm2	fy N/mm2	L mm	b mm	h mm	d* mm	w0 %	Pa kN/m	Pe kN/m	Pp kN/m	Pe/Pa -	Pe/Pp -
tests in bending failure with uniform loading	1	30,4	344,8	610	610	58,7	45	0,52	115,0	328,1	242,3	2,85	1,35
	2	29,4	344,8	610	610	58,7	45	0,52	114,7	218,7	236,3	1,91	0,93
	3	30,6	403,2	610	610	58,7	45	0,74	185,6	302,8	274,1	1,63	1,10
	4	29,4	403,2	610	610	58,7	45	0,72	178,3	298,6	264,7	1,67	1,13
	4A	28,7	403,2	610	610	58,7	45	0,72	177,8	290,2	261,2	1,63	1,11
	4B	29,0	403,2	610	610	58,7	45	0,72	178,0	323,9	262,7	1,82	1,23
	5	30,7	403,2	610	610	58,7	45	1,06	250,2	412,2	315,5	1,65	1,31
	6	29,5	403,2	610	610	58,7	45	1,06	248,3	382,7	310,4	1,54	1,23
	7	34,6	464,2	610	610	41,2	30	0,58	79,0	134,6	117,9	1,70	1,14
	8	34,3	464,2	610	610	41,2	30	0,58	78,9	96,7	117,3	1,23	0,82
	9	34,6	403,2	610	610	41,2	30	1,14	125,5	168,3	137,9	1,34	1,22
	9A	34,5	403,2	610	610	41,2	30	1,14	125,4	172,4	137,8	1,38	1,25
	10	34,3	403,2	610	610	41,2	30	1,14	125,3	-	137,5	-	-
	10A	34,2	403,2	610	610	41,2	30	1,14	125,2	-	137,3	-	-
	11	34,6	403,2	610	610	41,2	30	1,47	152,9	193,5	152,9	1,27	1,27
	12	34,3	403,2	610	610	41,2	30	1,47	152,5	92,5	153,5	0,61	0,60
										Mean value		1,59	1,12
										Standard deviation		0,49	0,21

* this value is not mentioned in the article and is an assumption

Table 4.1: Test values with the analytical (P_a), experimental (P_e) and predicted (P_p) solutions

As was to be expected, the value of the bending theory gives a better estimation than the analytical result. Furthermore it can be seen that Figure 4.2 also holds for these experiments, the estimation of Park is in most cases lower then the actual collapse load..

4.2. The punching model

4.2.1. Tests by J.S. Kuang and T. Morley

The article [4.2] presents the ultimate load for experiments, which failed in punch. The experiments consisted of 2-way slabs with different edge beam widths. Dimensions as shown in Figure 4.4 and Figure 4.5.

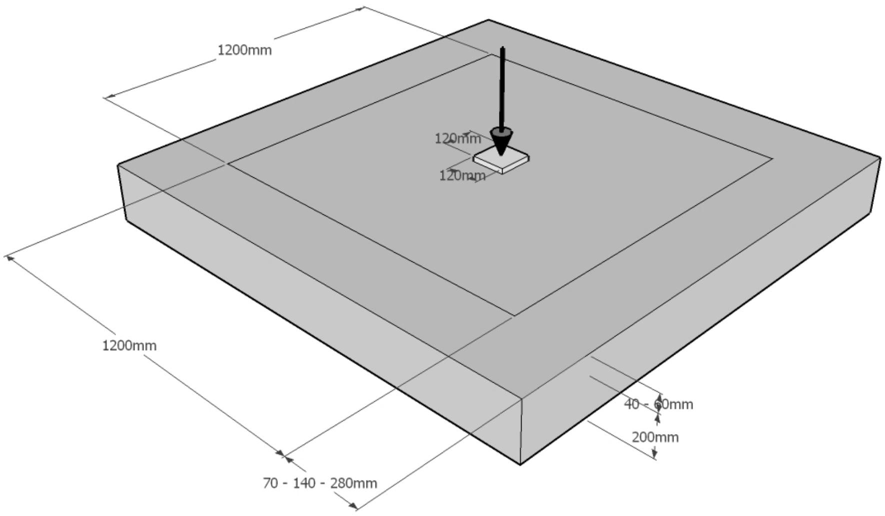

Figure 4.4: Overview of the experimental set-up

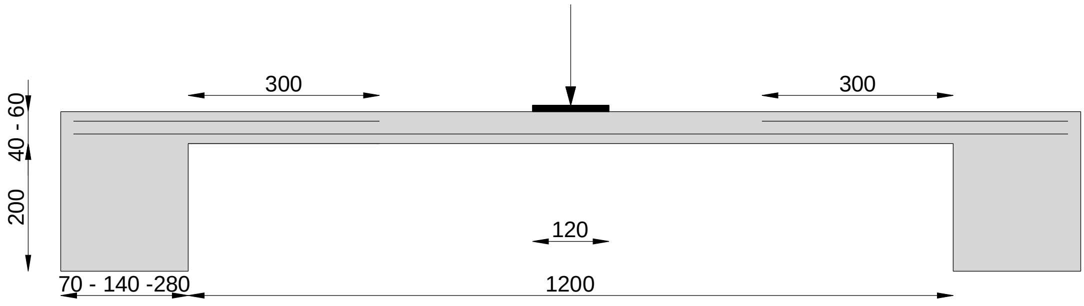

Figure 4.5: Dimensions of the test specimen

The results are presented Table 4.2.

Slab	fcu N/mm2	fy N/mm2	L mm	h mm	d mm	edgebeam mm	w0 %	c mm	Pa kN	Pe kN	Pp kN	Pe/Pa -	Pe/Pp -
S1-C03	48,7	400	1200	60	49	280	0,3	120	36	101	104	2,81	0,97
S1-C10	33,8	400	1200	60	49	280	1,0	120	29	118	64	4,07	1,85
S1-C16	41,2	400	1200	60	49	280	1,6	120	32	149	81	4,66	1,84
S2-C03	48,1	400	1200	40	31	280	0,3	120	20	49	63	2,45	0,78
S2-C10	45,8	400	1200	40	31	280	1,0	120	20	70	59	3,50	1,19
S2-C16	42,6	400	1200	40	31	280	1,6	120	19	68	53	3,58	1,29
S1-B10	45,9	400	1200	60	49	140	1,0	120	35	116	95	3,31	1,22
S1-B03	50,8	400	1200	40	31	140	0,3	120	21	42	67	2,00	0,63
S2-B10	59,5	400	1200	40	31	140	1,0	120	24	69	80	2,88	0,86
S1-A10	46,5	400	1200	60	49	70	1,0	120	36	99	96	2,75	1,03
S2-A03	47,8	400	1200	40	31	70	0,3	120	20	43	62	2,15	0,69
S2-A10	60,3	400	1200	40	31	70	1,0	120	24	63	81	2,63	0,78
										Mean value		3,06	1,09
										Standard deviation		0,79	0,41

Table 4.2: Test values with the analytical (P_a), experimental (P_e) and predicted (P_p) solutions

The factor P_e/P_p (P_p stands for predicted ultimate load and NOT Park's ultimate load, this value is calculated with the punch theory described in chapter 2.2) becomes smaller for smaller edge beam widths, which is to be expected. The presented bending theory does not include a rate of inclination, so for different edge beam widths, the predicted value will be the same. In reality the rate of inclination decreases for smaller edge beams, which will reduce the compressive membrane forces and thus the ultimate collapse load.

4.2.2. Tests by W. Salim and W.M. Sebastian

The authors of the theoretical punch model [2.3] did some experiments. See Figure 2.9 for the test set-up.

Slab	fcu N/mm2	fy N/mm2	L mm	h mm	d mm	w0 %	c mm	Pa kN	Pe kN	Pp kN	Pe/Pa -	Pe/Pp -
S1	63	500	1200	150	113	1,06	150	156,9	369,4	466,7	2,35	0,79
S2	52	500	1200	150	113	1,06	150	136,3	290,6	367,6	2,13	0,79
S3	56	500	1200	150	113	1,06	150	143,8	402,2	403,4	2,80	1,00
S4	53	500	1200	150	113	1,06	150	138,2	394,1	376,6	2,85	1,05
									Mean value		2,53	0,91
									Standard deviation		0,35	0,13

Table 4.3: Test values with the analytical (P_a), experimental (P_e) and predicted (P_p) solutions

As we put the data in a graph, we can see some scatter in the test results, since only the concrete strength is varied.

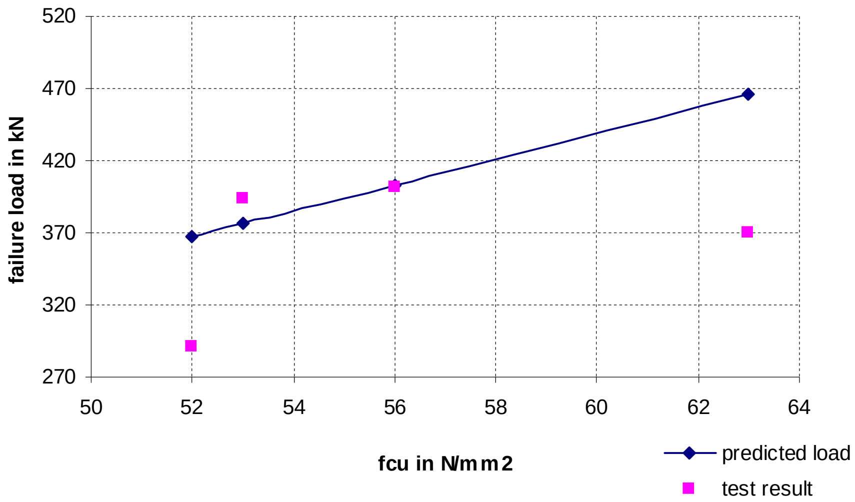

Figure 4.6: Predicted result versus test results

4.2.3. Tests by Holowka, Dorton and Csagoly

In the article which presents the theoretical punch failure solution [2.2], some test results from other parties where included. No information is given on how the test where carried out, but it still some good comparison data. One of these test results is shown in Table 4.4.

Slab	fcu N/mm2	fy N/mm2	h* mm	d mm	w0 %	c mm	Pa kN	Pe kN	Pp kN	Pe/Pa -	Pe/Pp -
A1-A3	27,4	310	48,1	38,1	0,2	127	19,1	42,4	42,1	2,22	1,01
B1-B2	27,7	310	41,8	31,8	0,2	127	15,5	36,8	35,8	2,37	1,03
C1-C3	28,4	310	35,4	25,4	0,2	127	11,8	23,1	30,2	1,96	0,76
D1-D3	25,9	310	48,1	38,1	0,3	127	18,5	49,1	39,3	2,65	1,25
E1-E3	26,9	310	41,8	31,8	0,3	127	15,2	34,9	35,1	2,30	0,99
F1-F3	27,0	310	35,4	25,4	0,3	127	11,7	23,8	29,4	2,03	0,81
G1	28,1	310	48,1	38,1	0,8	127	19,4	44,6	43,1	2,30	1,03
H1	28,2	310	41,8	31,8	0,8	127	15,6	37,9	36,7	2,43	1,03
I1-I3	28,1	310	48,1	38,1	1,0	127	19,4	47,3	42,6	2,44	1,11
J1-J2	27,8	310	41,8	31,8	1,0	127	15,5	37,2	35,8	2,40	1,04
K1-K2	27,9	310	35,4	25,4	1,0	127	11,9	25,2	32,0	2,12	0,79
* this value is not mentioned in the article and is an assumption								Mean value		2,29	0,99
								Standard deviation		0,20	0,15

Table 4.4: Test values with the analytical (P_a), experimental (P_e) and predicted (P_p) solutions

The span of the specimen is not given, but it is earlier stated that the influence of the length is not of much influence for a small d_0/L ratio, as is already mentioned in chapter 2.2. It can be seen that the predicted value gives a good indication. Only a few of the tested specimens have a somewhat larger difference. It can be that the height of the slab is not assumed correctly, or the tests may not have been carried out properly.

4.2.4. Full scale tests by S.E. Taylor, B. Rankin, D.J. Cleland and J. Kirkpatrick

Experiments done on a full-scale structure is described in the article [4.3]. The tests where done on several spans with loads up to three times the maximum wheel load of the British standards. The crack widths and the deflection at the midsection of the span where measured.

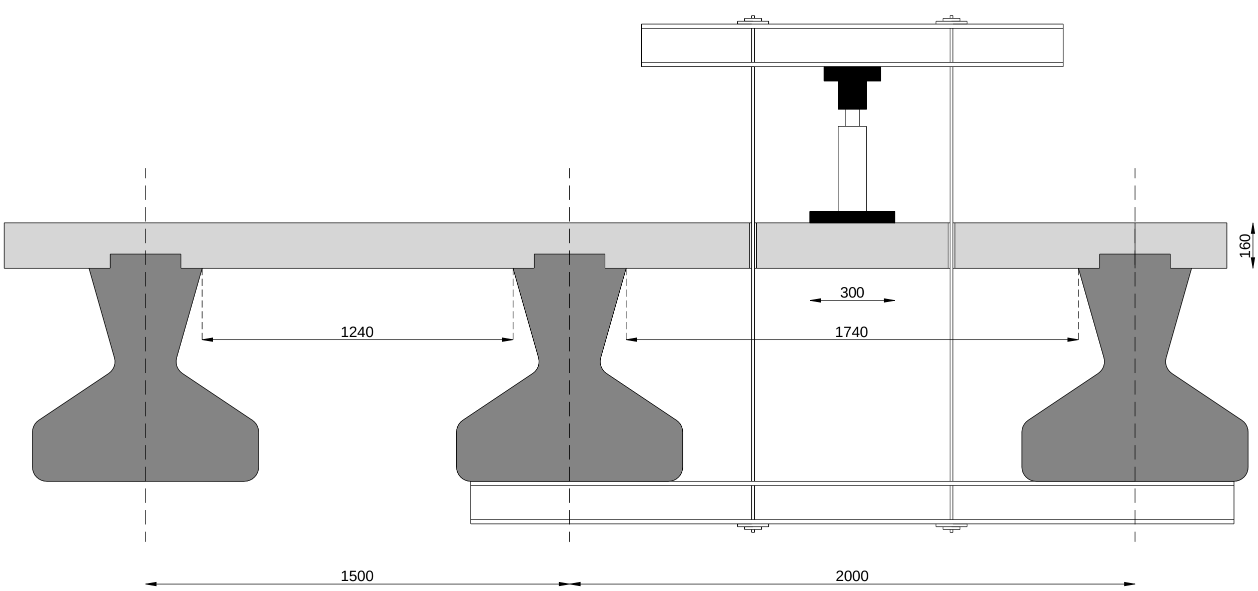

Figure 4.7: Overview of the test setup

Since they did not loaded the bridges till they collapsed, for now it can be only check if the analytical ultimate load is higher than the load level during the testing. After the finite element calculations, it can be checked whether the deflection and the crack widths calculated at the loading levels is in accordance with reality.

slab	fcu N/mm2	fs N/mm2	L mm	h mm	d mm	w0 %	anaytical collapse load	maximum test load	predicted ultimate load
A1	77,8	501	1740	160	82	0,5 + fibers	128,3	333	1240,1
A2	80,6	501	1240	160	74	0,5 + fibers	178,3	428	1279,6
B1	76,5	501	1740	160	75	0,25 + fibers	66,5	344	1280,5
B2	82,3	501	1240	160	75	0,25 + fibers	92,3	428	1314,9
C1	81,2	501	1740	160	75	0,25	66,6	333	1291,3
C2	78,2	501	1240	160	75	0,25	92,2	428	1239,3
D1	74,6	501	1740	160	75	0,5	127,9	368	1166,2
D2	74,6	501	1240	160	75	0,5	177,3	428	1169,1
E1	67,8	501	1740	160	105	0,6	202,1	392	1040,7
E2	67,8	501	1240	160	105	0,6	280,0	428	1043,1
F1	60,0	501	1740	160	103	0,6	199,5	371	899,8
F2	61,0	501	1240	160	103	0,6	275,2	428	919,8

Table 4.5: Test values and the predicted ultimate load

Part II: The finite element modelling

5. FINITE ELEMENT MODELS

The theory describes a one-way laterally restrained slab. Cracking of the concrete is the main reason compressive membrane forces are generated. The finite element package DIANA is capable to calculate concrete structures, including the cracking of the concrete. For bending a 2D model will be sufficient, but if punch is to be included, a 3D model must be used.
The loading steps on the structure can be applied in two different ways. There can be a given displacement and displacement steps, at which DIANA calculates the load, or there can be applied a load with a loading step and then DIANA calculates the displacement. Since Park's theory describes a plate with a distributed load, the input will be a load with a loading step.

Then there is the issue of which elements to use for the calculations. This will be discussed first.

5.1. The geometry of the model

Since the model must describe a reinforced concrete one-way slab with a unit width, the following models can be used:

– 2D beam model	bending
– 2D plane stress model	bending
– 3D curved shell model	bending
– axi-symmetric model	bending and punch
– 3D solids model	bending and punch

To make a choice of the above models, they will be used to calculate the following simply supported beam as shown below.

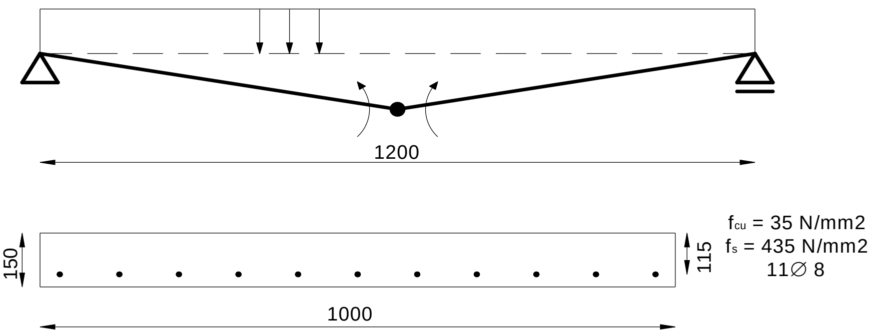

Figure 5.1: Simply supported beam used to determine a suitable finite element model

The analytical solution is

$$q_u = \frac{8M_u}{L^2}$$

$$M_u = 552,9.435\left(115 - 0,39\frac{4.552,9}{3.21.1000}\right) = 26,23kNm$$

$$q_u = 8.26,23.1,2^2 = 145,7\frac{kN}{m}$$

To make a choice which model to use the following factors are considered

- the deviation of the analytical solution presented in chapter 3
- the complexity of the input of the model
- the calculation time
- the output

For now the total strain rotating crack model, brittle in tension and ideal in compression will be used. The analytical solution is based on brittle cracking without tension softening, so this material model should give results close this solution and will be used for these calculations.

5.1.1. 2D beam model

The input model is presented in Figure 5.2.

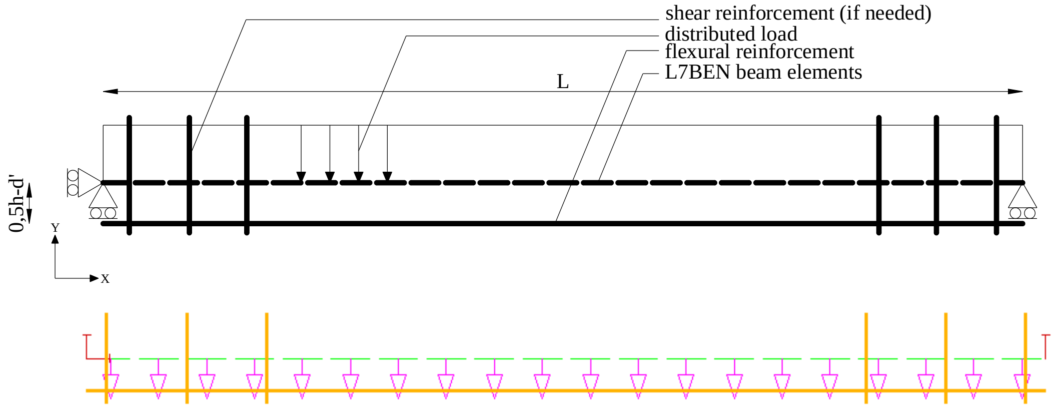

Figure 5.2: Schematic overview and iDIANA input for the finite element model

The manual of DIANA gives the following overview for beam elements. Only the class-II and class-III elements can be reinforced with embedded reinforcement bars.

Class	**Class-I**		**Class-II**		**Class-III**					
Theory	*Bernoulli*		*Bernoulli*		*Mindlin-Reissner*					
Type	L6BEN	L12BE	L7BEN	L13BE	CL9BE	CL12B	CL15B	CL18B	CL24B	CL30B
Dimension	2D	3D	2D	3D	2D	2D	2D	3D	3D	3D

Figure 5.3: Overview of the type of beam elements that can be used by DIANA

The L7BEN elements will be used for this calculation. The number of integration points over the height will be increased, so that the cracking will be taken into account more accurately. The difference is shown in the load-displacement graph below. The calculation stops before reaching the horizontal part when using only 2 integration points over the height of the beam.

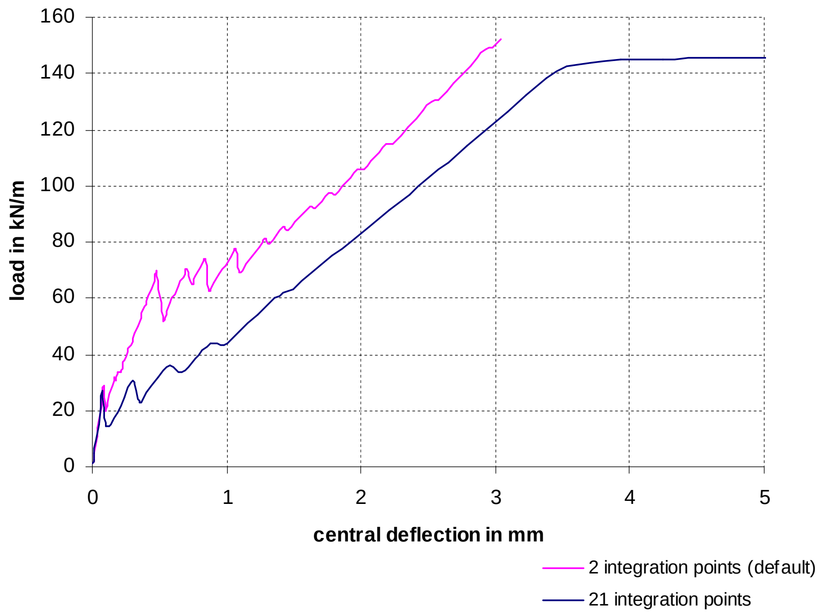

Figure 5.4: Difference between2 and 21 integration points over the height of a beam element

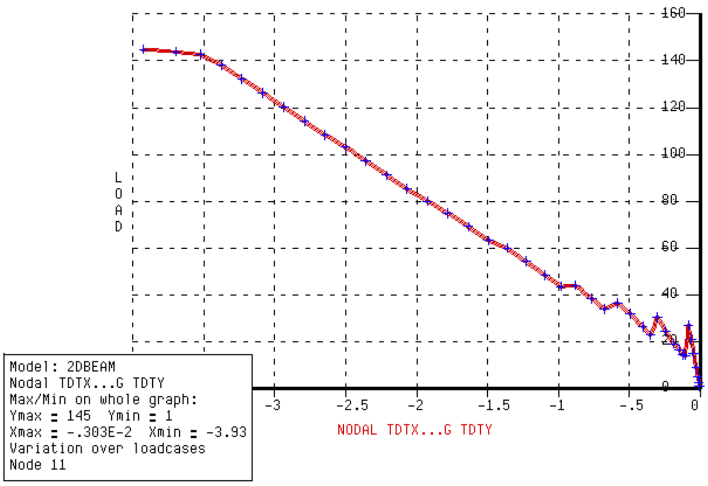

Figure 5.2 load-displacement graph for the middle node calculated by DIANA

Advantages

– easy and fast to build model
– little calculation time
– analytical and numerical solution are almost equal
– moment and shear forces as output

Disadvantages

– graphical output is minimal, since it is only a line model
– loads act over the whole width of the beam

5.1.2. 2D plane stress model

The input is presented below. It is common to make use of symmetry whenever possible, to reduce the calculation time.

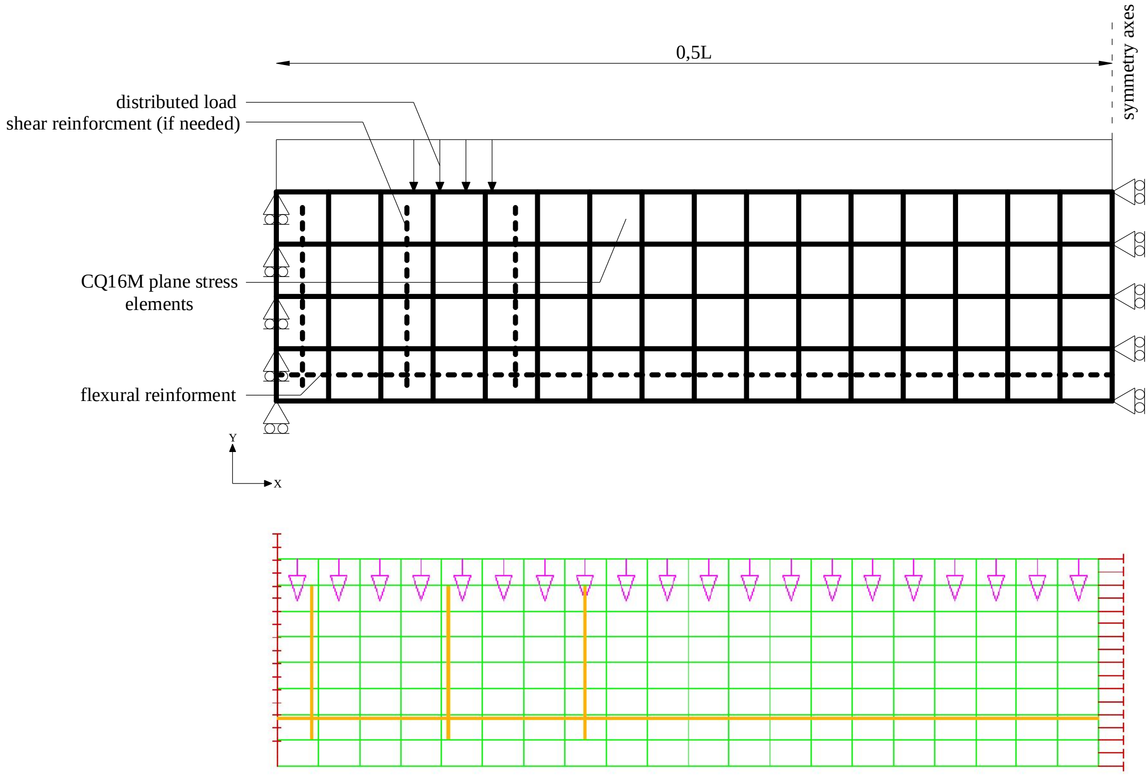

Figure 5.5: Schematic overview and iDIANA input for the finite element model

Plane stress elements are characterised by the fact that the stress components perpendicular to the face are zero, $\sigma_{zz} = 0$. DIANA can use the following regular plane stress elements. For this calculation, the CQ16M element will be used.

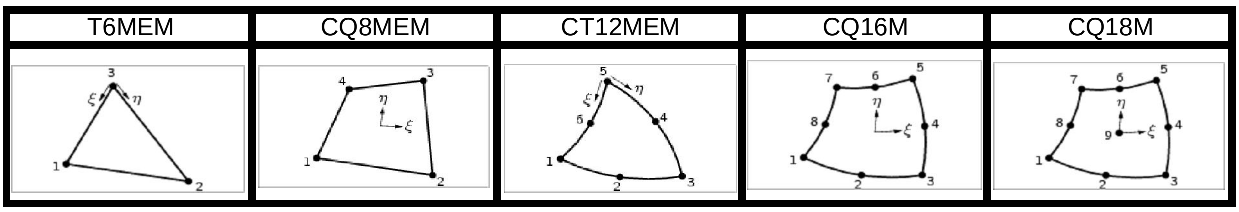

Figure 5.6: Overview of the type of 2D plane stress elements that can be used by DIANA

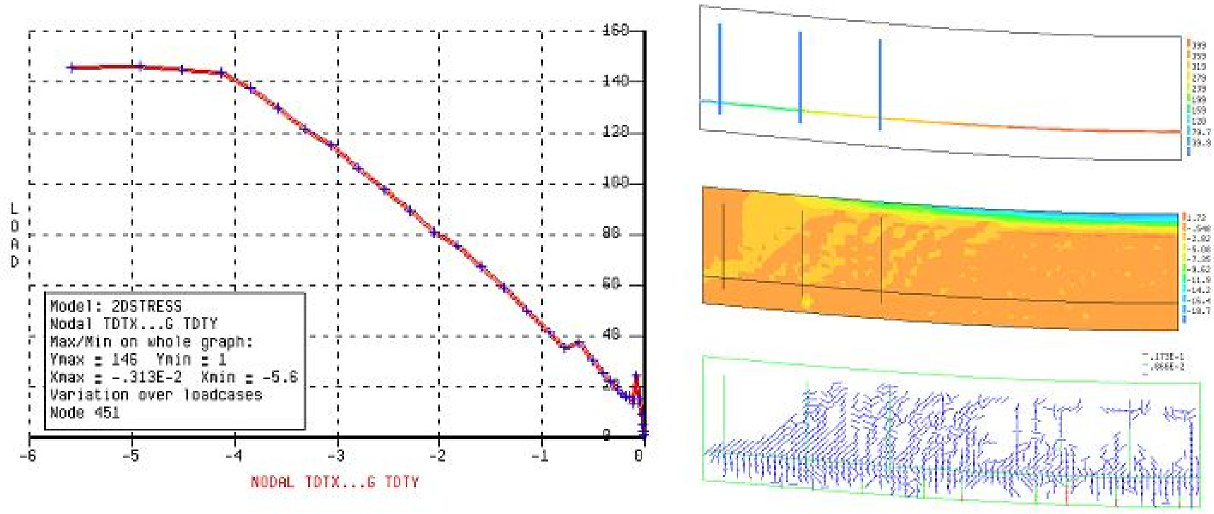

Figure 5.7: Output of iDIANA, stresses in the concrete and the reinforcement, the crack pattern and the load-displacement graph

Advantages

- easy and fast to build model
- little calculation time
- analytical and numerical solution are almost equal
- al the wanted output can be graphically presented

Disadvantages

- rotation is not a degree of freedom
- no moment and shear forces as output
- loads act over the whole width of the model

5.1.3. 3D curved shell model

For this model two symmetry axes will be used.

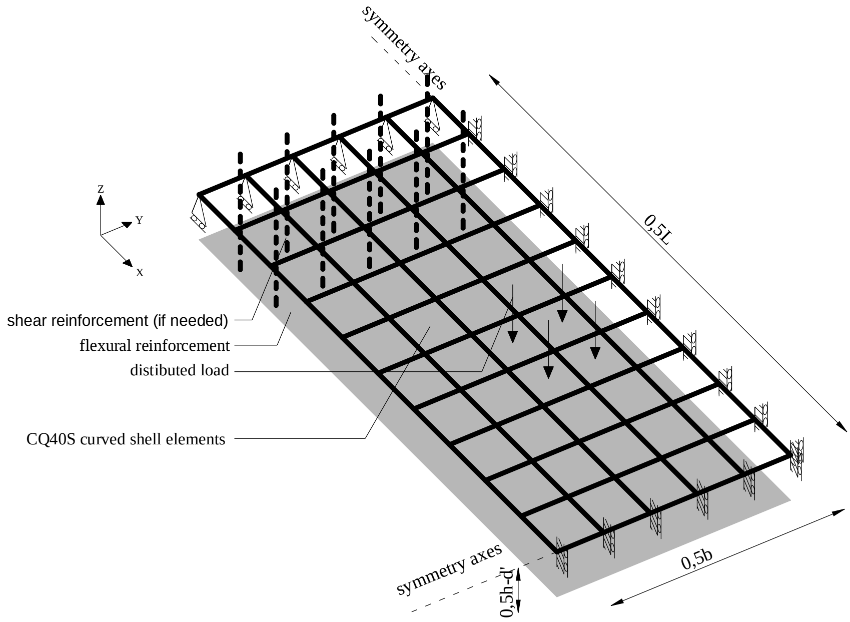

Figure 5.8: Schematic overview of the 3d curved shell model

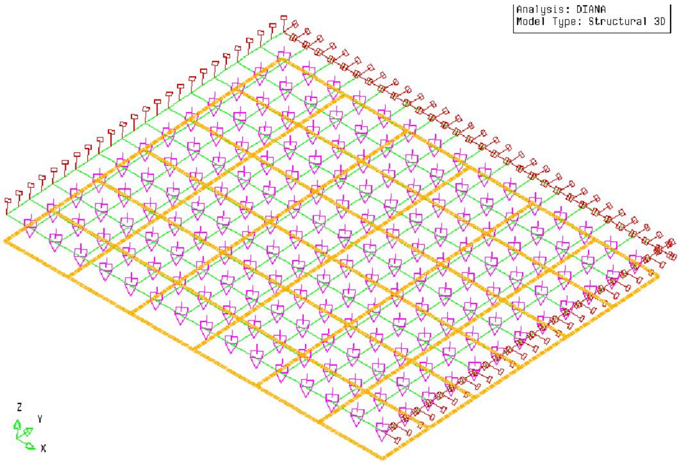

Figure 5.9: iDIANA input of the finite element model

The element CQ40S will be used for this calculation. The number of integration points over the height will be increased, so that the cracking will be taken into account more accurately, in the same way as for the 2D beam model, see chapter 5.1.1.

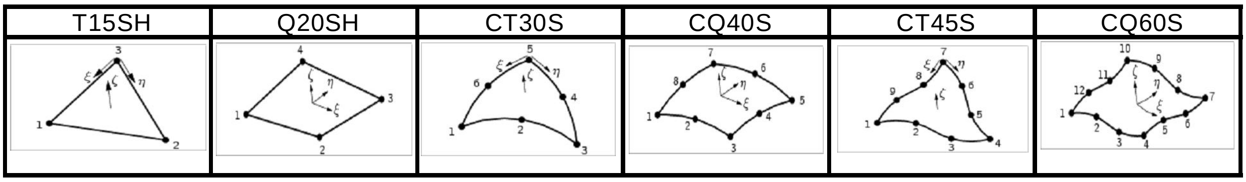

Figure 5.10: Overview of the type of 3D curved shell elements that can be used by DIANA

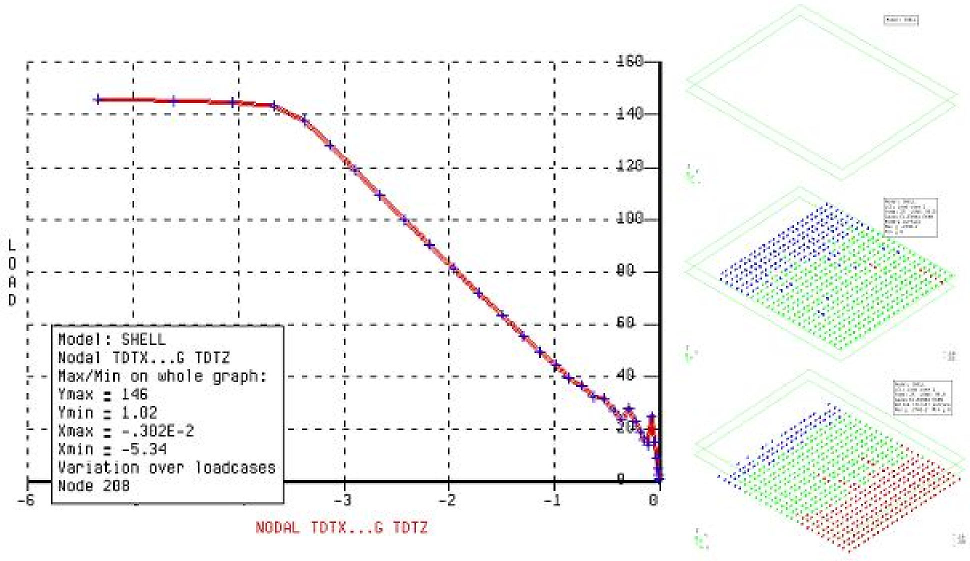

Figure 5.11: Some results, the load-displacement graph and cracking in the top, middle and bottom surface

Advantages

- analytical and numerical ultimate load are almost equal
- al the output can be graphically presented
- load can be distributed over an given area

Disadvantages

- rather long calculation time

5.1.4. 3D solid model

For the 3D solid model two symmetry axes will be used.

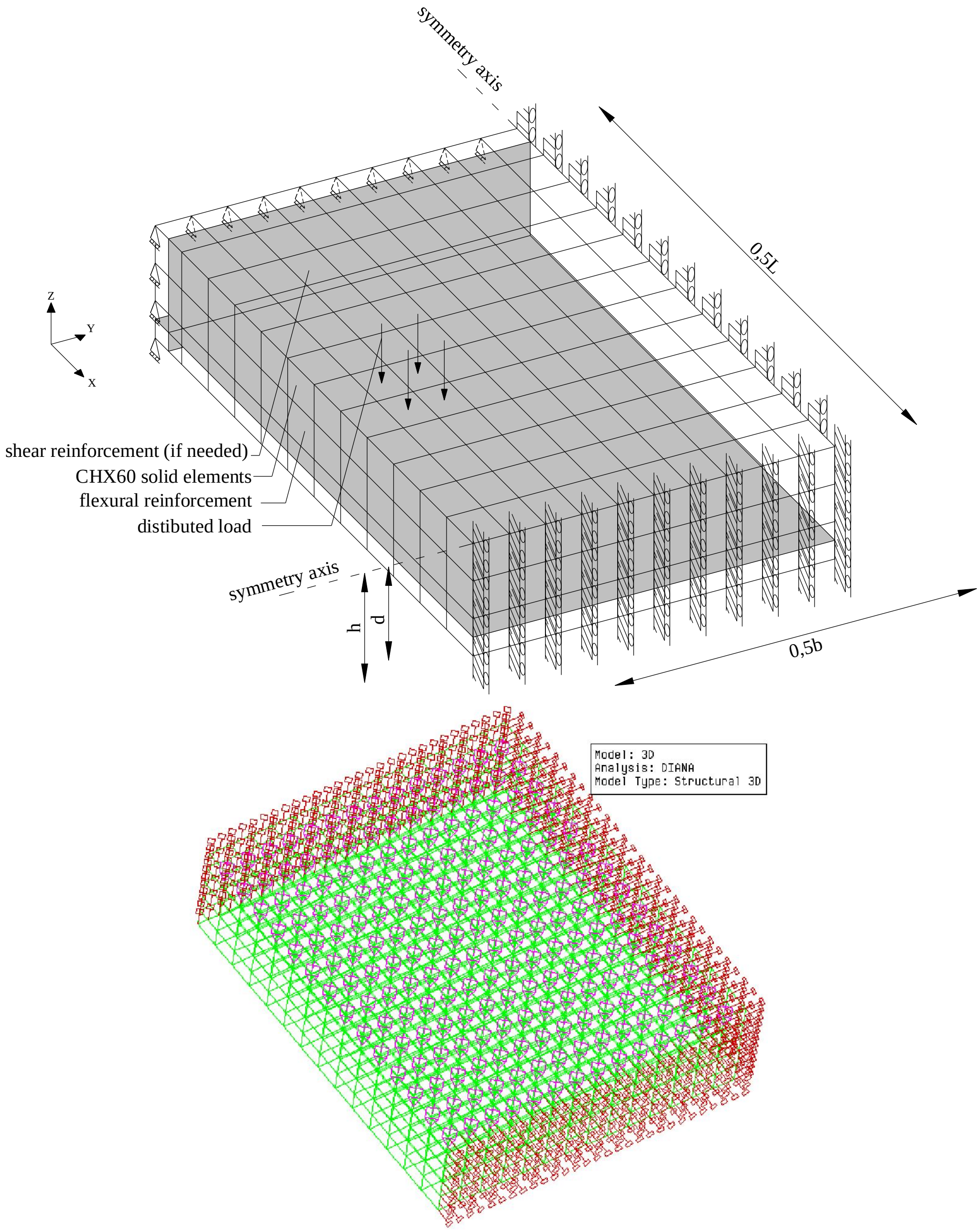

Figure 5.12: Schematic overview and iDIANA input for the finite element model

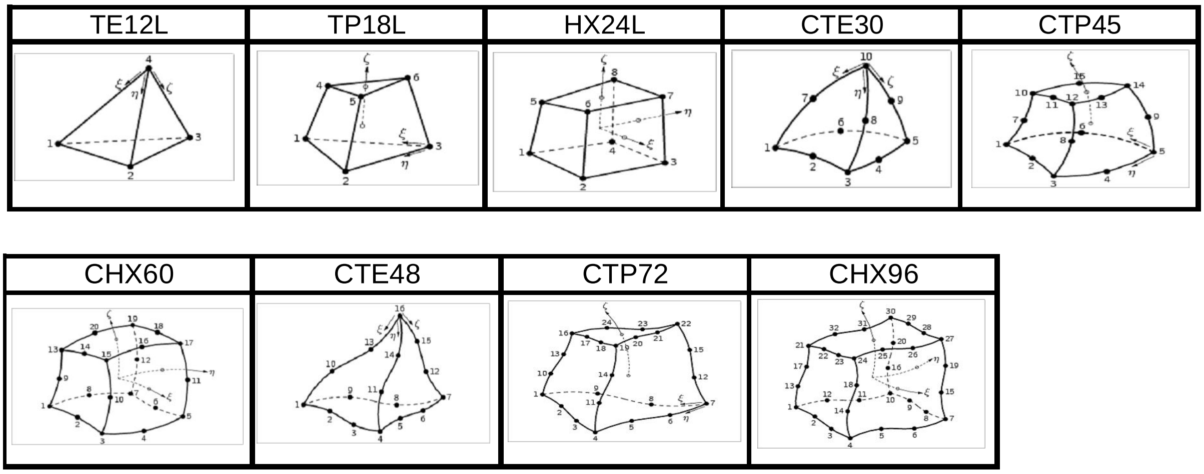

Figure 5.13: Overview of the type of 3D solid elements that can be used by DIANA

The element CHX60 is used for this calculation.

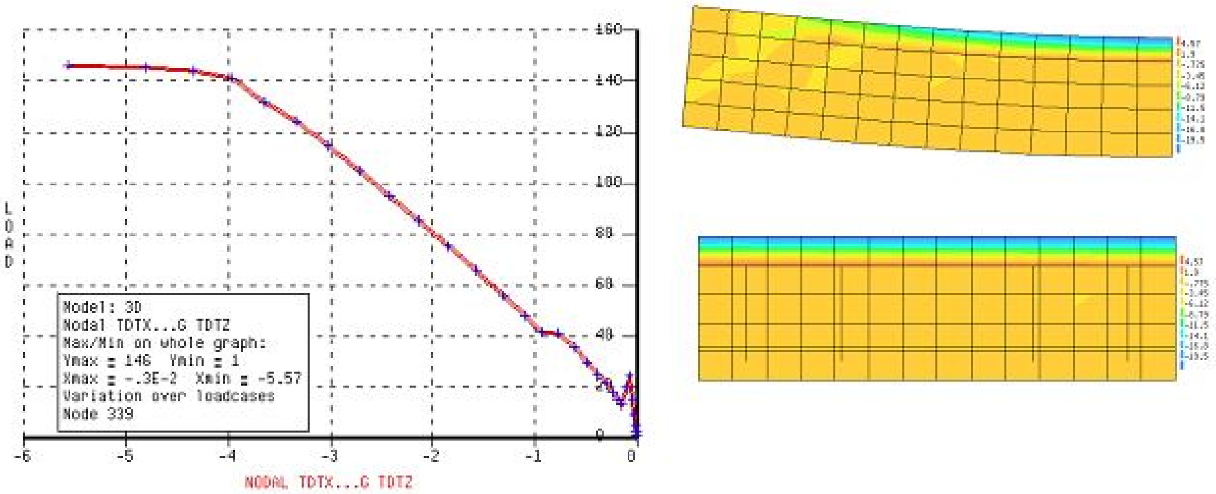

Figure 5.14: Output of iDIANA , the load-displacement graph and σ_{xx} in a x and y cross-section

Advantages

- the largest collection of output data
- load can be distributed over an given area

Disadvantages

- long calculation time
- most complex to build of all the models
- output can be difficult to understand

5.1.5. Axi-symmetric model

The axi-symmetric model will only be used for concentrated loads and will be further discussed in chapter 7.2.

5.1.6. Conclusion

The load-displacement graphs of all the models are compared below. All the models give a very accurate outcome compared to the analytically found load.

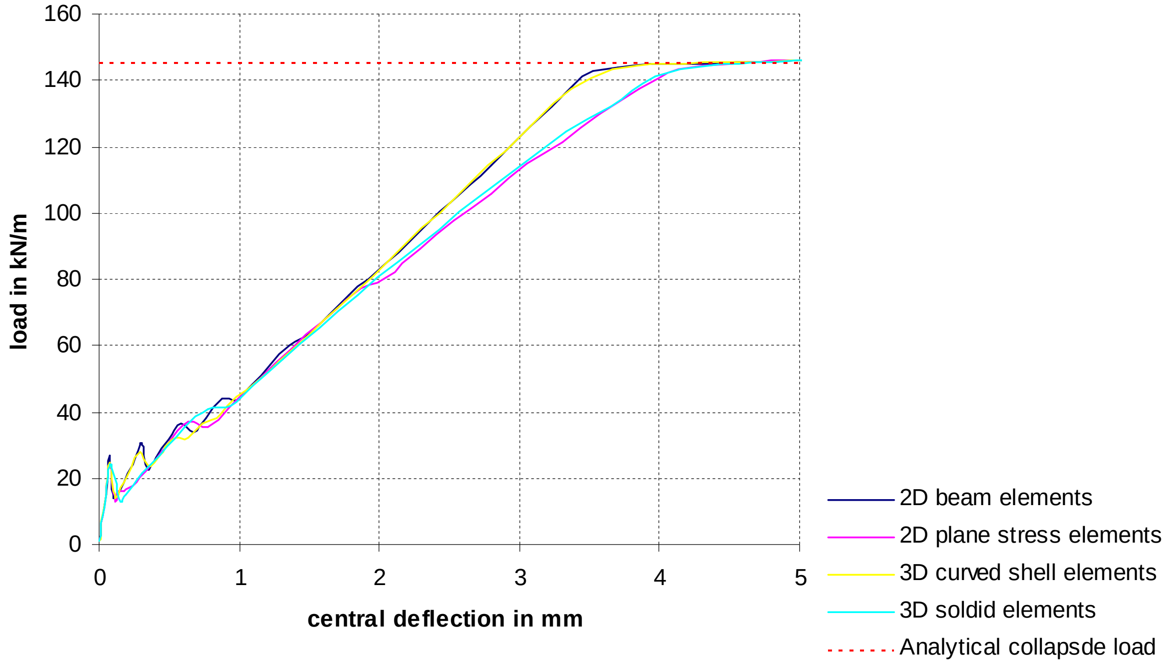

Figure 5.15: Comparison of the load-displacement graphs of the four models

It can be seen that all the models give a good approximation of the ultimate analytical load. The 2D beam model and the 3D shell model give almost the some solution. The same holds for the 2D plane stress and 3D solid model. The latter react somewhat less stiff at large loads.
An overview of the different models is given in Table 5.1.

	input	graphical output	realistic model	punch behaviour	calculation time
2D beam model	++	--	+	irrelevant	++
2D plane stress model	+	+	+	irrelevant	+
3D curved shell model	o	-	+	--	o
3D solids model	-	++	++	o	--
axi-symmetric model	+	+	-*	++	+

*** : rectangular slabs cannot be modelled with this model**

Table 5.1: overview of the different finite element models

5.2. Material properties

The material properties input in DIANA is numerous. Different models can be used for cracking, the tensile and compressive behaviour of concrete and the behaviour of the reinforcement steel. All of these will be discussed shortly in the next paragraphs. The most realistic material models will be used, since the model will be compared to experimental results.

5.2.1. Cracking

There are two cracking models that can be used, smeared cracking or total strain cracking. The smeared cracking model is depended on the principal stresses. This can be taken in to account for a constant or linear function.

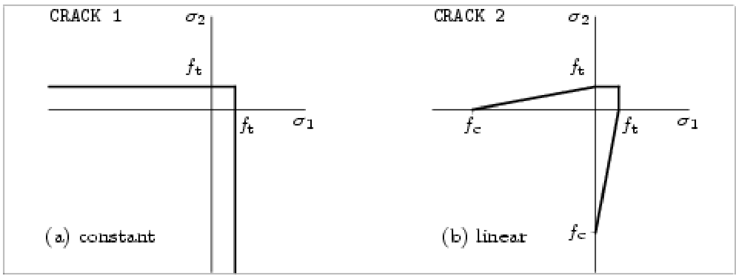

Figure 5.16: Two ways of smeared cracking

The total strain crack model describes the tensile and compressive behaviour of a material with one stress-strain relationship. This makes the model very well suited for Serviceability Limit State (SLS) and Ultimate Limit State (ULS) analyses which are predominantly governed by cracking or crushing of the material. Within this model, there can be chosen for rotating or fixed cracking. The difference between the two is that for fixed cracking the crack lies in the same direction for all the load steps, while by rotating cracking, the direction of the crack is calculated separately for each load step.

The total strain rotating crack model will be used for the calculations.

5.2.2. Concrete in tension

An overview of the different models DIANA can use for tension in the concrete is presented below.

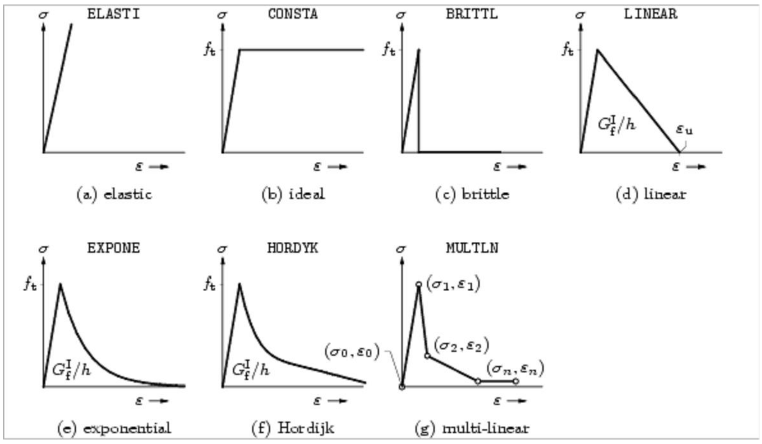

Figure 5.17: Different models for concrete behaviour after cracking

The options (d) till (g) show the possibilities to take into account tension softening.

The Dutch code is based on models with a brittle cracking model, but including tension softening may give results that lie closer to the real collapse load. So both options (c), brittle and (f), the Hordijk model will be used for the calculations.

5.2.3. Concrete in compression

An overview of the different models DIANA can use for compression in the concrete is presented below.

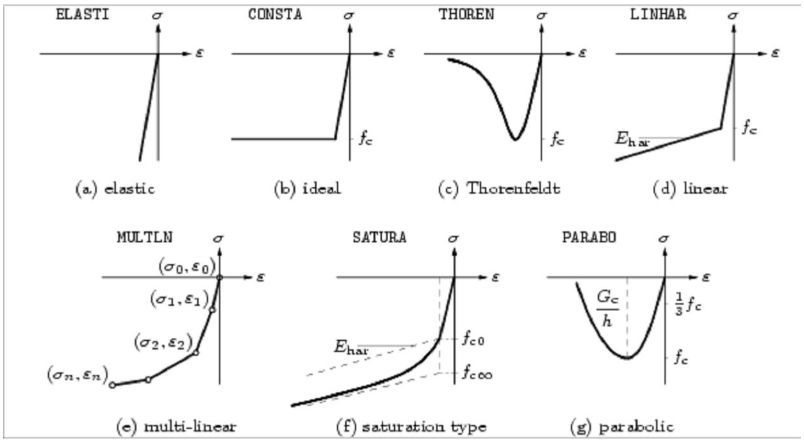

Figure 5.18: Different models for concrete behaviour after the yield strength is reached

Option (b), the ideal model will be used for the calculations.

5.2.4. Reinforcement steel

For the reinforcement there are three options, ideal plastic, a work-hardening diagram or a strain-hardening diagram. The ideal plastic model is used.

5.2.5. Conclusion

The material model that is used looks like this:

- total strain rotating crack model
- both brittle and Hordijk tension softening in tension
- ideal plastic model in compression
- ideal plastic model for the reinforcement

6. FINITE ELEMENT MODEL FOR BENDING ACTION

The 2D plane stress model will be used since this is an easy to build model with fast calculation time.

6.1. Total horizontal restrained clamped model

The same model as described in chapter 5.1 will be used, but now the edges will be totally clamped and horizontally restrained. The analytical and Park's solution are given below.

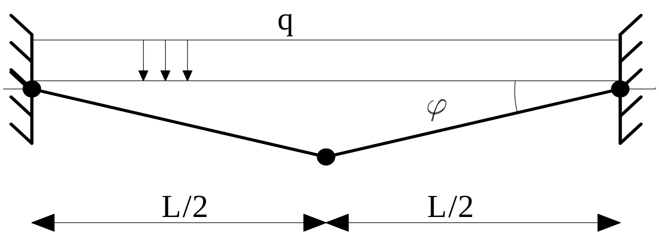

Figure 6.1: Schematic overview of the structure

$$q_{analytical} = 291{,}4 \frac{kN}{m}$$

$$q_{Park} = 706{,}7 \frac{kN}{m}$$

The schematic input in DIANA looks as follows

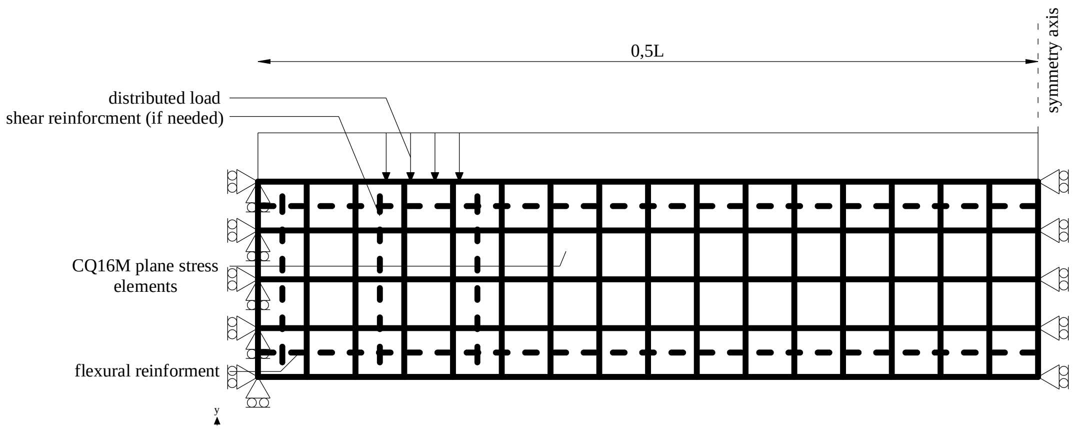

Figure 6.2: Schematic input of the finite element model

The difference between the earlier shown input is that the edge is now horizontally restrained and extra top reinforcement is added. Rotation is not a degree of freedom for these elements, but since the whole edge is restrained horizontally and vertically, it can not rotate.

The ultimate load calculated by DIANA is even higher than Park's prediction. This seems to be a good result since Park's values are in most cases somewhat lower than the experimental data (see chapter 4.1).

Since the code does not take into account tension softening, the solution with a brittle cracking model is compared to the tensile softening solution in the graph below.

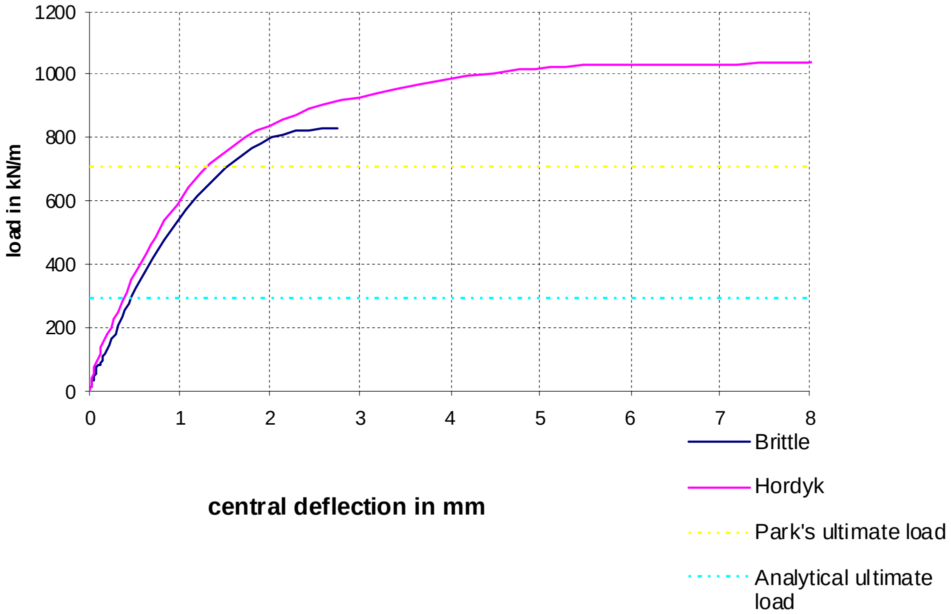

Figure 6.3: Difference between a calculation with brittle cracking and tension softening

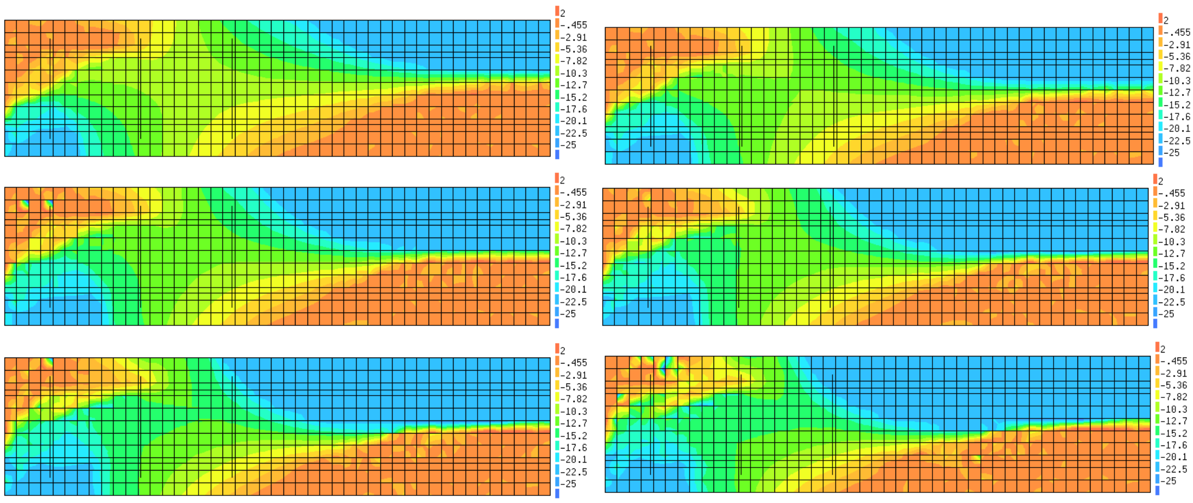

Figure 6.4: σ_{xx} over load steps 23 to 28, from 924 to 997 kN/m

In Figure 6.4, the shifting of the neutral axis can be seen.

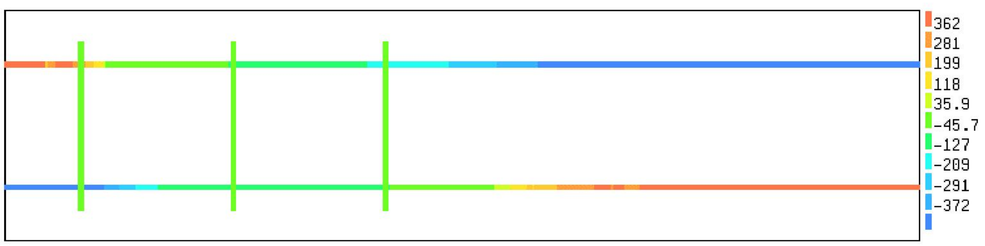

Figure 6.5: Stresses in the steel, the steel is loaded in compression and tension

6.1.1. Model without shear reinforcement

The maximum analytical solution for the shear failure depends on τ_1 when no shear reinforcement is used.

$$f_{cu} = 35\frac{N}{mm^2}$$

$$f'_c = 1{,}4\frac{N}{mm^2}$$

$$k_\lambda = 1{,}0$$

$$k_h = 1{,}6 - h = 1{,}35$$

$$\omega_0 = 0{,}37\%$$

$$\tau_1 = 0{,}4.f_c'.k_\lambda.k_h.\sqrt[3]{\varpi_0} \nless 0{,}4.f'_c = 0{,}56\frac{N}{mm^2}$$

$$V_d = \tau_1.b.d = 64{,}4kN$$

$$q_{\max} = \frac{2.V_d}{L} = 107{,}3\frac{kN}{m}$$

In the bending theory presented in chapter 2.1, a compressive normal force is introduced, and the value τ_1 may be increased by τ_n according to the Dutch code[5.1]. This value holds only for linear elastic calculations, which means it may not be used in this case. Yet it is interesting to see what the influence might be on the shear strength. The value of N_u follows for the calculation of the bending theory and is calculated with the excel sheet from Appendix A.

$$N_u = 1293kN$$

$$\sigma_{bmd} = \frac{N_u}{h.b} = 8{,}62\frac{N}{mm^2}$$

$$\tau_n = 0{,}15.\sigma_{bmd} = 1{,}29$$

$$\tau_{1,increased} = \tau_1 + \tau_n = 1{,}85$$

$$q_{\max} = 354{,}6\frac{kN}{m}$$

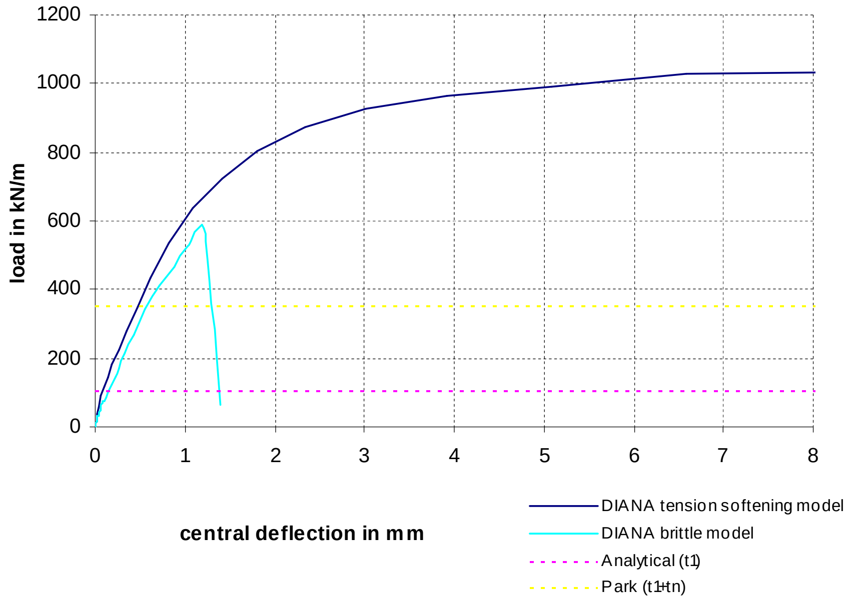

Figure 6.6: Load-displacement graph for a model without shear reinforcement

The ultimate load calculated by DIANA is the same as for the model with shear reinforcement in the case of a model which includes tension softening, which means shear failure is not governing in this model. For the brittle material behaviour shear failure is governing. The ultimate load for the brittle model is thus less than the model without shear reinforcement.

6.1.2. Variation in reinforcement layout

As can be seen in Figure 6.5 the flexural reinforcement is loaded in both tension and compression. The following graph shows the ultimate load for a model with only reinforcement in the tensile zones, and for a model with no reinforcements at all. The models are all <u>without</u> any <u>shear reinforcement.</u>

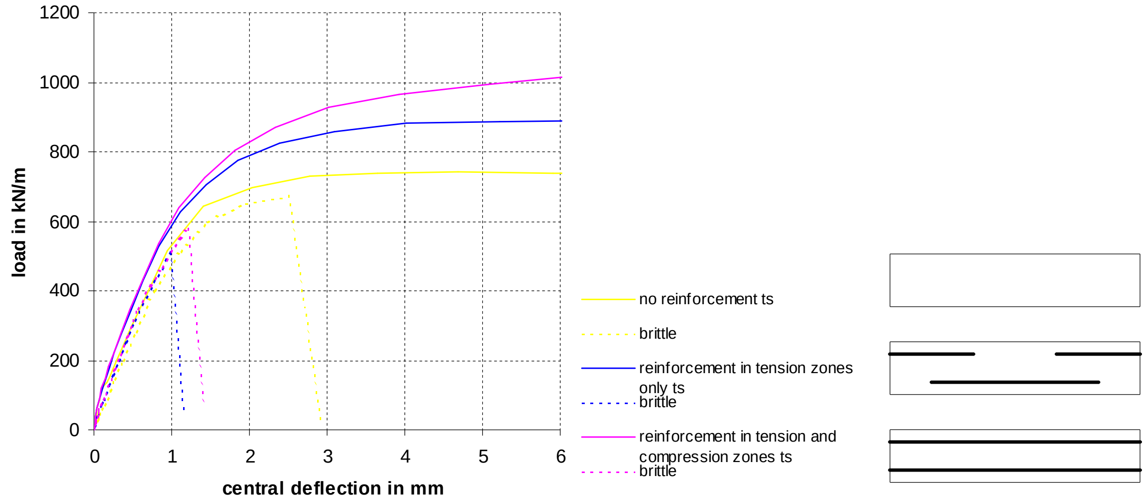

Figure 6.7: Load-displacement graphs for different reinforcement placements (ts stands for tension softening)

First of all, taking into account tension softening enhances the shear capacity considerably. All of the tension softening models failed in bending. All the brittle models fail in shear. Noticeable is that the model without any reinforcement has the highest shear capacity of the brittle models. This is probably due to the fact that large crack widths occur in an un-reinforced structure, which enlarges the compressive membrane force that is introduced by the lateral restraint edges. This compressive force has a positive effect on the shear capacity of the one-way slab.
Testing is required to prove that un-reinforced lateral restrained slabs have a greater shear capacity then reinforced lateral restrained slabs.

6.1.3. Enhancement factors

The enhancement factor $\frac{q_{DIANA}}{q_{analytic}}$ is calculated for variation in the slenderness, the concrete and steel strength and the reinforcement percentage. The reinforcement is taken in both the upper and lower layer, according to the first used model, which can be seen in figure 5.12.

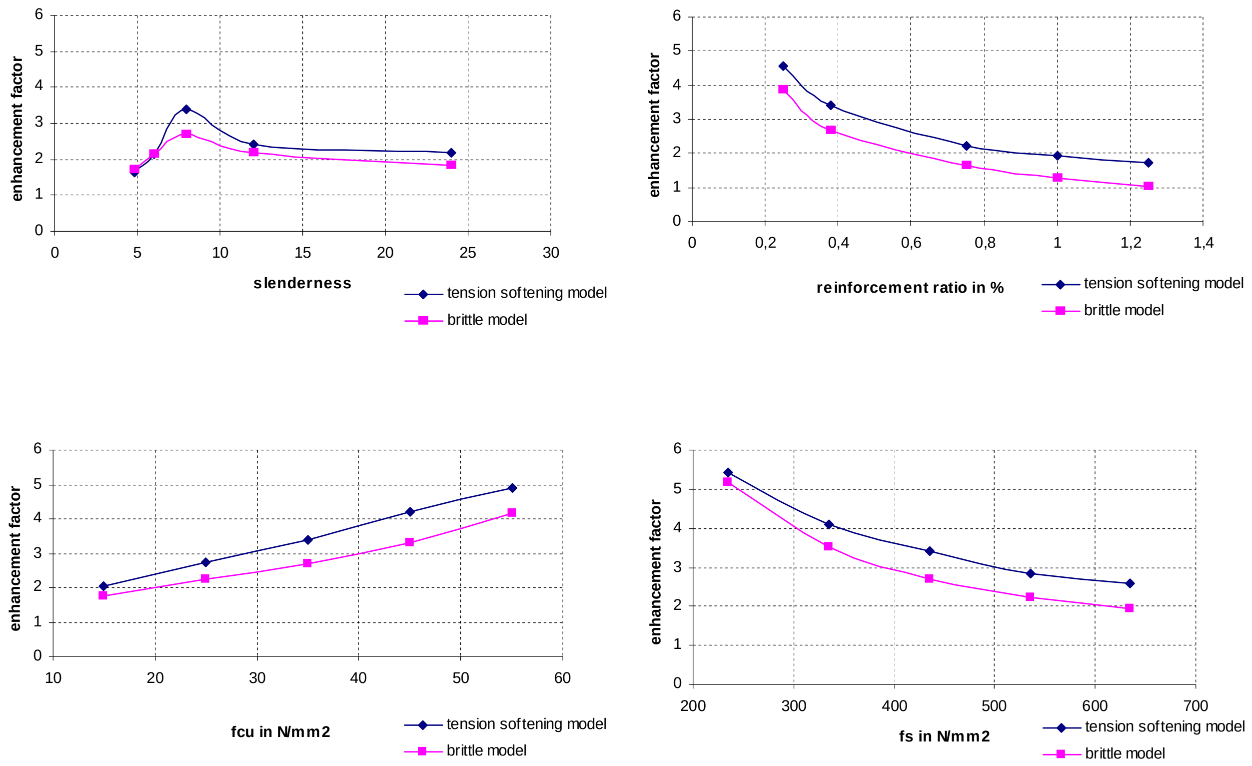

Figure 6.8: Enhancement factors according to the finite element model

In all cases the brittle material behaviour gives slightly less enhancement factor then the model with tension softening, as was to be expected. For low slenderness, the load capacity gets so high that the value of τ_2 gets exceeded. This means that the slab is failing in the line of pressure thrust, which means it fails at a lower load than it would in pure bending. Therefore the enhancement factor predicted by the theory of chapter 2.1 is not reached for small values of the slenderness. All other values are in good comparison with the presented theory.

6.1.4. Conclusions

Thus far the following conclusions can be drawn:

- with a simple non-linear finite element calculation it can be shown that the ultimate load of a horizontal restrained one-way slab is much higher than the analytical virtual work solution
- the theory presented by Park gives a better estimation of the ultimate load than the virtual work theory, and it is a safe approximation
- even slabs without flexural reinforcement have more capacity then is shown analytically
- due to introduction of normal compressive forces, the shear capacity is improved greatly
- even structures with a high slenderness the enhancement is noticeable
- for high reinforcement ratios and low slenderness, shear failure might become governing
- the presented model is only useable for totally horizontal restrained slabs, for partly restrained slabs, see the next paragraph

6.2. Partly horizontal restrained model

In reality a horizontal restrained edge is, in most cases not totally, but only partly restrained so the model will be extended to the model as shown below.

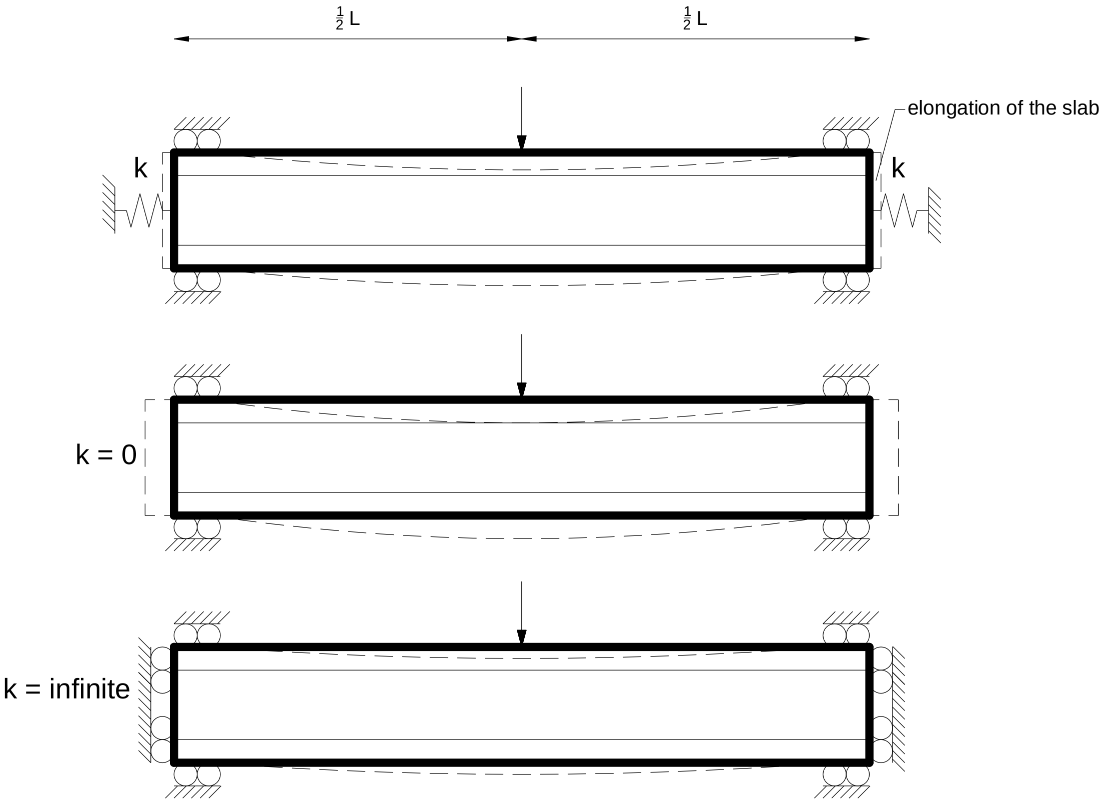

Figure 6.9: Schematic overview of a slab, which is partly horizontal restrained

To convert the schematic of Figure 6.9 to a finite element model, there need to be added springs on the left side so that it can translate. Since rotation is not a degree of freedom for 2D plane stress elements, a beam element is introduced, which is very stiff and is prevented from rotating at the edges, see Figure 6.10.

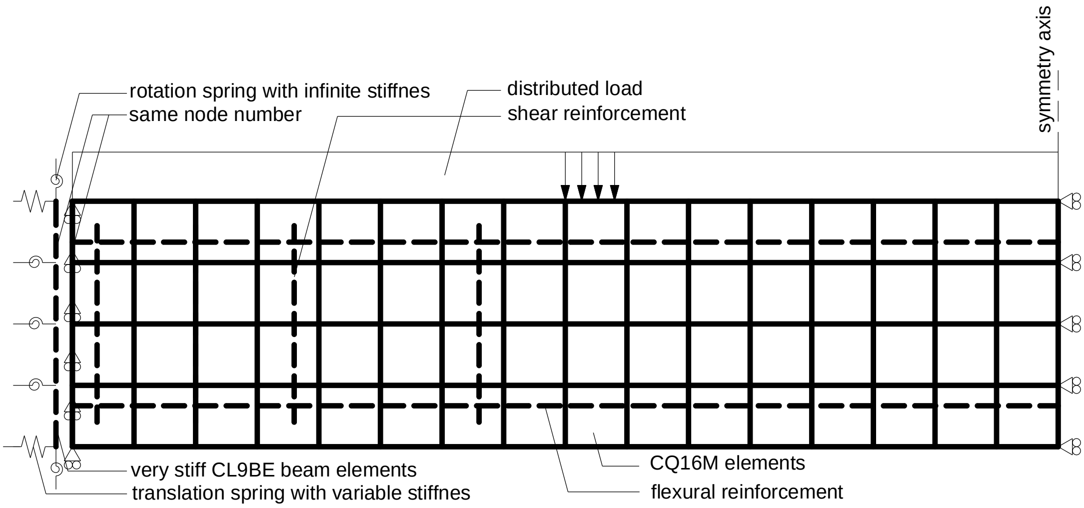

Figure 6.10: Schematic input for the finite element model

For the beam elements, the L7BEN element can not be used since this is element has only two nodes and a linear shape function. A quadratic beam element with three nodes is needed to get the right connectivity. This is explained in Figure 6.11.

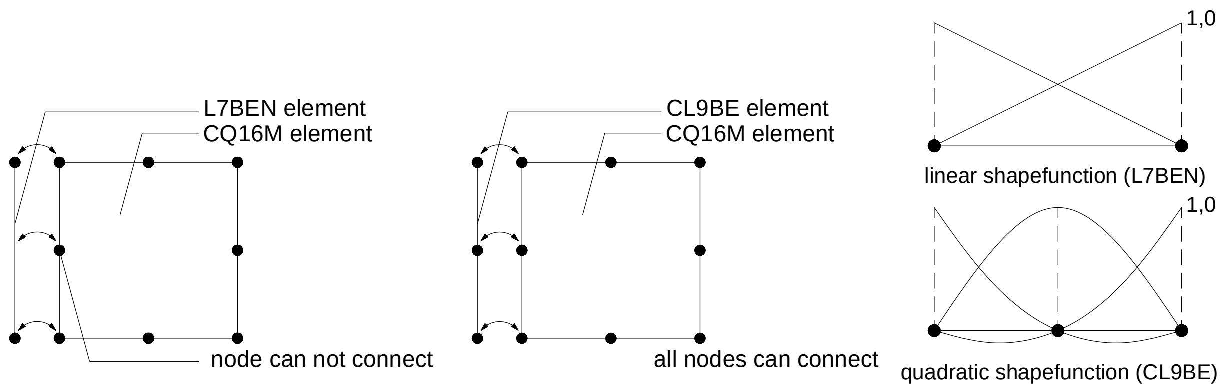

Figure 6.11: L7BEN elements can not be used

In Figure 6.12 the variation in spring stiffness is plotted against the ultimate load, for both the theory of Park and the finite element model. In the finite element model shear reinforcement is included, so that bending failure will be governing.

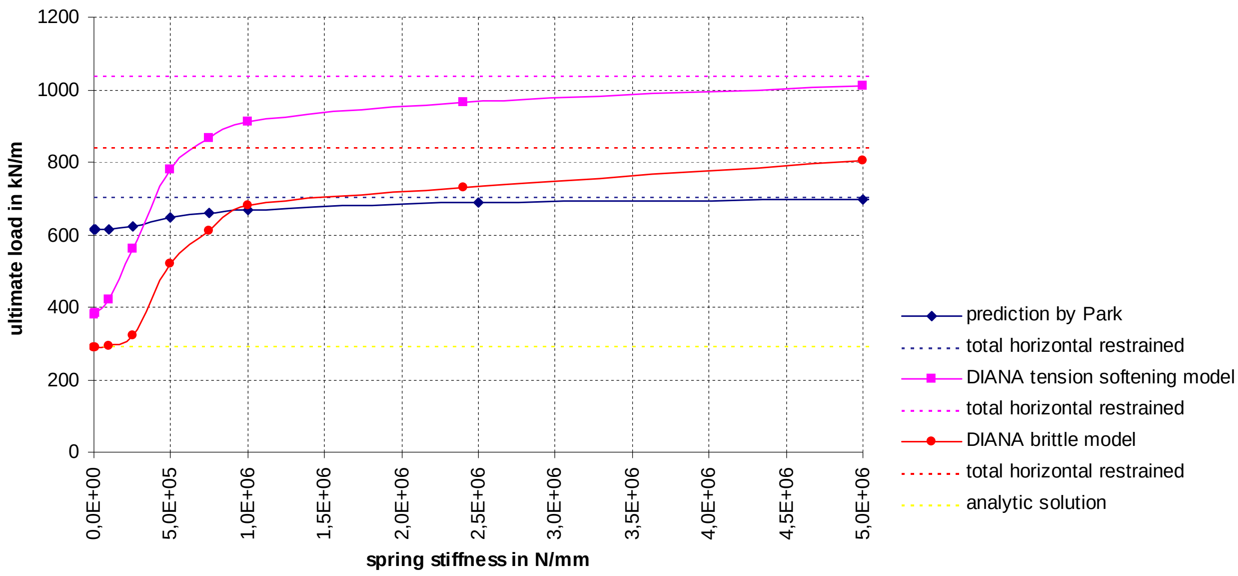

Figure 6.12: Ultimate load for different spring stiffnesses and models

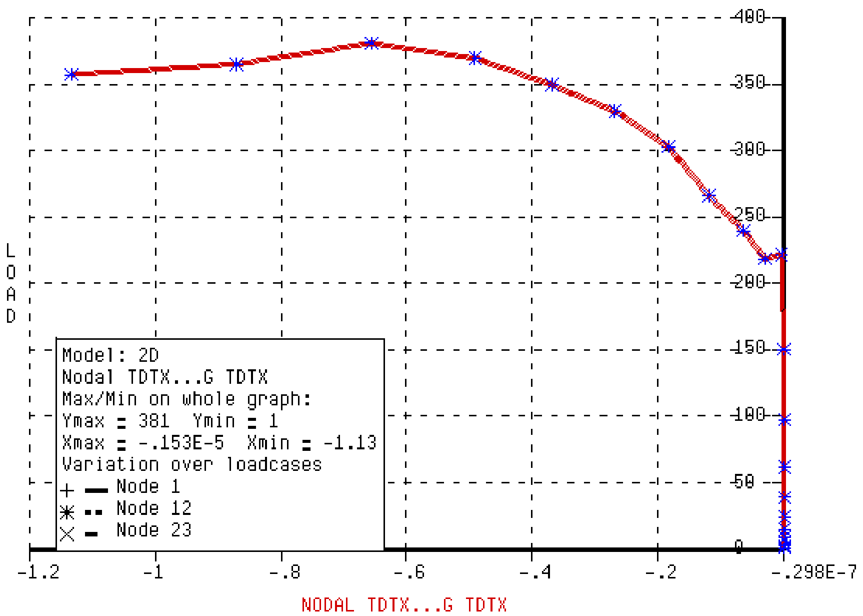

Figure 6.13: Horizontal displacement of a horizontal unrestrained edge

In Figure 6.13 it can be seen that the restrained edge does not move horizontally until cracking load of the slab is reached. This is in accordance with the theory, which states that compressive membrane forces will be generated after cracking of the concrete.

The normal compressive force that is generated can be calculated by multiplying the maximum horizontal displacement of the edge of the slab by the spring stiffness, which is a known parameter since it needs to be inputted in the finite element model. These values are shown in Figure 6.14 and Figure 6.15.

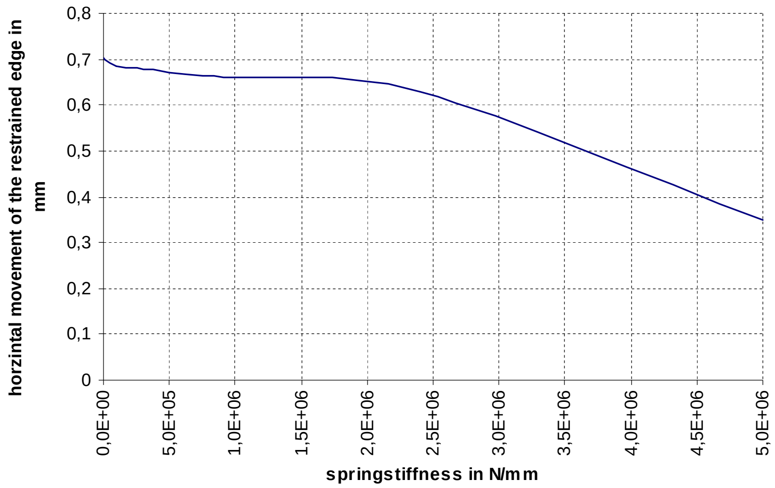

Figure 6.14: Maximum horizontal displacement of the edge

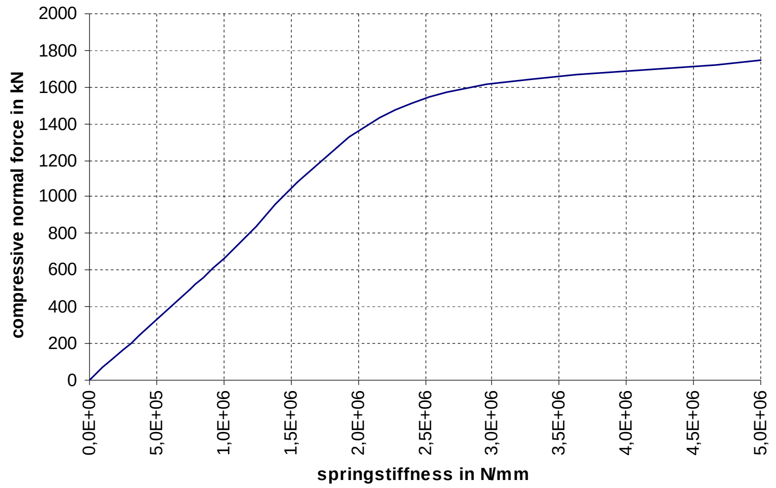

Figure 6.15: Compressive normal force in the slab

Now that the restraining edge forced can be calculated, it will be checked if this force is bigger for unreinforced slabs, as was suggested by evaluating Figure 6.7.

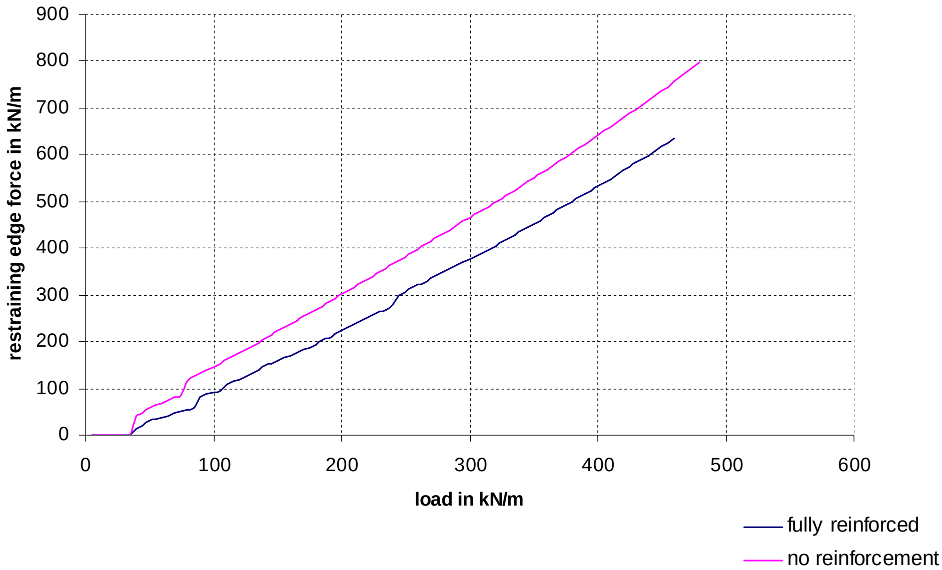

Figure 6.16: restraining edge force for a reinforced and unreinforced slab

The graph starts with a horizontal part with a value of zero. In this part the concrete is not cracked yet and the edge does not move laterally. Then, after the cracking load is reached the restraining force starts to develop. The unreinforced slab has indeed a large restraining force for the same loading as the reinforced slab.

6.3. Comparison with test results

The results as in chapter 4.1.1 will be used. See Table 4.1 for an overview.

In Table 6.1 the finite element calculations are compared to experimental and the predicted results. This is performed for a model with brittle cracking and a model that takes into account tension softening.
If the three slabs with the highest deviations (slab 1, 8 and 12) are excluded from the calculation of the mean value and standard deviation, the test results correspond very well with the finite element models. Even when these experimental results are included, the results lie in between an acceptable range.

Slab	Pe	Pp	Pfem,ts	Pfem,brit	Pfem,ts/Pp	Pfem,brit/Pp	Pfem,ts/Pe	Pfem,brit/Pe
	kN/m	kN/m		kN/m	-			-
1	328,1	242,3	288	232	1,19	0,96	0,88	0,71
2	218,7	236,3	282	227	1,19	0,96	1,29	1,04
3	302,8	274,1	356	320	1,30	1,17	1,18	1,06
4	298,6	264,7	348	309	1,31	1,17	1,17	1,03
4A	290,2	261,2	343	305	1,31	1,17	1,18	1,05
4B	323,9	262,7	345	309	1,31	1,18	1,07	0,95
5	412,2	315,5	414	380	1,31	1,20	1,00	0,92
6	382,7	310,4	401	376	1,29	1,21	1,05	0,98
7	134,6	117,9	184,0	140	1,56	1,19	1,37	1,04
8	96,7	117,3	182,0	132	1,55	1,13	1,88	1,36
9	168,3	137,9	215	186	1,56	1,35	1,28	1,11
9A	172,4	137,8	215	184	1,56	1,34	1,25	1,07
10	-	137,5	214	178	1,56	1,29	-	-
10A	-	137,3	214	173	1,56	1,26	-	-
11	193,5	152,9	236	193	1,54	1,26	1,22	1,00
12	92,5	153,5	234	188	1,52	1,22	2,53	2,03
				Mean value	1,42	1,19	1,31	1,10
				Standard deviation	0,15	0,11	0,42	0,30
						Mean value, slab 1, 8 & 12 excluded	1,19	1,02
						Standard deviation, slab 1, 8 & 12 excluded	0,11	0,05

Table 6.1: Finite element calculations compared to experimental- and predicted results

Figure 6.17 and Figure 6.18 show the finite element results of a brittle cracking model and the experimental results.

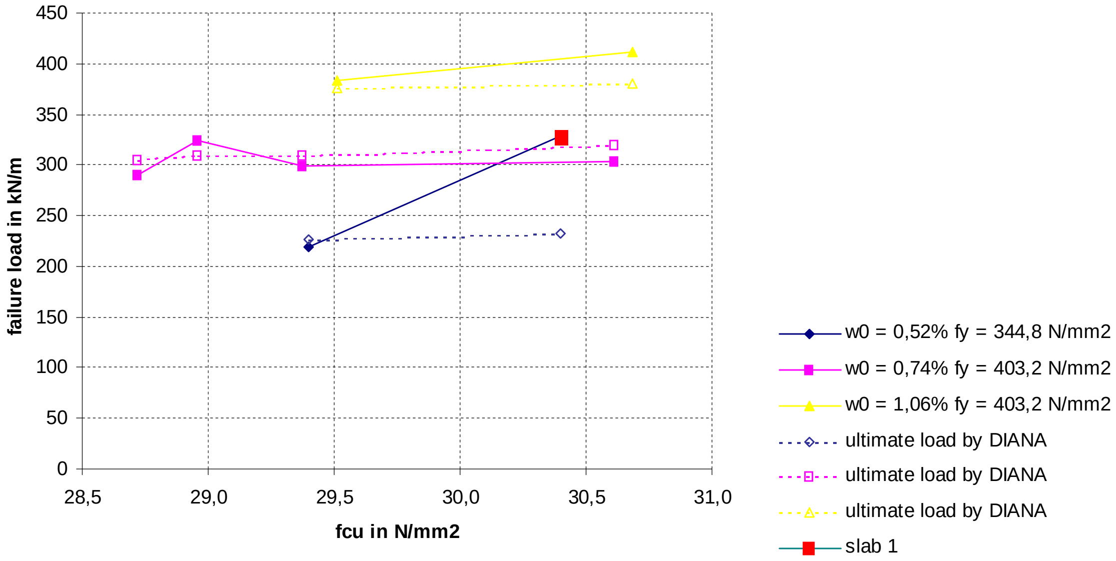

Figure 6.17: Test results versus finite element (brittle model) calculations for the thick slabs of 58,7 mm

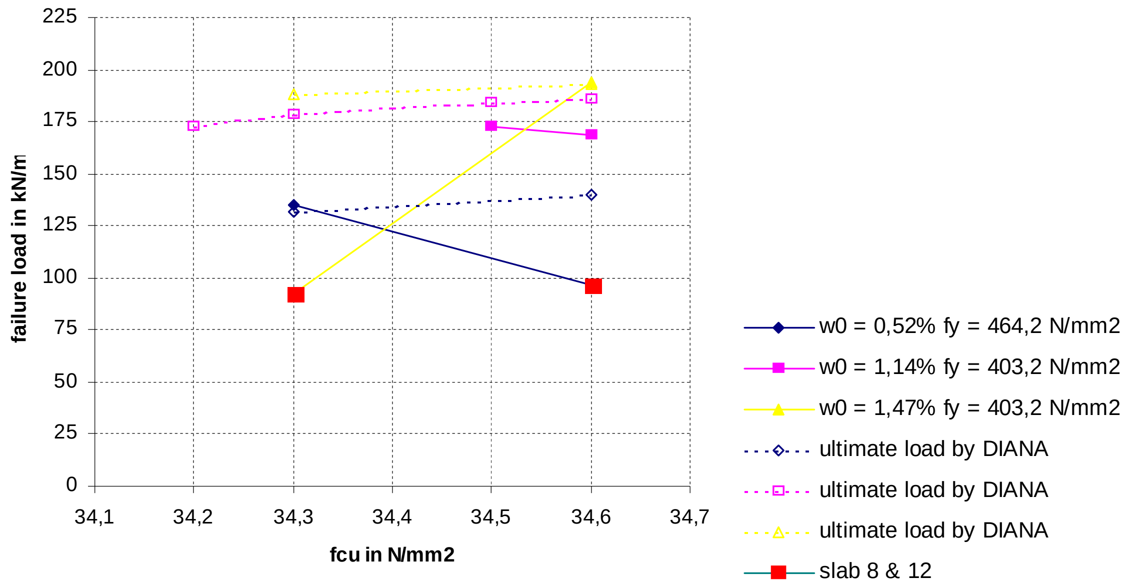

Figure 6.18: Test results versus finite element (brittle model) calculations for the thin slabs of 41,2 mm

6.4. Brittle versus tension softening cracking model

To get a better view of the difference between the tension softening and the brittle cracking model, the factor $\frac{P_{fem}}{P_e}$ of test results is plotted in Table 6.1. It can be clearly seen that the calculations with a brittle cracking model lies in between upper and lower 15% boundaries. Further more it can be seen that the model that includes tension softening gives results that are around 20% to high.

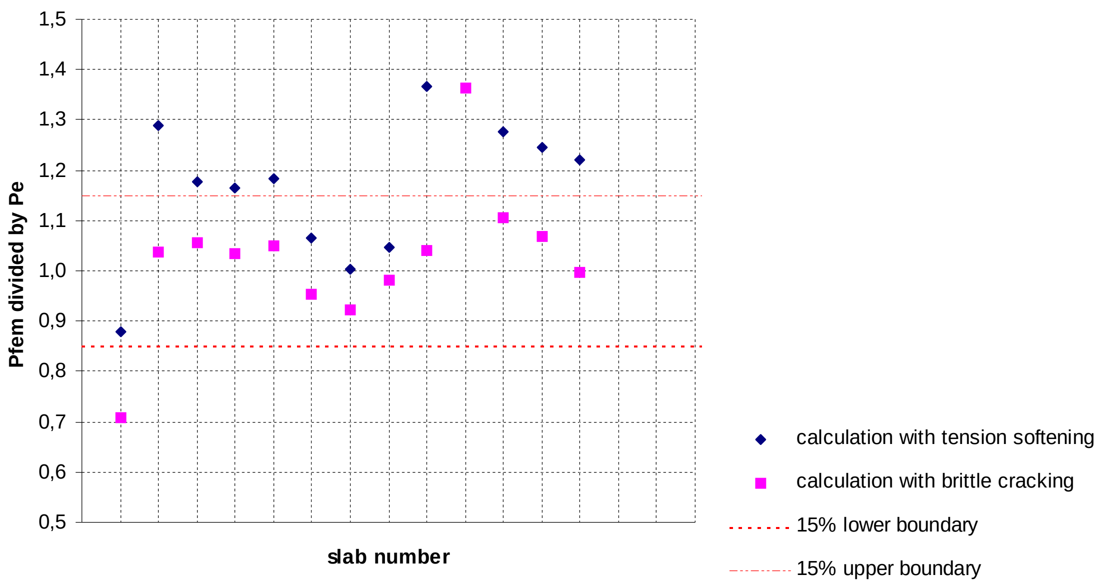

Figure 6.19: The brittle versus the tension softening model

Looking at Figure 6.12 some things can be noticed. The analytical solution is determined without the use of tension softening. This corresponds very well with the brittle finite element calculation without any spring stiffness. The finite element model with tension softening gives a higher ultimate load of approximately 30% for an unrestrained edge. For a totally horizontal restrained edge the following factors can be determined:

$$\frac{q_{fem,brittle}}{q_{bendingtheory}} = 1{,}19$$

$$\frac{q_{fem,tensionsoftening}}{q_{bendingtheory}} = 1{,}47$$

$$\frac{q_{\exp erimets}}{q_{bendingtheory}} = 1{,}12$$

The last factor is the mean value from the test data as shown in Table 4.1. Comparing those three factors and the finite element calculations of the experimental results, it seems that the brittle finite element model will give a better approximation of the collapse load then the finite element model that includes tension softening.

The difference in ductility between the brittle and tension softening model is very large. Including tension softening makes the behaviour of the material much more ductile. This can be clearly seen in Figure 6.3, Figure 6.6 and Figure 6.7.

Another difference between the brittle and the tension softening is the calculation time. The brittle material model needs more iterations to reach its convergence criterion in each step. This increases the calculation time considerably. For this 2D plane stress model it is not much of an influence, the calculation time stays within reasonable limits. For a fully 3D solids model however this will be something to keep in mind.

.

7. FINITE ELEMENT MODEL FOR PUNCHING FAILURE

A punch cone can only occur in a 3D or an axi symmetric model (the latter is discussed in chapter 7.2). The 2D plane stress model used in chapter 6 is thus not suitable for punching analysis. First, the 3D solid model, as presented in chapter 5.1.4 will be evaluated.

7.1. 3D solids model

The model that will be evaluated is shown in Figure 7.1. The dimensions are chosen equal to the 2D plane stress model.

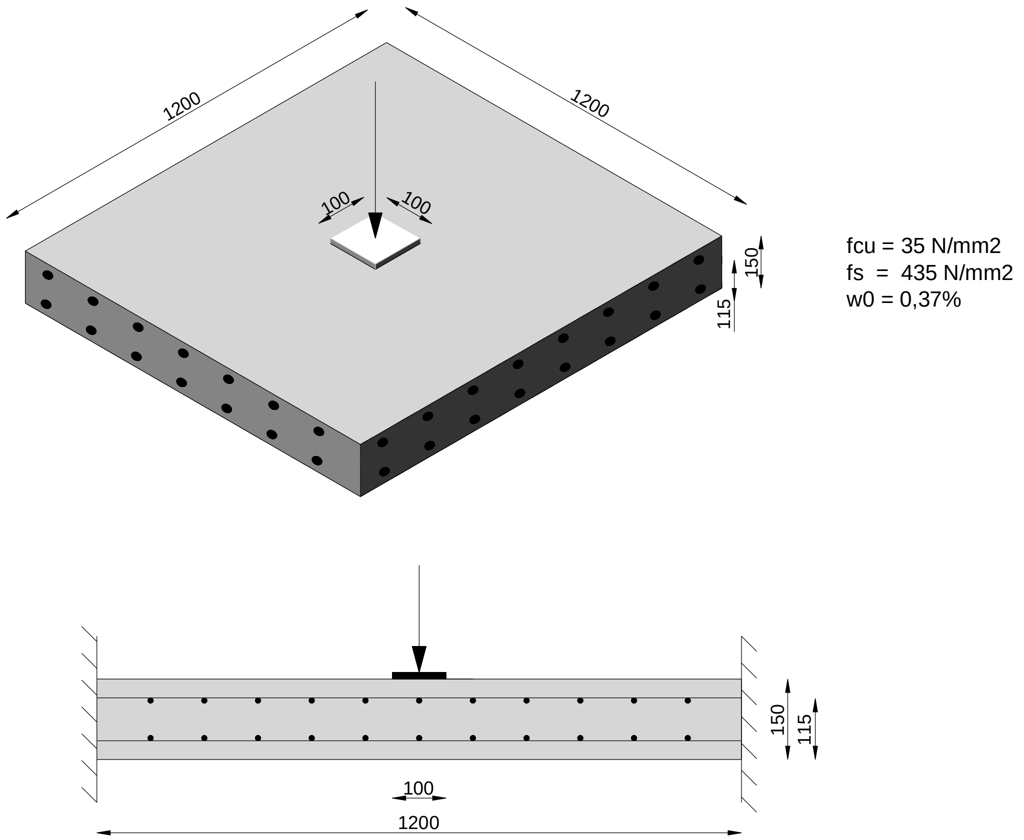

Figure 7.1: Dimensions of the 3D solid model, all the edges are clamped and totally horizontal restrained

The analytic solution for this plate is the lowest value of the maximum bending or punching load.

$$A_s = w_0 bd = 510{,}6 mm^2$$

$$n_s = \frac{A_s f_s}{b} = 185{,}1 \frac{N}{mm}$$

$$m_u = n_s z = n_s \left(d - 0{,}39 \frac{4 A_s f_s}{3 f'_c b} \right) = 20438{,}1 \frac{Nmm}{mm}$$

See chapter 3.1.1.

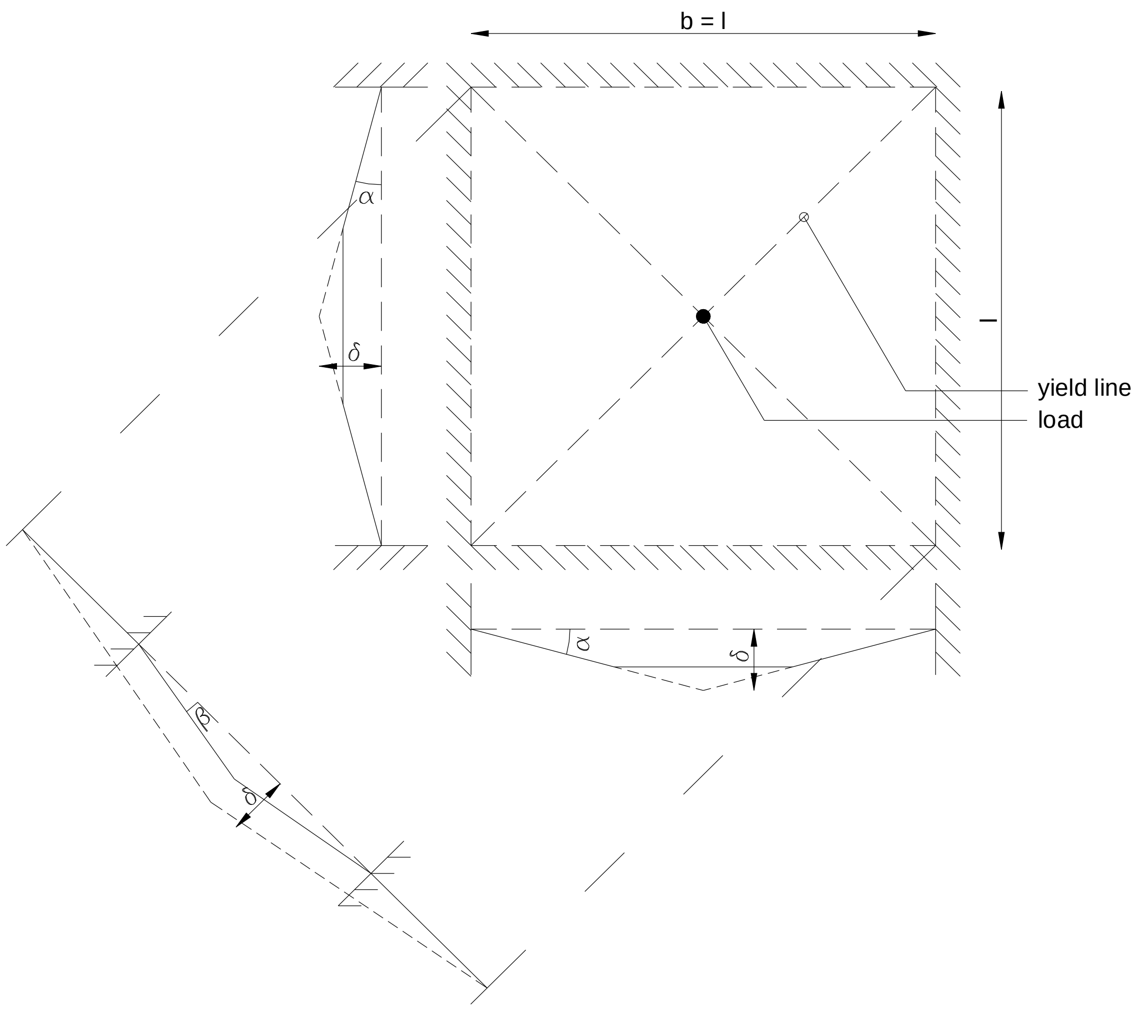

Figure 7.2: Yield lines in a clamped square slab

The ultimate bending load is determined with the virtual work theory, as presented in a reader [7.1]. To do the calculation, a few simplifications are made:

- the load is located in one point, and not distributed over the give area
- the ultimate moment of the slab is the same in all directions

$$W_{external} = F\delta$$

$$\alpha = \frac{2\delta}{b}$$

$$\beta = \frac{2\delta}{\sqrt{2b^2}}$$

$$W_{internal} = \alpha(4b)m_u + 2\beta\left(2\sqrt{2b^2}\right)m_u$$

$$W_{external} = W_{internal} \rightarrow F_u = 8m_u + 8m_u = 16m_u$$

$$F_u = 327kN$$

The ultimate punching load is calculated as presented in chapter 3.1.2.

$$f'_c = 1{,}4\frac{N}{mm^2}$$
$$a_1 = 100mm$$
$$a = \frac{4a_1}{\pi} = 127{,}3mm$$
$$k_d = 1{,}5 - 0{,}6d = 1{,}431$$
$$\tau_1 = 0{,}8 f'_c\, k_d \sqrt[3]{w_0} = 1{,}15$$
$$p = \pi(a+d) = 761{,}36mm$$
$$F_u = \tau_1 pd = 100{,}7kN$$

As was to be expected $F_{u,\ punch} < F_{u,\ bending}$, so the punching failure mode is governing. The predicted collapse load including compressive membrane action calculated by the method as described in chapter 2.2 is 161 kN (calculated with maple). An overview of the found values is shown below.

$$F_{analytic} = 100{,}7kN$$
$$F_{predicted} = 161kN \text{ (including compressive membrane action)}$$

In the figures below, the DIANA output of laterally restrained clamped slab is presented. The load is distributed over an area of 100 x 100 mm. Only a quarter of the slab is modelled, since the slab has two symmetry axes. The model will be build up just like the model presented in chapter 5.1.4, but now with boundary conditions of the two supported sides fixed in lateral and z-direction. Both brittle and tension softening models will compared to each other. To check whether DIANA can calculate punch. So four models will be compared to each other:

– brittle material model, all sides simply supported
– brittle material model, all sides clamped
– tension softening material model, all sides simply supported
– tension softening material model, all sides clamped

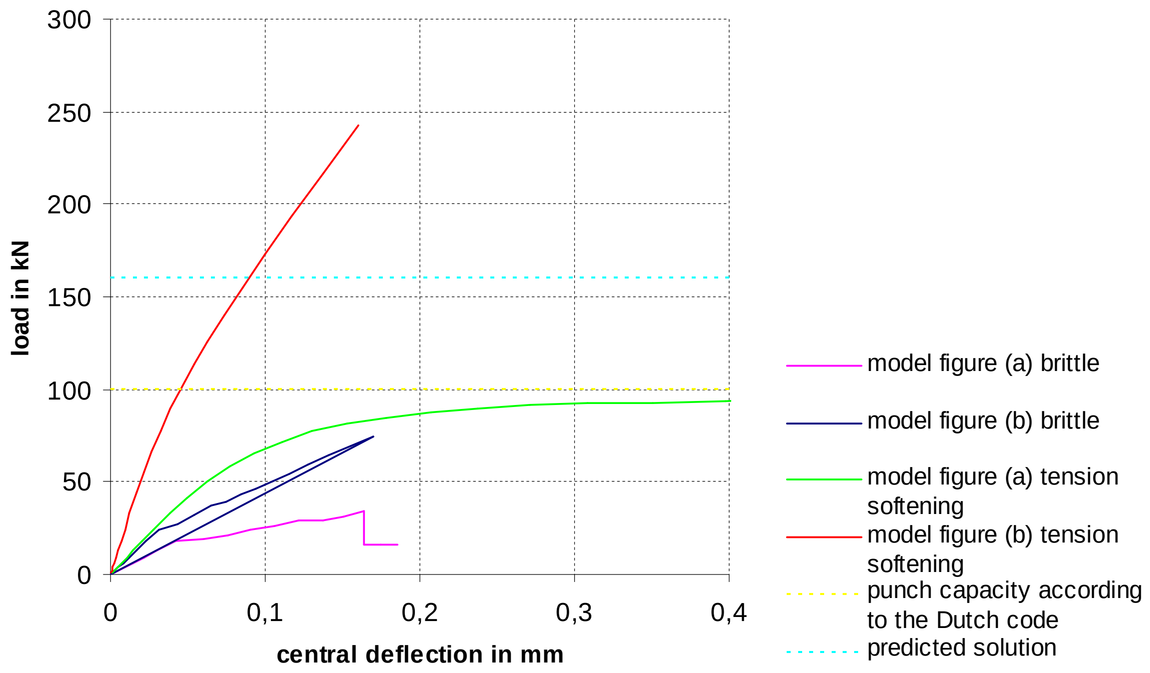

Figure 7.3: The 4 load-displacement graphs of the 3D solids model

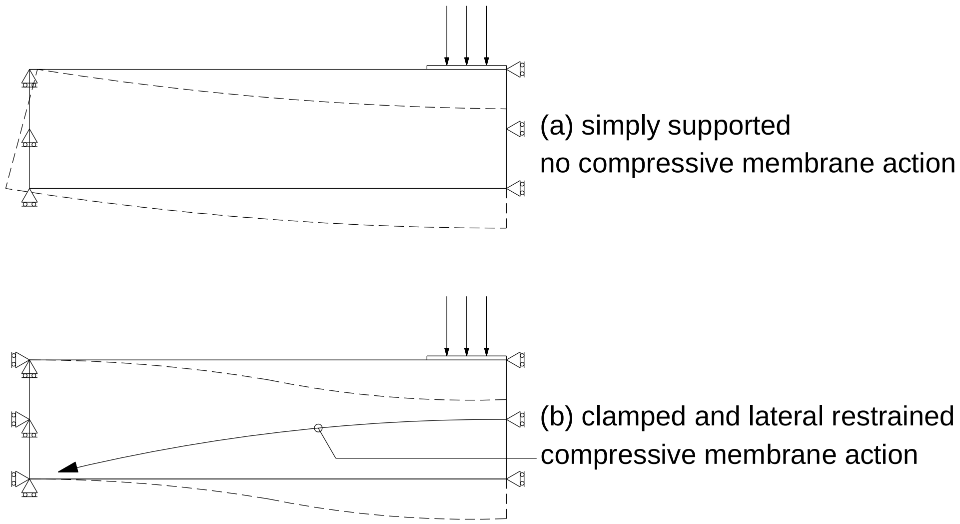

Figure 7.4: Difference between the simply supported and clamped model

As already noticed in chapter 6, there is a big difference in a model with and without tension softening. Furthermore it can be seen that the brittle material models collapse before reaching the punching shear load as calculated according the Dutch code. The clamped model with the tension softening material model comes closest to failure in punching shear. For this model, the load-displacement graph, the displacement fields and the cracking pattern are shown in Figure 7.5 to Figure 7.7. This model seems to give a collapse load that might be too high, as the predicted value was more or less in agreement with experimentally found results, see chapter 4.2.

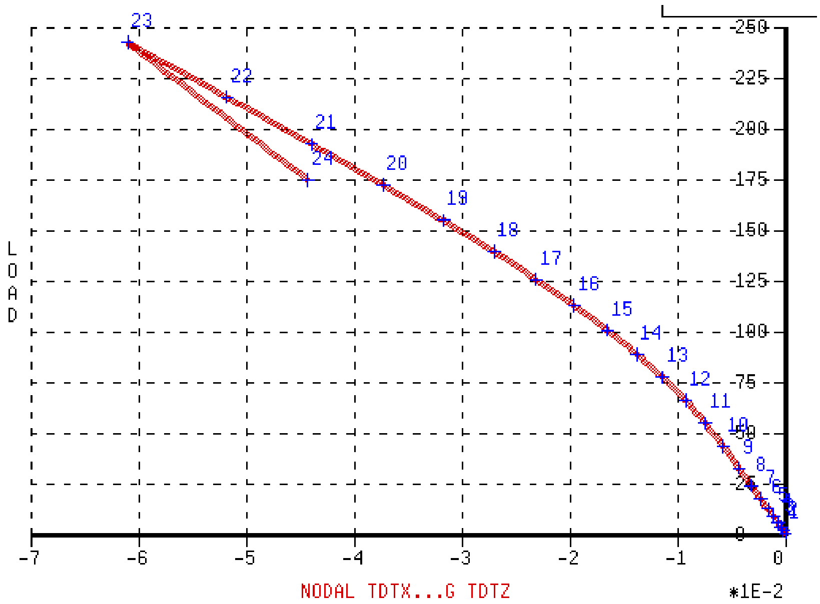

Figure 7.5: Load displacement graph for the 3D solid clamped tension softening model, the model fails between loadstep 23 and 24

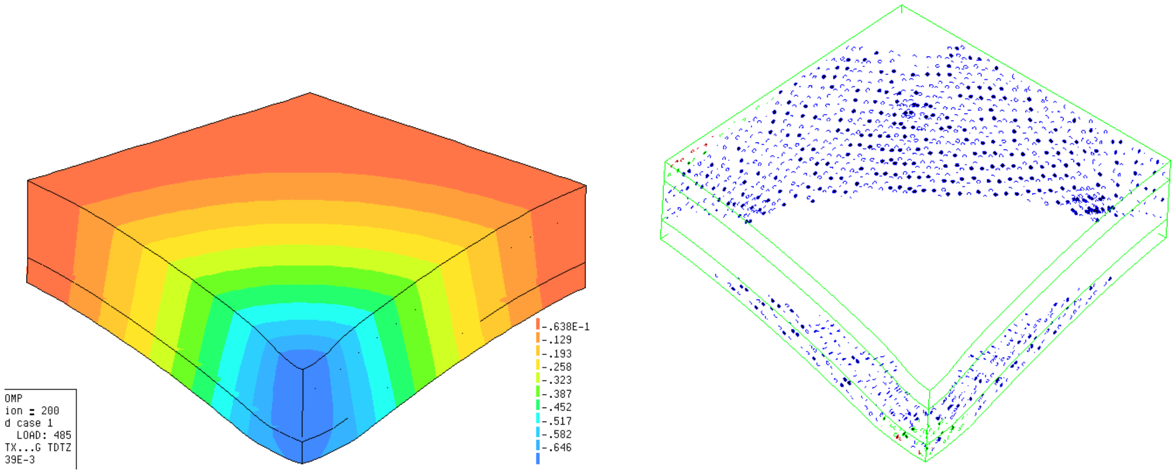

Figure 7.6: Displacement field in Z-direction and cracking pattern of the slab just before failure (loadstep 23)

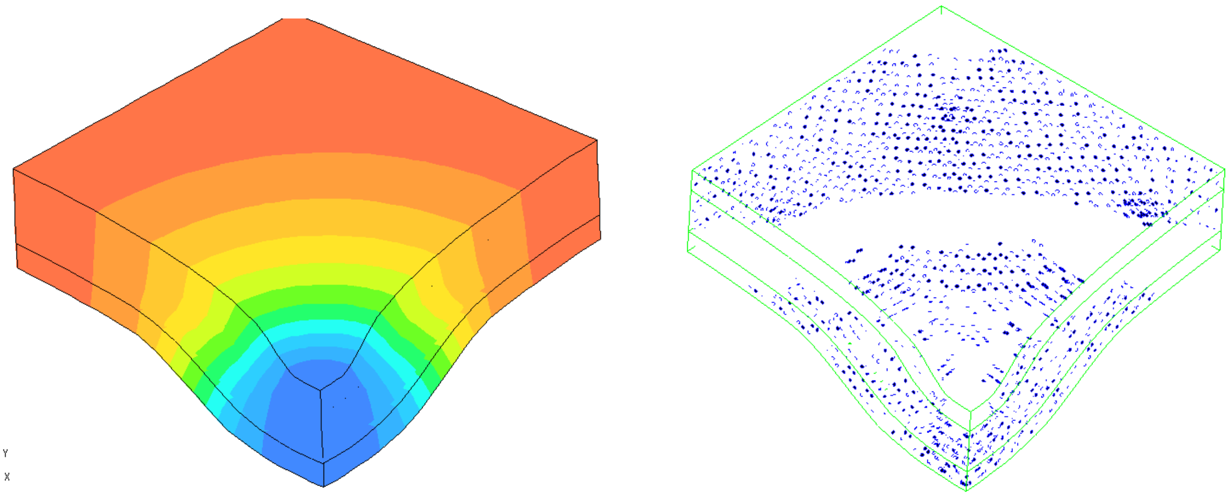

Figure 7.7: Displacement field in Z-direction and cracking pattern of the failed slab (loadstep 24)

The results of the 3D solids model seem not to correspond to the expected values, see Figure 7.3. Varying parameters to see what influence they have is very time consuming, since each calculation takes a long time. To spare time an axi symmetric model will be evaluated. Since punch is the governing failure mode, this model might give good results.

7.2. axi-symmetric model

In this model a 2D slice is modelled in DIANA, and is then rotated 360 degrees around the y-axis. See Figure 7.8. To get a good comparison, the input is the same as the 3D solids model. This model can only be used to model circular shaped structures. This holds also for the loaded area, which is not square, but circular shaped. The diameter of the area is 127,3 mm.

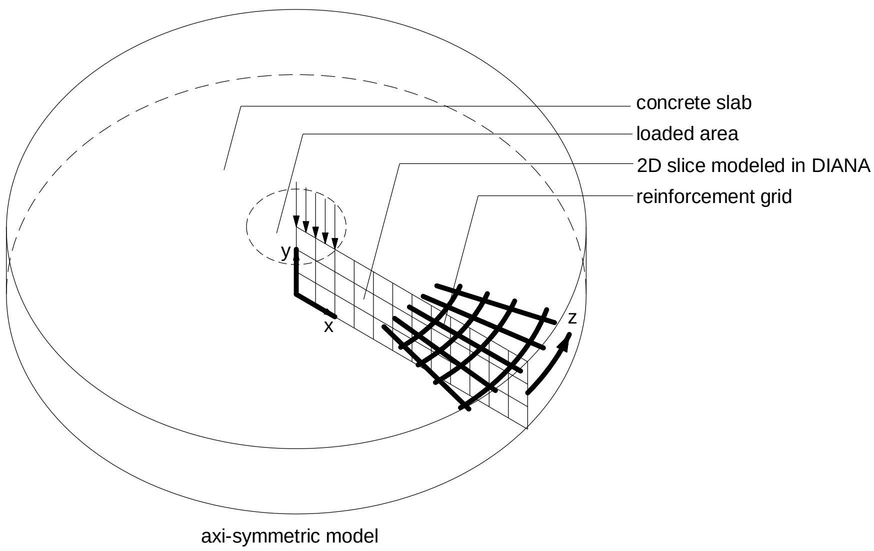

Figure 7.8: axi-symmetric model

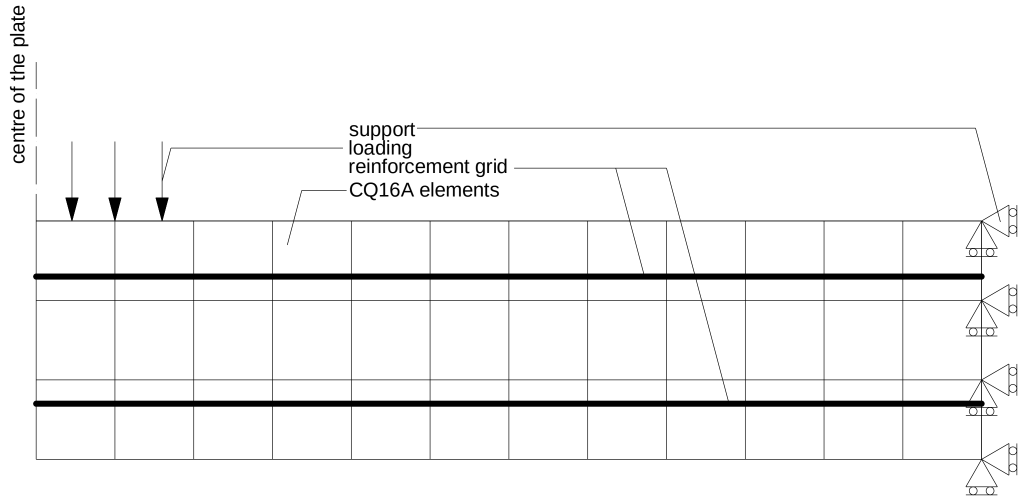

Figure 7.9: Schematic input of the axi-symetric model

This model is again evaluated for the same four cases as the 3D solids model. For the difference between (a) and (b) see Figure 7.4.

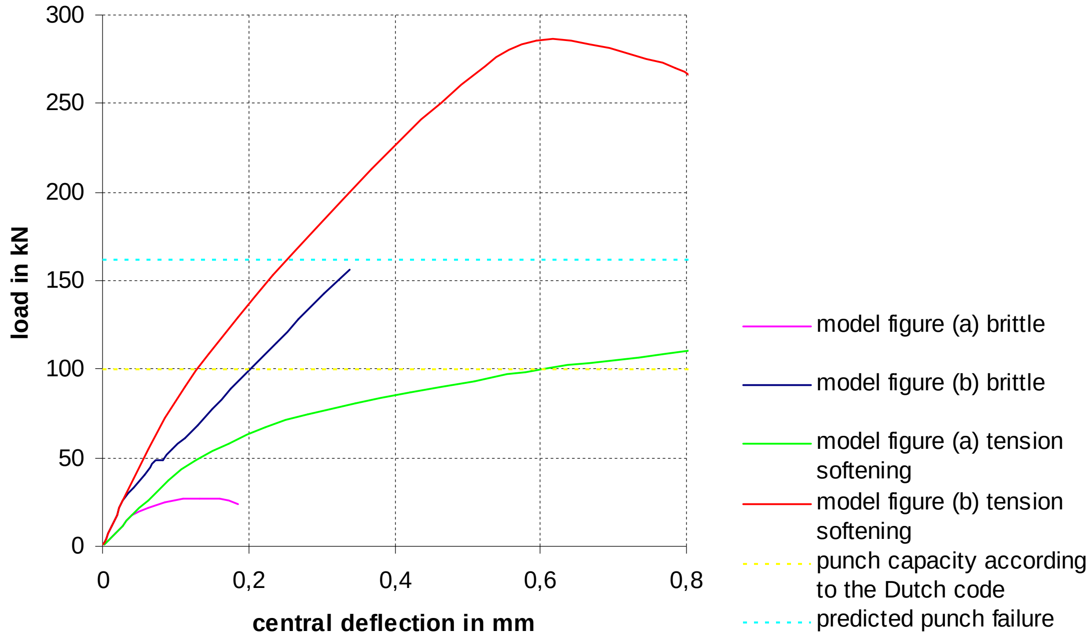

Figure 7.10: Load-displacement graphs for 4 different models of the axi-symmetric model

The difference between the brittle and tension softening material behaviour can be clearly seen again. The tension softening material model is again much more ductile. The simply supported variant with a brittle material model seems to fail in bending, this can be seen because it has a horizontal part in load-displacement graph.
The lateral restrained model with the brittle material behaviour is almost equal to the predicted punching load failure as described in chapter 2.2. To check whether this is a coincidence or that the

models really give the same results, a parameter study is done and the factor $\frac{P_p}{P_{fem}}$ is calculated. The values of the steel ratio and steel strength are not taken into account, since these have little influence on the punching capacity.

d0 mm	Pp kN	Pfem kN	Pa kN	Pfem/Pa -	Pfem/Pp -
50	78,5	76,8	74,2	1,04	0,98
100	161	156	100,7	1,55	0,97
150	228,2	222	127,1	1,75	0,97
200	295,3	281	153,6	1,83	0,95
250	362,5	359	180,1	1,99	0,99
	Mean value			1,63	0,97
	Standard deviation			0,37	0,01

h mm	Pp kN	Pfem kN	Pa kN	Pfem/Pa -	Pp/Pfem -
50	46,3	24,8	24,9	1,00	0,54
100	100,6	92	61	1,51	0,91
150	161	156	100,7	1,55	0,97
200	227,5	222	166,1	1,34	0,98
250	299,4	292	249,2	1,17	0,98
	Mean value			1,31	0,87
	Standard deviation			0,23	0,19

fcu N/mm2	Pp kN	Pfem kN	Pa kN	Pfem/Pa -	Pp/Pfem -
15	49,1	87	63	1,38	0,56
25	102,5	128	85	1,51	0,80
35	161	156	100,7	1,55	1,03
45	222,7	188	115,6	1,63	1,18
55	286,1	223	133,1	1,68	1,28
	Mean value			1,55	0,97
	Standard deviation			0,11	0,29

Table 7.1: The difference between the predicted, analytical and finite element values

Looking at Table 7.1 it can be seen that for the concrete strength f_{cu} = 35 N/mm^2 the predicted value and the finite element value correspond very well. Only for very large slenderness (L/h = 24 in this cases) the results do not match. The punch load according to the Dutch code for this plate with a height of 50 mm is 24,9 kN. This value corresponds very will with the finite element result. This indicates that for a finite element calculation in DIANA, in slabs with a large slenderness no compressive membrane action is generated. The theoretical model presented in chapter 2.2 gives a result that does include compressive membrane action for a large slenderness. The influence of the concrete strength differs. The finite element results show that it has less influence than the predicted solution. To determine which model is more accurate, they have to be compared to experimental results.

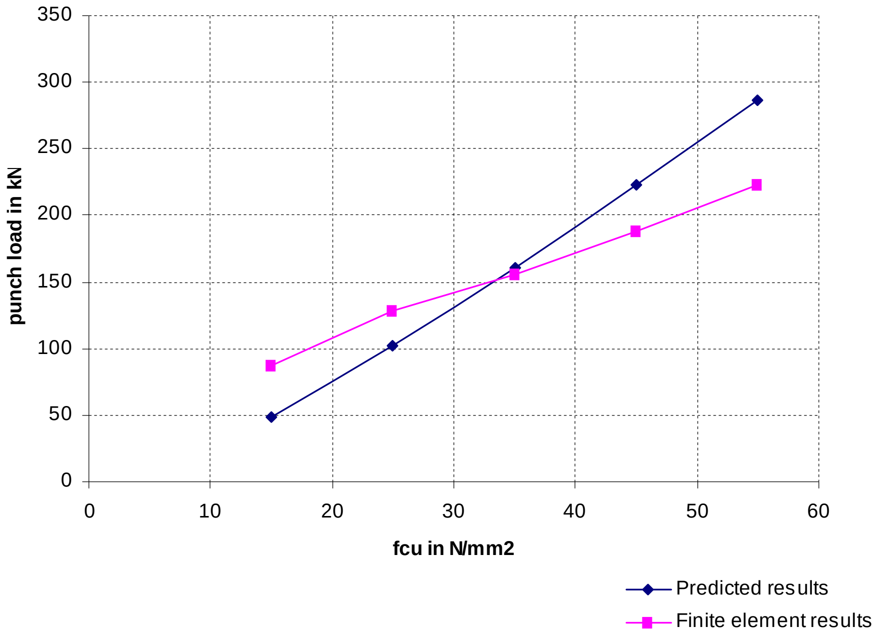

Figure 7.11: Difference between the predicted and finite element value for different concrete strengths

In Figure 7.12 and Figure 7.13 the load-displacement graph and the crack patterns are shown for a axi-symmetric model with a brittle material behaviour. It can be seen that this model is failing in punch.

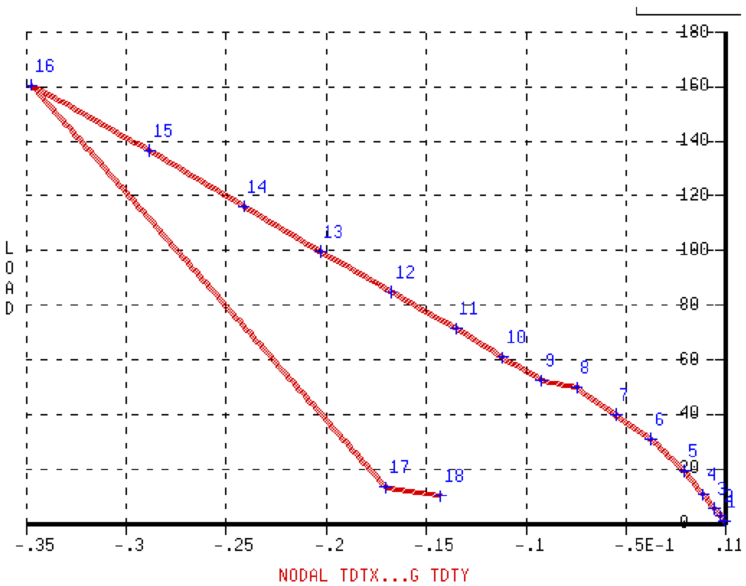

Figure 7.12: Load-displacement graph for the clamped model, with a brittle material behaviour, force controlled

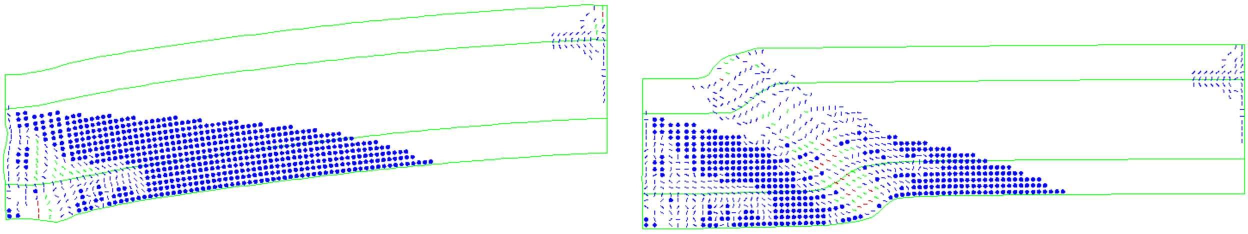

Figure 7.13: Crack pattern just before (loadstep 16) and after (loadstep 17) failure

From now on the axi-symmetric model with a brittle material behaviour will be used. This model is chosen above the 3D solids model based on the following points

- all tests described in chapter 4.2 failed in punch and the axi-symmetric model predicts punch well
- the model is fast and easy to build
- the calculation time is much less than that of a 3D solids model

7.3. Enhancement factors

The enhancement factors for variation in the length of the loaded area, the height of the slab and the concrete strength are shown in Figure 7.14.

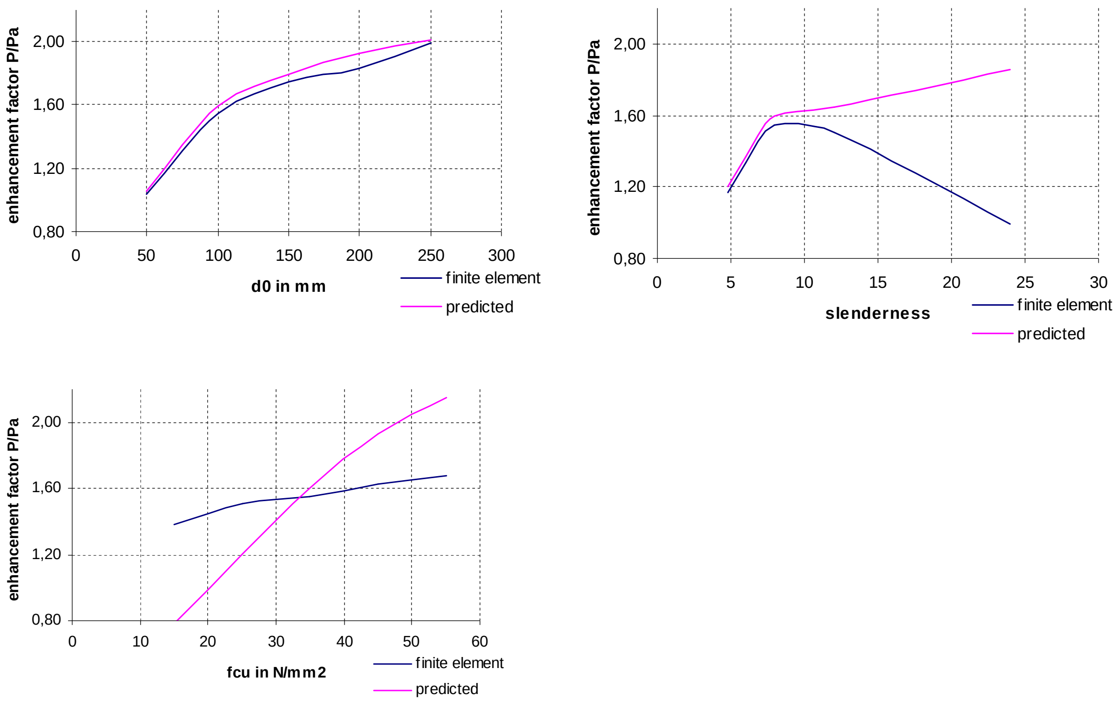

Figure 7.14: Enhancement factor P_{fem}/P_a and P_p/P_a for variation in d0, slenderness and fcu

The theory of chapter 2.2 does not take into account that compressive membrane action is not present in slabs with a high slenderness. This can be concluded from the high enhancement factors given by this theory for a high slenderness. These values are in contradiction with the finite element results.

The reinforcement placement is varied from no reinforcement to reinforcement in tension zones to continuos reinforcement. The un-reinforced slab has a higher collapse load then the slabs that does include reinforcement. A similar result as already been seen for the bending model presented in chapter 6.1.2. The higher punch resistance of the un-reinforced slab might be explained by the fact that the compressive membrane force generated in the un-reinforced slab is higher than that of a reinforced slab, see Figure 6.16. Unfortunately, no experimental data was found that includes different reinforcement layouts, so it can not be verified if these results are right at this moment.

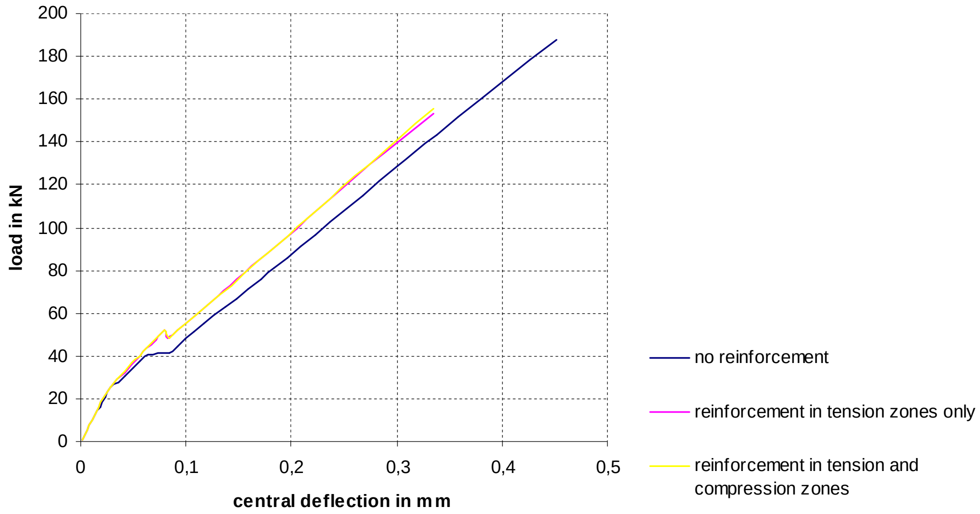

Figure 7.15: ultimate punch load for different reinforcement locations

7.4. Comparison with test results

The experimental results described in chapter 4.2.1 are compared to a finite element calculation. The results are presented in Table 7.2.

Pfem kN	Pfem ts kN	Pe kN	Pp kN	Pfem,ts/Pe -	Pfem,ts/Pp -
46	118	101	104	1,17	1,14
35	97	118	64	0,82	1,52
44	105	149	81	0,70	1,30
25	60	49	63	1,22	0,95
23	63	70	59	0,90	1,08
16	61	68	53	0,90	1,15
46	115	116	95	0,99	1,21
24	65	42	67	1,55	0,97
27	73	69	80	1,06	0,91
46	120	99	96	1,21	1,25
25	62	43	62	1,44	0,99
28	83	63	81	1,32	1,02
		Mean value		1,11	1,13
		Standard deviation		0,26	0,18

Table 7.2: experimental results presented in chapter 4.2.1 compared to finite element results

The slenderness of the tested slabs are respectively 20 and 30. As already mentioned in chapter 7.2 the used finite element model does not take into account compressive membrane action for these high values of the slenderness. This is not in comparison with the experimental results. Therefore, a second finite element analysis is done, but now with the use of the tension softening model. The result from these analyses seems to be in better accordance with the experimental result.

In Table 7.3 the experimental result presented in chapter 4.2.2 are compared to the finite element results. Since the concrete strength is rather high in these experiments, the brittle material model might give values that might be somewhat lower than the experimental result, see Figure 7.11. Therefor the finite element calculation will also be done with a tension softening material model. The tension softening material model gives results that lie in acceptable range of the experimentally found values.

Pfem kN	Pfem ts kN	Pe kN	Pp kN	Pfem,ts/Pe -	Pfem,ts/Pp -
95	416	369,4	466,7	1,13	0,89
79	372	290,6	367,6	1,28	1,01
85	380	402,2	403,4	0,94	0,94
81	368	394,1	376,6	0,93	0,98
		Mean value		1,07	0,96
		Standard deviation		0,16	0,05

Table 7.3: experimental results presented in chapter 4.2.2 compared to finite element results

The results of the measurements on the bridge decks presented in chapter 4.2.4 are compared to finite element models in Table 7.4.

	measured values			
slab	cracking load kN	deflection at 112,5 kN in mm	deflection at 330 kN in mm	deflection at 430 kN in mm
C1	118	0,35	2,6	-
C2	143	0,25	-	1,2
D1	154	0,4	1,85	-
D2	143	0,25	-	1,75

	finite element results (totally horizontal restrained)			
slab	cracking load kN	deflection at 112,5 kN in mm	deflection at 330 kN in mm	deflection at 430 kN in mm
C1	120	0,175	0,815	-
C2	112	0,08	-	0,5
D1	150	0,12	0,55	-
D2	112	0,08	-	0,5

Table 7.4: experimental results presented in chapter 4.2.4 compared to finite element results

The slabs A1 to B2 included reinforcement in the form of fibres, which can not (yet) be included in the finite element model. The results of the finite element model do not match at all with the experimental found values. However, the goal of this study is to predict the ultimate load of the structures, and not an accurate value for deflections and crack widths.

7.5. Partly horizontal restrained axi-symmetric model

To make the model as described in chapter 7.2 partly horizontal restrained, springs will be added, just like is done for the 2D plane stress model as described in chapter 6.2. However, the use of a stiff edge beam is not a possibility anymore. These stiff beam elements will be rotated over 360 degrees, which creates a shell of revolution. This shell of revolution acts as a stiff ring element which can not deform horizontally freely and is thus not useful. Instead the tying option will be used. With this input, a group of nodes can be tied togheter, so they have the same displacement in a chosen direction. Tying the nodes of the edge together will create the boundary condition that is needed, an edge that can move latterly but does not rotate.

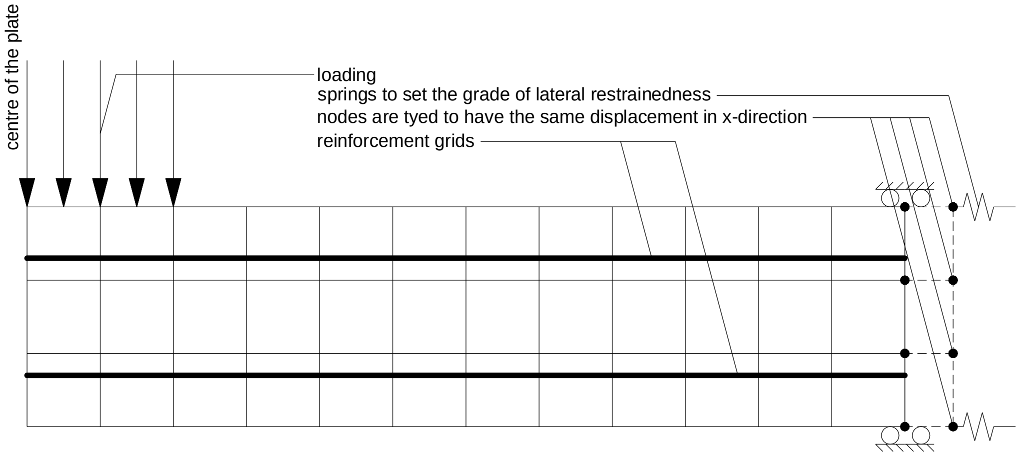

For low spring stiffness the slab is failing in bending, which can be identified in the load displacement curve, which ends in a horizontal part if it fails in bending. Shear or punch failure can be identified by abrupt ending of a rising curve, or by a fallback of the load. For higher spring stiffness the slab fails in punching shear.

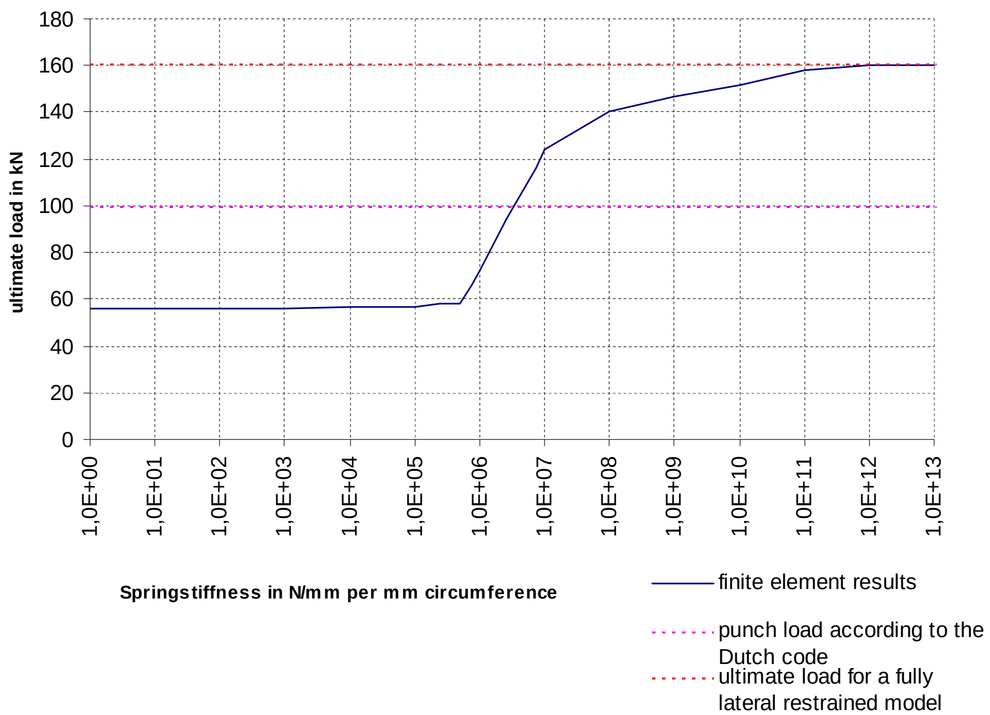

Figure 7.16: Ultimate load of the finite element calculation for different spring stiffnesses

With the spring stiffness per m circumference and the horizontal displacement known, the value for the force generated by the lateral restraint can be calculated by multiplying the horizontal displacement by the spring stiffness.

$$N = u_x.S.$$

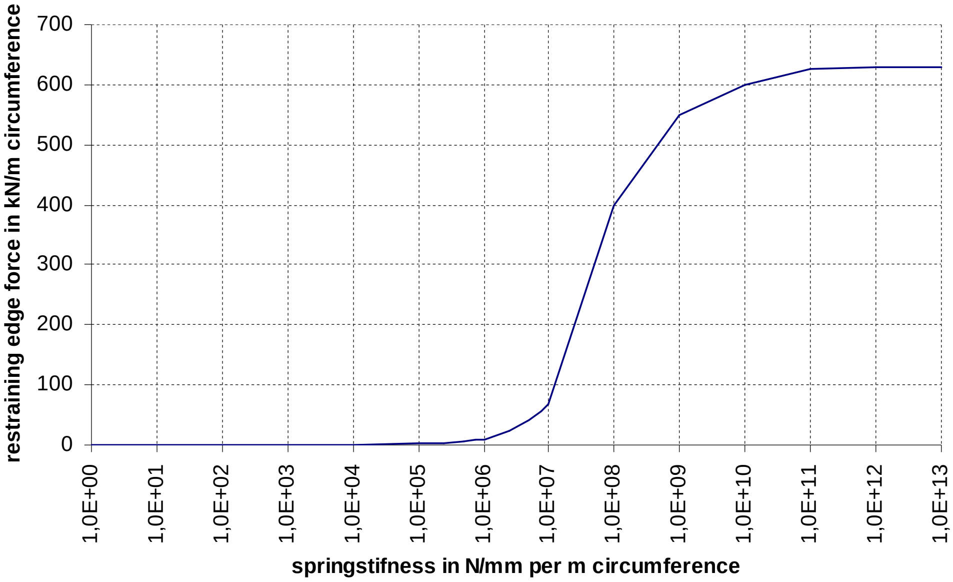

Figure 7.17: Nrs for an increasing spring stiffness

7.5.1. Ontario experimental results

In Ontario some experiments where done on bridge decks, see appendix D. Some small scale experiments where done, at which the membrane forces where measured by the expansion of a steel ring. The test set-up is shown in Figure 7.18.

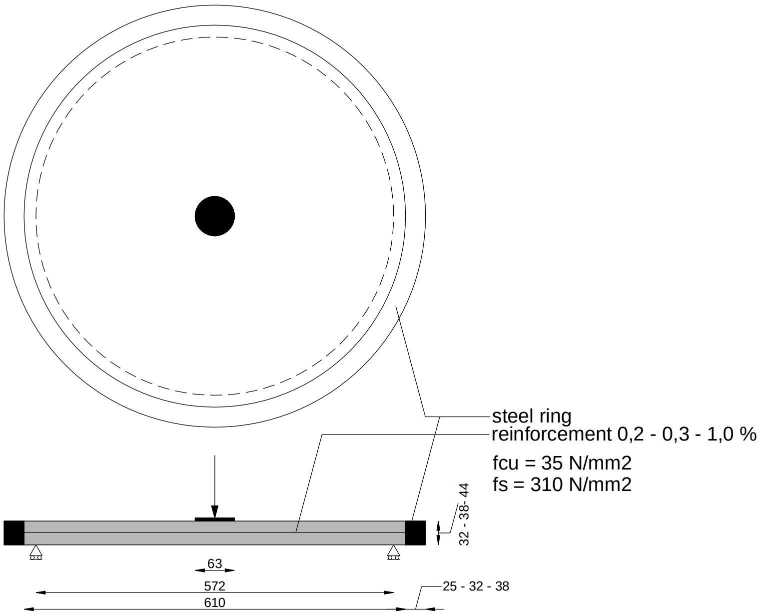

Figure 7.18: test set-up of small-scale test

For the calculation of the spring stiffness the linear relationship between spring and force will be used, F = k.u.

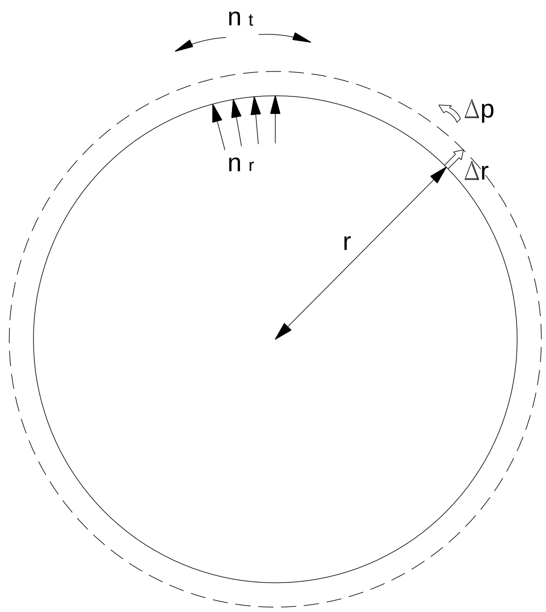

Figure 7.19: deformation in lateral direction before and after loading

In the formula r is the radius and p the perimeter of the slab.

$$p = 2\pi r$$

$$\Delta p = \frac{n_t . p}{E.A}$$

$$n_t = n_r . r$$

$$r + \Delta r = \frac{p + \Delta p}{2\pi}$$

$$\Delta r = \frac{2\pi r + \dfrac{n_r r . 2\pi r}{E.A}}{2\pi} - r = \frac{n_r r^2}{E.A}$$

$$n_r = S.\Delta r$$

$$S = \frac{EA}{r^2} \frac{N / mm^2}{mm\, circumference}$$

For the conversion of radial into tangential stresses, the formula $\sigma = \dfrac{pr}{t}$, in which p is a pressure and not the perimeter, is used[7.2]. For the input in the finite element model the found value has to be multiplied with a factor 1000, since the input is in $\dfrac{N / mm^2}{m\, circumference}$.

A finite element model will be used to calculate the restraining force and will then be compared to the values presented in the Ontario code, see appendix D Figure 18. It is not clear in the Ontario code what dimensions each of the samples have, so for the finite element model, the average of the values presented in Figure 7.18 are used.

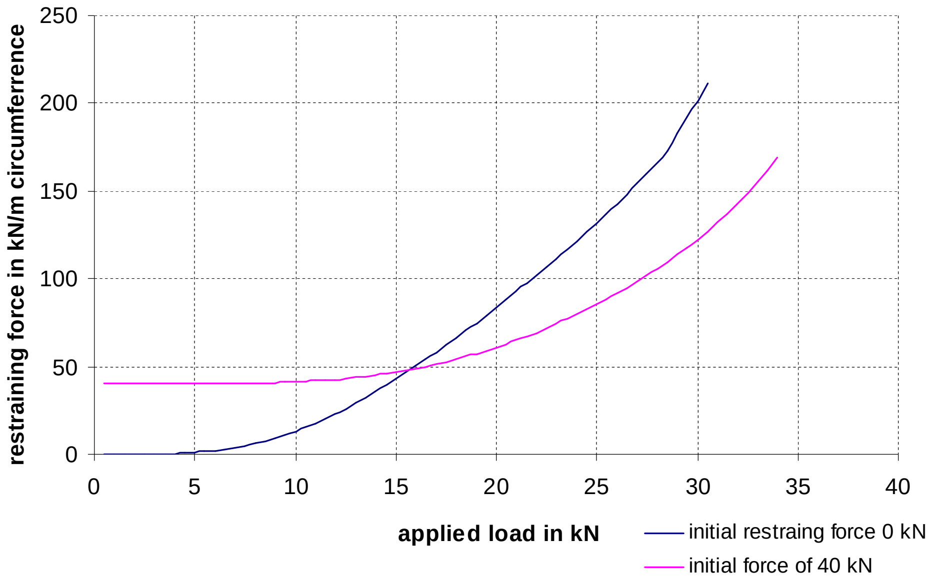

Figure 7.20: restraining force calculated by multiplying the spring stiffness with the lateral displacement

Comparing Figure 7.20 with the one presented in appendix D, a few differences can be noticed.

– the ultimate load of the Ontario specimens is higher than the load found with the finite element model
– the maximum restraining load of both methods is about the same
– the Ontario specimens started with a restraining load for a unload slabs, which might indicate that the steel ring was attached tightly to the specimen, this is not modelled in the finite element model

It is not clear why the graph given in the Ontario report does not show a horizontal part at the beginning. Even when a starting with a compression force on the edge, the cracking load still has to be reached, before the compressive membrane action starts to form.

Part III: A Practical example

8. THE DECK OF A COMMON GIRDER BRIDGE

As an example, a ZIP-girder system will be evaluated, which is a commonly used system in the Netherlands. This system has already been introduced in chapter 1. The system will be designed according to the guidelines of the Dutch company Spanbeton. All information according to dimensions is downloaded from their Internet page [8.1]. The thickness of the compression layer (the concrete slab) is the same for every case, 230 mm. This means the span is not an influence factor for the height of the slab. Chosen is for a ZIP 1200 system.

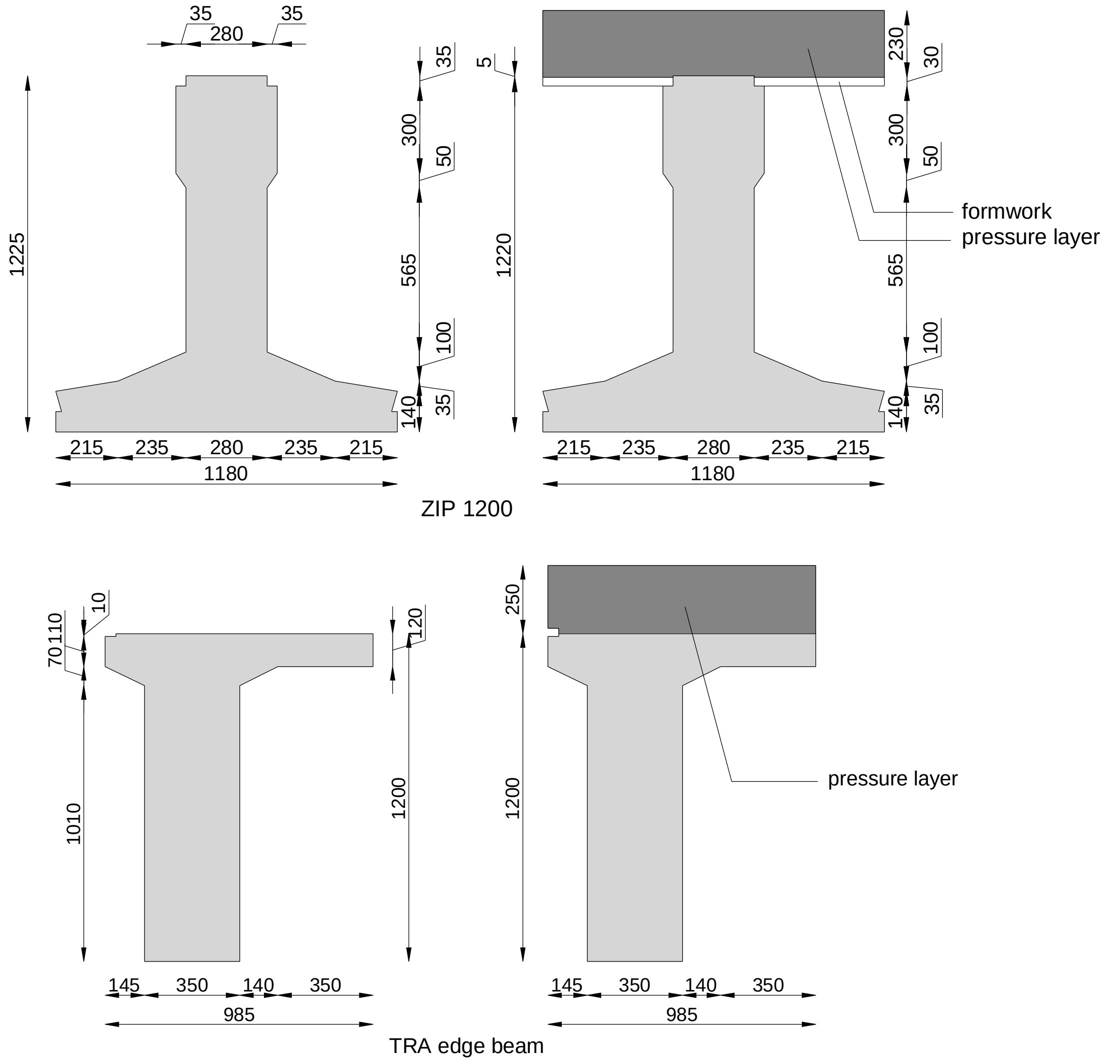

Figure 8.1: Dimension of the ZIP profile and the edge beam

The system has the following quantities:

- the concrete quality of the deck is C28/35
- the top reinforcement is Ø12 – 150 and the bottom reinforcement is Ø16 -100
- the concrete cover is 35 mm (according to the code [5.1])
- the effective height is 187 mm
- the area over which the load is spread is 350 x 600 mm

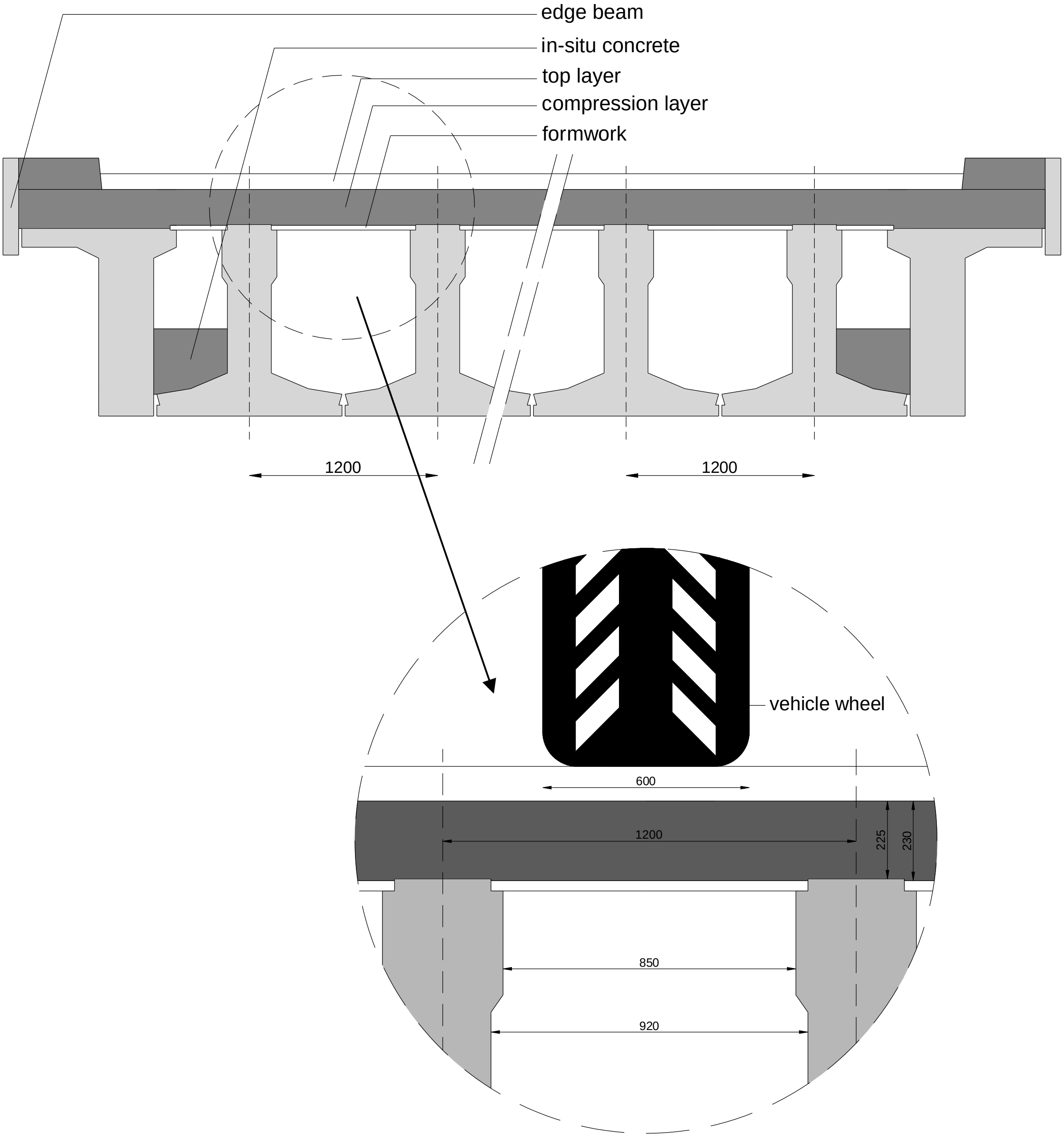

Figure 8.2: Cross-section of the bridge and one span of the compression layer zoomed in to

Since punch failure is governing in the most cases, only load configuration 2 (see Figure 1.2) with the high axle loads will be discussed here.

8.1. Analytical solutions

The ultimate load for both bending and shear will be calculated. Some assumptions that are made for these calculations are:

- the top layer does not contribute to the bearing capacity
- the form work does not contribute to the bearing capacity
- the length of the mechanical system is the distance between the centre lines

8.1.1. Bending

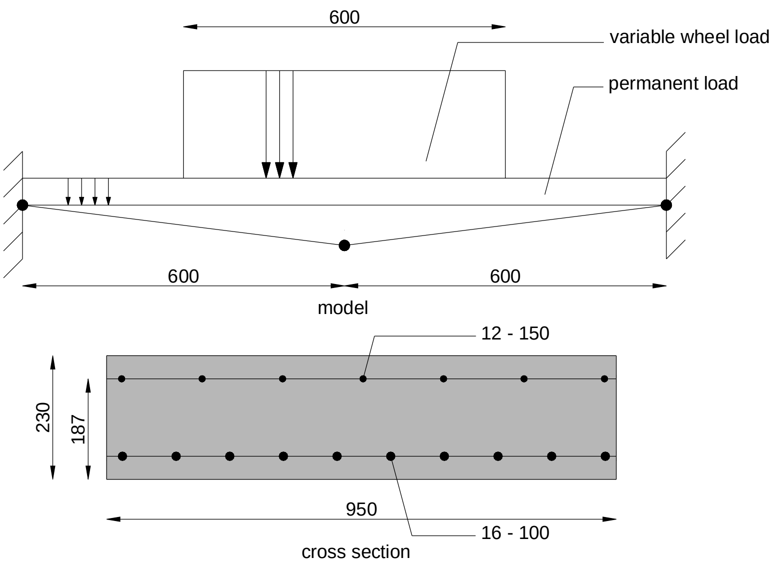

Figure 8.3: Model for the calculation of the bending capacity

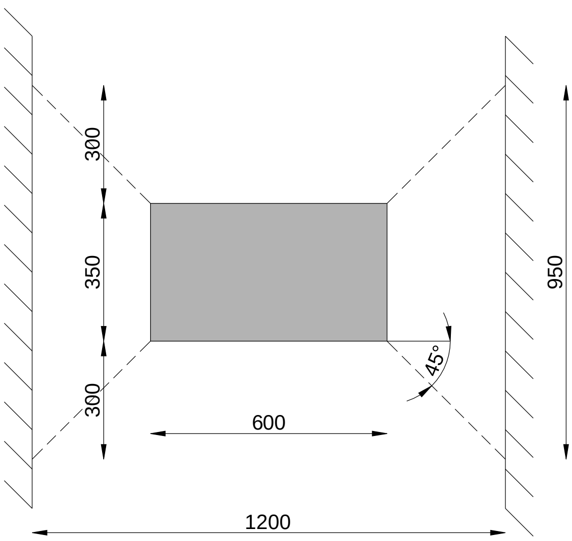

Figure 8.4: Width over which the wheel load has influence

$$A_{s,top} = \frac{950}{150}.\pi.6^2 = 716{,}3mm^2$$

$$A_{s,bottom} = \frac{950}{100}.\pi.8^2 = 1910{,}1mm^2$$

$$M_{u,top} = 716{,}3.435.\left(187 - 0{,}39.\frac{4.716{,}3.435}{3.21.950}\right) = 55{,}7kNm$$

$$M_{u,top} = 1910{,}1.435.\left(187 - 0{,}39.\frac{4.1910{,}1.435}{3.21.950}\right) = 137{,}4kNm$$

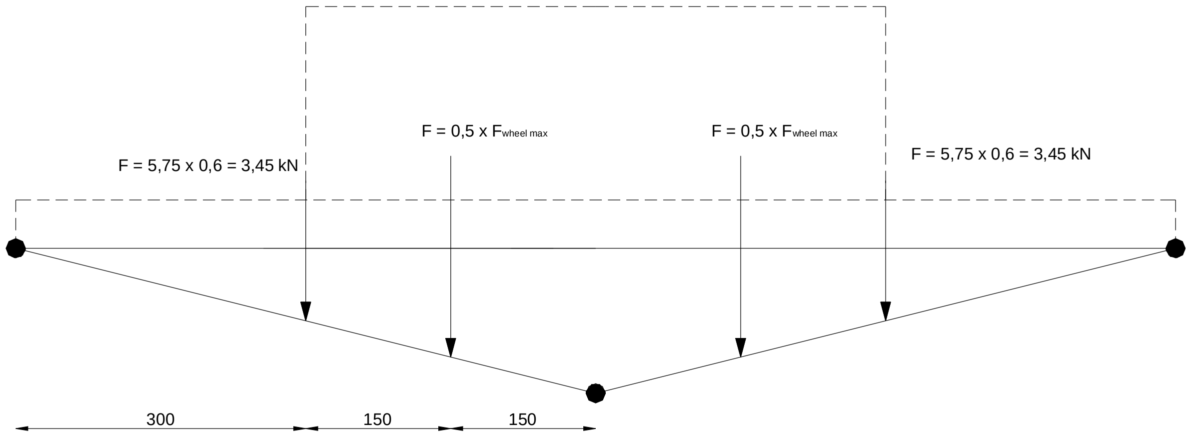

Figure 8.5: load positions to calculate the virtual work

$$W_{extern} = 2.(3{,}45.0{,}3)\theta + 2.(0{,}5F_{wheel,\max}\,0{,}45)\theta$$

$$W_{\text{int}\,ern} = 2M_{u,top}\theta + 2M_{u,,bottom}\theta$$

$$W_{extern} = W_{\text{int}\,ern} \rightarrow F_{wheel,\max} = 853{,}6kN$$

The analytic value is higher than the 200 kN wheel load which is prescribed in the code.

8.1.2. Punch

The l/b ratio of the loaded area is less then 2, which means the slab will fail in pure punch, and not a combination of punch and shear.

$$\varpi_{o,top} = \frac{A_{s,top}}{b.d} = 0{,}40\%$$

$$\varpi_{o,bottom} = \frac{A_{s,top}}{b.d} = 1{,}08\%$$

$$a = \frac{2.(600 + 350)}{\pi} = 604{,}8mm$$

$$p = \pi(604{,}8 + 187) = 2487{,}5mm$$
$$k_d = 1{,}5 - 0{,}6.0{,}187 = 1{,}39$$
$$\tau_1 = 0{,}8.1{,}4.1{,}39.\sqrt[3]{0{,}74} \geq 1{,}4.0{,}8 \rightarrow \tau_1 = 1{,}41$$
$$F_{wheel,\max} = 1{,}41.2487{,}5.187 = 655{,}9kN$$

The slab will fail in punching shear, and not in bending, at least for the analytic solution.

8.2. solutions including compressive membrane action

The example structure will be calculated with the bending and punch theory described in chapter 2 and with an axial symmetric finite element model. The example will be calculated according to the New Zealand code, which takes into account compressive membrane action by using a restrained factor (see appendix E).

8.2.1. Bending

The theory predicts the ultimate distributed load, which is 1436,4 kN/m (calculated with the excel sheet presented in appendix A). To calculate the maximum wheel load, it is assumed tat the maximum bending moment in the middle will be the same for the total distributed load, and the system with the more concentrated wheel load, see Figure 8.6.

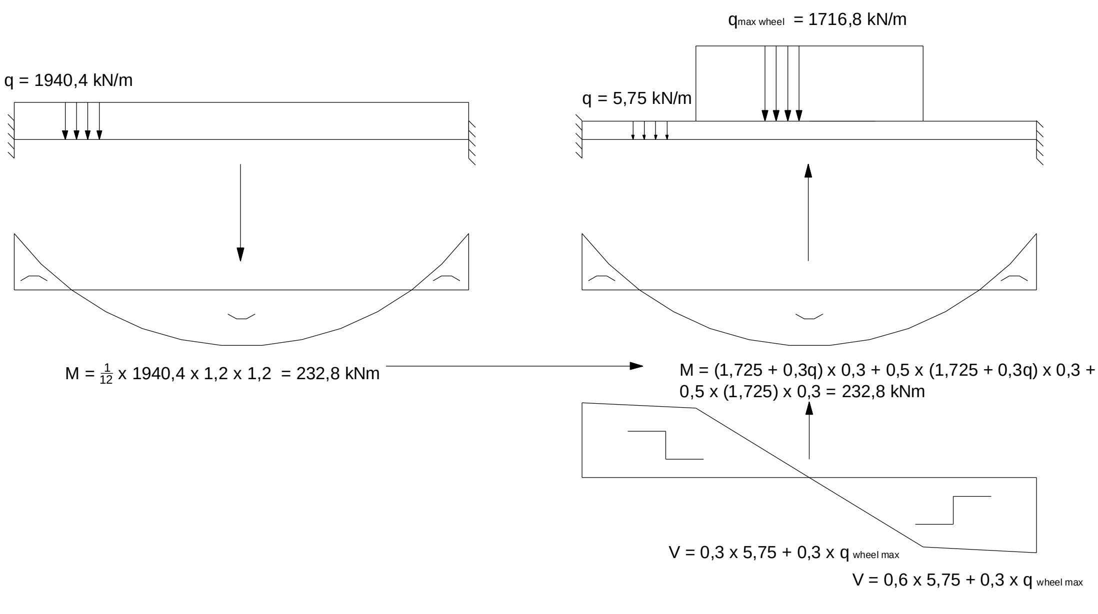

Figure 8.6: conversion from a full distributed to a wheel load

$$F_{wheel,\max} = 1716{,}8.0{,}6 = 1030{,}1N$$

Using the compressive membrane action for bending gives an enhancement factor of $\frac{1030{,}1}{655{,}9} = 1{,}57$.

8.2.2. Punch

To calculate the ultimate punch load with the theory presented in chapter 2.2, the loaded area has to be square. To calculate the length of the square, it is assumed that the square and rectangle have the same area.

$$600.350 = l_{square}{}^{2} \rightarrow l_{square} = 458{,}3\,\text{mm}$$

The maximum wheel load calculated with punching shear theory is 1012,8 kN (calculated with maple, see appendix B). The enhancement factor now becomes $\frac{1012{,}8}{655{,}9} = 1{,}54$

8.2.3. Finite element model

The axi-symmetric finite element model will be used. The brittle material model should give reasonable results, as the concrete strength is 35 N/mm^2 and the slenderness is 5,2 (see Figure 7.14). In the axi-symmetric model, only circular loaded areas can be created. The diameter of the loaded area is $\frac{4.458{,}3}{\pi} = 583{,}5mm$. The fully restrained model will be used.

The ultimate load of the finite element model is 900 kN. The enhancement factor is $\frac{910}{655{,}9} = 1{,}38$.

8.2.4. New Zealand code

The New Zealand code is one of the first international codes that takes into account compressive membrane action in bridge decks (see Appendix E, section 6.5). The empirical method described in this code may be used if the following conditions are met:

- the supporting beams are steel or concrete
- the diaphragms are continuos and present at all supports for pre-stressed concrete beams
- the slenderness does not exceed 20
- the span length does not exceed 4,5 meter
- the concrete strength f'_c is not less then 20 N/mm^2
- the minimum slab thickness is 150 mm
- the overhang of the outer beam is at least 80 mm

The example bridge deck meets all of the above requirements, and may thus be analysed with the empirical method.

The maximum wheel load in kg can be calculated with the following empirical method. Since no safety factors are taken into account so far, the value for γ_L will be assumed 1,0 to get a fair comparison of the values.

$$\left[\frac{\phi(0{,}6R_i)}{\gamma_L.40.I}.8200\right]$$

$$f'_c = 21\frac{N}{mm^2}$$

$$L = 1200mm$$

$w_0 = 0{,}74\%$ (called q in the New Zealand code)

$R_i = 1575kN$ (figure 6.4 appendix E)

$\phi = 0{,}90\phi_D$ (table 6.6 appendix E)

$\phi_D = 0{,}5$

$\gamma_L = 1{,}9$ (table 6.3 appendix E)

$I = 1{,}3$

$$\left[\frac{0{,}45.0{,}6.1575}{1{,}0.40.1{,}3}\right].8200 = 67058{,}7kg$$

$$F_{wheel,\max} = \frac{67058{,}7}{98} = 684{,}3kN$$

The enhancement factor is $\frac{684{,}3}{655{,}9} = 1{,}04$

8.3. Overview of results

For the analytical solution, which does not take into account compressive membrane action into account, the collapse load is 655,9 kN and the deck fails in punch.

The enhancement factors of the four methods to take compressive membrane action into account from low to high are:

– New Zealand code (appendix E)	1,04
– finite element model (chapter 7.5)	1,38
– punch theory (chapter 2.2)	1,54
– bending theory (chapter 2.1)	1,57

The minimum concrete strength for the deck subscribed by Spanbeton is C28/35, but in practice C50/60 is commonly used. If this concrete strength is used in the calculations, the bearing capacity and enhancement factors are:

– bending analytic	887,0 kN	
– punch analytic	888,5 kN	
– New Zealand code	899,3 kN	1,01
– finite element model	1360,0 kN	1,53
– bending including compressive membrane action	1415,4 kN	1,60
– punch including compressive membrane action	1794,7 kN	2,02

8.4. Existing bridges

Existing bridges are a point of discussion in the Netherlands, as already mentioned in the article in chapter 1. To see whether these bridges meet the bearing capacity as prescribed in the NEN-EN 1991-2, the minimum enhancement factor will be determined and then checked if it can hold the wheel load of 200 kN (load configuration 2, see Figure 1.2). The above used dimensions are only for new to build bridges, for this calculation commonly used dimensions in the 1970's will be used. These dimensions of are given in Figure 8.7. A recent study showed that the concrete quality of the decks of this existing bridges is at least C50/60. For more information on this study Dr.ir. C. van der Veen from Delft University of Technology can be contacted.

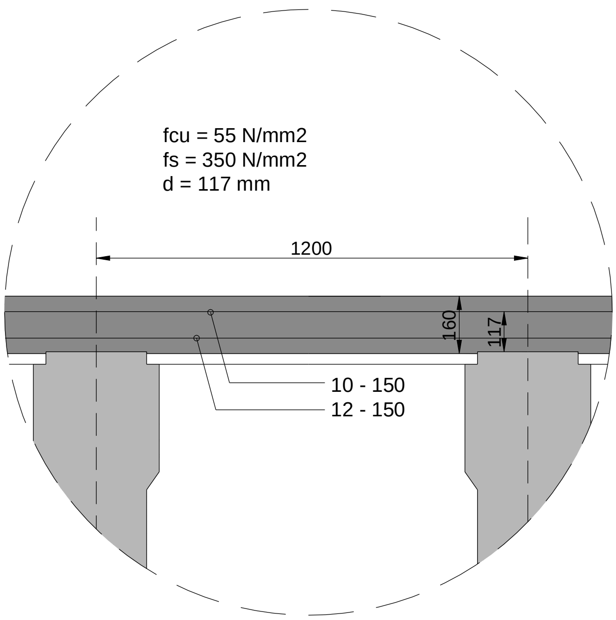

Figure 8.7: Commonly encountered dimensions of existing bridge decks

The bearing capacity and enhancement factors are:

– bending analytic	220,3 kN	
– punch analytic	477,6 kN	
– New Zealand code	488,8 kN	2,22
– bending including compressive membrane action	597,4 kN	2,71
– finite element model	600,0 kN	2,72
– punch including compressive membrane action	1225,4 kN	5,56

It can be concluded that a 200 kN wheel load, as prescribed in the EN-NEN 1991-2 can be carried if compressive membrane action is taken into account.

The enhancement factor found by the bending theory lies again between 2,2 and 2,7. Looking at the similarity of the bending enhancement factors and taking into account that this method gives a lower bound vale, it can be concluded that the enhancement factor for these kind of bridge decks and load configuration 2 (see Figure 1.2) is at least 2,7 and increases for higher concrete strengths.

The presented calculation does not include any safety factors for the loading. The load factor for live loads on bridges is 1,35 according to the European code [8.2]. This means that the deck must have the capacity to withstand an wheel load of 1,35 x 200 = 270 kN. The lower-bound value found by the theory's including compressive membrane action is significant higher then this prescribed load. It can be concluded that the deck can withstand the 270 kN wheel load if compressive membrane action is taken into account.

Not taking into account the load safety factor for the does not chance the value of the enhancement factors, since the load safety factors are equal for both calculations.

9. CONCLUSIONS AND RECOMMENDATIONS

9.1. Conclusions

The goals as described in chapter 1.1 are met. This rapport describes finite element models, for bending and punch failure, to predict the bearing capacity of latterly restrained concrete slabs.

From this rapport the following things can be concluded:

- if a concrete slab is laterally restrained, the bearing capacity is higher than can be shown with a linear analytic calculation

- the finite element program DIANA takes into account compressive membrane action and gives acceptable results (compared to experimental data) if
  - the calculation method used is non-linear
  - the material is modelled as total strain rotating brittle cracking model
  - the 2D plane stress model is used for bending failure, or the axi symmetric model is used for punch or a combination of punch and bending failure
  - the concrete strength f_{cu} lies around 35 N/mm^2
  - he slenderness is less than 15

- for lower values of the concrete strength the found values are to high, but compression membrane action is still taken into account. For higher values of the concrete strength the found values are to low, but compression membrane action is still taken into account

- for higher values of the slenderness DIANA does not take predict compressive membrane action, while experimental results show that the phenomenon is still present

- the enhancement factor, which is the ultimate load from the finite element solution divided by the ultimate load of the analytic solution, differs for different input parameters
  - for a higher concrete strength the enhancement factor will increases
  - for a higher reinforcement percentage the enhancement factor will decrease
  - for a higher reinforcement yielding strength the enhancement factor will decrease
  - for a higher slenderness the enhancement factor will decrease
  - for a low slenderness failure of the trust relieving arch might become governing (the value τ_2 gets exceeded), in which case the enhancement factor will be lower
  - if a concentrated load is spread over a larger area the enhancement factor increases

- the finite element model can include partly laterally restrained edges, this lowers the enhancement factor

- the decks of the in the Netherlands commonly used ZIP girder structures have a minimum enhancement factor of approximately 1,5

- using compressive membrane action to determine the bearing capacity of existing decks of ZIP girder bridges shows that these decks can carry the loads prescribed by the newest Euro codes

9.2. Recommendations

Recommendations for further research on the following subjects are done.

9.2.1. Tension softening

Using a tension softening instead of a brittle material behaviour, the results seem to be too ductile. The model does not fail in punch shear anymore, but fails in bending. Test specimens do fail in punch. Research has to be done to verify the different parameters such as the tensile fracture energy and the crack bandwidth, to come to a more accurate model.

9.2.2. Reinforcement layout

Finite element results show that an un-reinforced slab has a higher punch capacity than a reinforced slab provided that only flexural and no shear reinforcement is included. This might be due to the fact that in an un-reinforced slab the generated compression membrane force is larger, which makes the enhancement of the punch capacity larger. However, no test results where found to confirm this, so it is recommended to do testing on slabs with and without reinforcement to see if the results of the finite element model can be verified.

9.2.3. 3D solids model

Doing research on a 3D solids model is still very time consuming due to convergence difficulties and is therefore not continued in this thesis. However, this model might give very accurate results if the model is build-up in accordance with the specimen (which is not the case in an axi-symmetric model, since only circular structures can be modelled with this model). Research has to be done, to see if the 3D solids model can give an accurate value for the collapse load. If that is the case, this model can be extended for more complex structures, including irregular edges or holes for example.

9.2.4. Serviceability limit state

This study only checks the bearing capacity for bridge decks in the ultimate limit state. The serviceability limit state has to be checked to see if the decks fulfil all the requirements of the latest Codes.

10. REFERENCES

1.1 P. de Waard, De volkskrant, 4 oktober 2007

2.1 A. Hon, G. Teplin and R.S. Al-Mahaidi, Structural journal June 2005 "Strength of reinforced concrete bridge decks under compressive membrane action"

2.2 R. Park and W. L. Gamble, "Reinforced concrete slabs, 2nd edition" 2000, chapter 12

2.3 W. Salim and W. M. Sebastian, Structural journal July 2003 "Punching shear failure in reinforced concrete slabs with compressive membrane action"

2.4 J. S. Kuang and C. T. Morley, International journal of mechanical sciences 1993 "A plasticity model for punching shear of laterally restrained slabs"

2.5 B. Mullin, The structural engineer 2003 "Arching action in concrete slabs with novel reinforcement"

3.1 C. Hartsuijker and H. Welleman, "Toegepaste mechanica deel 3: Statisch onbepaalde constructies en bezwijkanalyse" module 2chapter 5.3

3.2 R. Sagel and A. J. van Dongen, "Constructeileer gewapend beton" 2000, chapter 11

3.3 "NEN 6706, traffic loads on bridges" 2007, chapter 7.2

4.1 L. K. Guice and E. J. Rhomberg, Structural journal July 1988 "Membrane action in partially restrained slabs"

4.2 J.S. Kuang and C.T. Morley, Structural journal January 1992 "Punching shear behaviour of restrained reinforced concrete slabs"

4.3 S.E. Talor, B. Rankin, D.J. Cleland and J. Kirkpatrick, Structural journal January 2007 "Serviceability of bridge deck slabs with arching action"

5.1 "NEN 6720 Voorschriften beton, constructieve eisen en rekenmethoden"

7.1 A.C.W.M. Vrouwenvelder and Witteveen, "The plastic behaviour and the calculation of plates subjected to bending"

7.2 J.M. Gere and S.P. Timoshenko, "Mechanics of materials"

8.1 www.spanbeton.nl

8.2 NEN 6702 "Technische grondslagen voor bouwconstrcuties –TGB 1990– Belastingen en vervormingen"

Appendix A: Excel sheet for bending capacity

General input		
L	1200	mm
b	1200	mm
h	150	mm
d0	127,3	mm
l/h	8	-
c (concrete cover)	27	mm
F steel top	8	mm
F steel bottom	8	mm
number of bars top	13	-
number of bars bottom	13	-
d	115	mm
fck	35	N/mm2
fbm	2,8	N/mm2
fc	1,4	N/mm2
f'c	21	N/mm2
T2	4,2	N/mm2
Ec	31000	N/mm2
Es	210000	N/mm2
As,top	653,4512719	mm2
As,bot	653,4512719	mm2
fs	435	N/mm2
S	1,00E+11	N/mm/mm width
wo	0,36%	passes
wmin	0,18%	
wmax	1,94%	

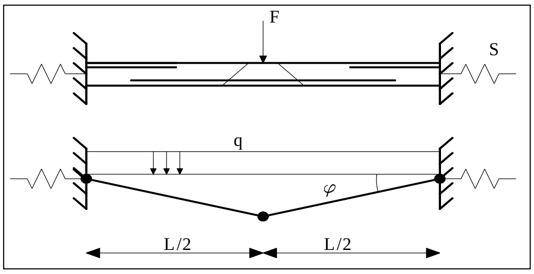

$$W_{load,q} = \frac{qL^2}{4}\varphi$$

$$W_{load,F} = \frac{FL}{2}\varphi$$

$$W_{int} = 2M_{p,support}\varphi + 2M_{p,field}\varphi$$

$$q_{max} = \frac{8M_{p,support}}{L^2} + \frac{8M_{p,field}}{L^2}$$

$$F_{max} = \frac{4M_{p,support}}{L} + \frac{4M_{p,field}}{L}$$

$$\frac{\varepsilon_c}{0{,}375h} = \frac{\varepsilon_s}{d-0{,}625h}$$

$$\varepsilon_s = 0{,}002625\frac{(d-0{,}625h)}{0{,}375h}$$

$$C_s = \frac{A_s E_s \varepsilon_s}{b} = 0{,}002625.\frac{A_s E_c (d-0{,}625h)}{0{,}375bh}$$

Standaard virtual work theory		
Ns,sup	284251,3033	N
xu,sup	15,0397515	mm
z,sup	109,1344969	mm
Mu,sup	31021622,98	Nmm
Ns,field	284251,3033	N
xu,field	15,0397515	mm
z,field	109,1344969	mm
Mu,field	31021622,98	Nmm
qmax	**344,7**	**kN/m**
Fmax	**207**	**kN**

Including compressive mebrane action (Park's theory)		
B1	0,85	-
T	236,88	N/mm width
T'	236,88	N/mm width
Cs	113,40	N/mm width
Cs'	113,40	N/mm width
maxium qpark/qmax	**2,45**	**-**
qpark max	**845,9**	**kN/m**
sagg at qpark max	**1**	**mm**

Punching		
wo,bottom	0,36%	
kd	1,431	-
t1	1,12	N/mm2
P	761,2079	mm
Fmax	98043,57752	N
Fmax	**98**	**kN**
Fshear maple		**kN**

Shear (no shear reinforcement included)		
Md max	31021622,98	Nmm
Vd max	206820	N
λv	1,940869565	-
A0	138000	mm2
gλ	4,77	-
kλ	2,52	-
kh	1,45	-
ω0	0,36	%
t1,increased	1,46	N/mm2
t1 (0,4fb)	0,56	N/mm2
qmax	**335**	**kN/m**
qmax (t2)	**966**	**kN/m**

q	q/qmax	sagg/h
#DEEL/0!	#DEEL/0!	0
816,6282	2,369098	0,001667
837,1984	2,428774	0,003333
844,0778	2,448732	0,005
845,8533	2,453882	0,006667
845,4427	2,452691	0,008333
844,0147	2,448549	0,01
842,0917	2,44297	0,011667
839,9261	2,436687	0,013333
837,6468	2,430075	0,015
835,3215	2,423329	0,016667
832,9869	2,416556	0,018333
830,6628	2,409814	0,02
828,3595	2,403132	0,021667
826,0821	2,396525	0,023333
823,8328	2,389999	0,025
821,6117	2,383556	0,026667
819,4185	2,377193	0,028333
817,2519	2,370908	0,03
815,1105	2,364695	0,031667
812,993	2,358552	0,033333
810,8977	2,352474	0,035
808,8234	2,346456	0,036667
806,7686	2,340495	0,038333
804,732	2,334586	0,04
802,7124	2,328728	0,041667
800,7089	2,322915	0,043333
798,7203	2,317146	0,045
796,7458	2,311418	0,046667
794,7844	2,305728	0,048333
792,8356	2,300074	0,05
790,8985	2,294454	0,051667
788,9724	2,288867	0,053333
787,057	2,28331	0,055
785,1514	2,277782	0,056667

Appendix B: Maple sheet for punch capacity

The maple sheet in which the ultimate punching shear load is calculated looks as follows:

```
> restart;
```

This sheet works as follows:

(1) fill in the variables (blue fields) in N and mm

(2) run the sheet and fill in d1 as a smaller value than d1start

(3) run again

(4) change the value 'angle' to the value 'nextangle' (3 decimals)

(5) run again and repeat step (4) till dP is approximately zero

(5) write down the value of P (this value is shown in kN!)

(6) slightly decrease d1 and repeat step 3 till 6 untill a minimum is reached for P

(7) this minimum is the value P at which the plate will fail in shear mode (mind that d1 can reach d0 closely)

```
> L:=2250;
```

$L := 2250$

```
> h:=150;
```

$h := 150$

```
> d:=135;
```

$d := 135$

```
> d0:=300;
```

$d0 := 300$

```
> fcu:=35;
```

$fcu := 35$

```
> fy:=435;
```

$fy := 435$

```
> W0:=0.0075;
```

$W0 := 0.0075$

```
> fca:=0.85*fcu;
```

$fca := 29.75$

```
> fc:=0.85*fca;
```

$fc := 25.2875$

```
> fta:=0.7*(1.05+0.05*fcu);
```

$fta := 1.960$

```
> ft:=fc/400;
```

$ft := 0.06321875000$

```
> Ec:=evalf((4730*sqrt(fca)));
```

$Ec := 25799.10415$

```
> Es:=210000;
```

$Es := 210000$

```
> ck:=sqrt(1+fc/fta)-1;
```

$ck := 2.728509851$

```
> d1start:=solve((d1/d0)^d1=exp(ck*h), d1);
```
d1start := 596.0873953

```
> d1:=350;
```
d1 := 350

```
> angle:=4.988;
```
angle := 4.988

```
> beta:=convert(angle*degrees,radians);
```
b := 0.02771111111p

```
> tb:=evalf(tan(beta));
```
tb := 0.08727762478

```
> a:=L/2;
```
a := 1125

```
> R:=L/2;
```
R := 1125

```
> As:=evalf(W0*L*d);
```
As := 2278.1250

```
> x:=1.76*d*W0*(fy/fcu);
```
x := 22.14771428

```
> S:=1/((a*R)/(0.8*Ec*L*d+Es*As)+a/(0.5*Ec*(x+h)));
```
S := 1440.547813

```
> phi:=(a*fc)/(2*h*S);:
```
f := 0.06582782200

```
> wi:=0.03*h;
```
wi := 4.50

```
> w0:=0.5*h;
```
w0 := 75.0

```
> N0:=0.5*h*fc-(As/L)*fy;
```
N0 := 1456.125000

```
> n0:=(N0/(h*fc));
```
n0 := 0.3838853188

```
> k:=(0.5*n0+0.25+0.25*phi-0.25*(wi/h))*exp(wi/(h*phi));
```
k := 0.7112180663

```
> na:=-1*(k*exp(-(w0/h)/phi)-0.5*(n0+0.5+0.5*phi)+0.25*(w0/h));
```
na := 0.3330421055

```
> B:= fsolve(d1/2=(d0/2+tan(beta)/B)*exp(B*h)-tan(beta)/B,B);
```
B := 0.0004890077716

```
> A:=d0/2+tb/B;
```

$$A := 328.4790137$$

```
> d0/2=A-tb/B;
```

$$150 = 150.0000000$$

```
> d1/2=A*exp(B*h)-tb/B;
```

$$175 = 175.0000000$$

```
> r:=A*exp(B*y)-tan(alpha)/B;
```

$$r := 328.4790137\,\mathbf{e}^{(0.0004890077716\,y)} - 2044.957275\tan(a)$$

```
> dr:=diff(r,y);
```

$$dr := 0.1606287905\,\mathbf{e}^{(0.0004890077716\,y)}$$

```
> nr:=na+(w0/(2*h))*(1-(r/a));
```

$$nr := 0.5830421055 - 0.07299533640\,\mathbf{e}^{(0.0004890077716\,y)} + 0.4544349500\tan(a)$$

```
> Nin:=int(nr*2*Pi*r,y=0..h);
```

$$Nin := 1.629455225\ 10^{5} - 8.317644672\ 10^{5}\tan(a) - 8.758446696\ 10^{5}\tan(a)^{2}$$

```
> Nrscont:=fc*Nin;
```

$$Nrscont := 4.120484900\ 10^{6} - 2.103324396\ 10^{7}\tan(a) - 2.214792208\ 10^{7}\tan(a)^{2}$$

```
> Nrs:=2*Pi*fc*(na+(w0/(2*h)))*((A/B)*(exp(B*h)-1)-(h/B)*tan(alpha))-
Pi*fc*(w0/(a*h))*((A^2/(B*2))*(exp(2*B*h)-1)-((2*A)/B^2)*(exp(B*h)-
1)*tan(alpha)+(h/B^2)*(tan(alpha))^2);
```

$$Nrs := 29.48735448\,p\,(51123.93190 - 3.067435912\ 10^{5}\tan(a))$$
$$- 0.01123888889\,p\,(1.743218788\ 10^{7} - 2.090925128\ 10^{8}\tan(a) + 6.272775384\ 10^{8}\tan(a)^{2})$$

```
> diff(Nrs,alpha);
```

$$29.48735448\,p\,(-3.067435912\ 10^{5} - 3.067435912\ 10^{5}\tan(a)^{2}) - 0.01123888889\,p\,(-2.090925128\ 10^{8}$$
$$- 2.090925128\ 10^{8}\tan(a)^{2} + 1.254555077\ 10^{9}\tan(a)\,(1 + \tan(a)^{2}))$$

```
> F:=r*(dr-tb+(ck^2/4)*((1+dr*tb))^2/(dr-tb));
```

$$F := (328.4790137\,\mathbf{e}^{(0.0004890077716\,y)} - 2044.957275\tan(a))\left(0.1606287905\,\mathbf{e}^{(0.0004890077716\,y)}\right.$$
$$\left. - 0.08727762478 + \frac{1.861191502\,(1 + 0.01401929931\,\mathbf{e}^{(0.0004890077716\,y)})^{2}}{0.1606287905\,\mathbf{e}^{(0.0004890077716\,y)} - 0.08727762478}\right)$$

```
> Pin:=int(F,y=0..h);
```

$$Pin := -7.440824738\ 10^{6}\tan(a) + 1.238993219\ 10^{6}$$

```
> P:=2*Pi*ft*((A^2/2)*(exp(2*B*h)-1)-((2*A)/B)*(exp(B*h)-1)*tan(alpha)+(h/B)*(tan(alpha))^2)+Pi*ft*(ck^2/2)*(h/B+((2*A)/B)*(exp(B*h)-1)*tan(alpha)+(A^2/2)*(exp(2*h*B)-1)*(tan(alpha))^2)+Nrs*tan(alpha);
```

$$P := 0.1264375000\, \pi\, (8524.475350 - 1.022478638\ 10^5 \tan(\alpha) + 3.067435912\ 10^5 \tan(\alpha)^2) + 0.2353244005\, \pi\, (3.067435912\ 10^5 + 1.022478638\ 10^5 \tan(\alpha) + 8524.475350 \tan(\alpha)^2) + (29.487354\backslash 48\, \pi\, (51123.93190 - 3.067435912\ 10^5 \tan(\alpha)) - 0.01123888889\, \pi\, (1.743218788\ 10^7 - 2.090925128\ 10^8 \tan(\alpha) + 6.272775384\ 10^8 \tan(\alpha)^2)) \tan(\alpha)$$

```
> Pcontr:=evalf(2*Pi*ft*Pin+Nrs*tb);
```

$$Pcontr := -4.791339674\ 10^6 \tan(\alpha) + 8.517729766\ 10^5 - 1.933018034\ 10^6 \tan(\alpha)^2$$

```
> dP:=(diff(P,alpha))/(1+(tan(alpha))^2);
```

$$dP := \frac{1}{1+\tan(\alpha)^2} (0.1264375000\, \pi\, (-1.022478638\, 10^5 - 1.022478638\, 10^5 \tan(\alpha)^2 + 6.134871824\ 10^5 \tan(\alpha)\, (1 + \tan(\alpha)^2)) + 0.2353244005\, \pi\, (1.022478638\ 10^5 + 1.022478638\ 10^5 \tan(\alpha)^2 + 17048.95070 \tan(\alpha)\, (1 + \tan(\alpha)^2)) + (29.48735448\, \pi\, (-3.067435912\ 10^5 - 3.067435912\ 10^5 \tan(\alpha)^2) - 0.01123888889\, \pi\, (-2.090925128\ 10^8 - 2.090925128\ 10^8 \tan(\alpha)^2 + 1.254555077\ 10^9 \tan(\alpha)\, (1 + \tan(\alpha)^2))) \tan(\alpha) + (29.48735448\, \pi\, (51123.93190 - 3.067435912\ 10^5 \tan(\alpha)) - 0.01123888889\, \pi\, (1.743218788\ 10^7 - 2.090925128\ 10^8 \tan(\alpha) + 6.272775384\ 10^8 \tan(\alpha)^2)) (1 + \tan(\alpha)^2))$$

```
> rad:=max(solve(dP=0,alpha));
```

$$rad := 0.08706146960$$

```
> nextagle:=evalf(convert(rad,degrees));
```

$$nextagle := 4.988254766\, degrees$$

```
> alpha:=beta;
```

$$\alpha := 0.02771111111\pi$$

```
> dPcontr:=Pi*ft*(ck^2/2)*(((2*A)/B)*(exp(B*h)-1)+A^2*(exp(2*B*h)-1)*tan(alpha))-2*Pi*ft*(((2*A)/B)*(exp(B*h)-1)-((2*h)/B)*tan(alpha))-2*Pi*fc*(na+(w0/(2*h)))*(h/B)*tan(alpha)+Pi*fc*(w0/(a*h))*(((2*A)/B^2)*(exp(B*h)-1)-((2*h)/B^2)*tan(alpha))*tan(alpha)+Nrs;
```

$$dPcontr := 0.2353244005\, \pi\, (1.022478638\ 10^5 + 17048.95070 \tan(0.02771111111\, \pi)) - 0.1264375000\, \pi\, (1.022478638\ 10^5 - 6.134871824\ 10^5 \tan(0.02771111111\, \pi)) - 9.045057010\ 10^6\, \pi \tan(0.02771111111\, \pi)$$

$$+ 0.01123888889\,p\,(2.090925128\,10^{8} - 1.254555077\,10^{9}\tan(0.02771111111\,p))\tan(0.02771111111\,p)$$

$$+ 29.48735448\,p\,(51123.93190 - 3.067435912\,10^{5}\tan(0.02771111111\,p)) - 0.01123888889\,p$$

$$(1.743218788\,10^{7} - 2.090925128\,10^{8}\tan(0.02771111111\,p) + 6.272775384\,10^{8}\tan(0.02771111111\,p)^{2})$$

```
> evalf(Pcontr)/1000;
```

418.8716901

```
> evalf(P)/1000;
```

418.8716902

```
> evalf(dP)/1000;
```

0.2392902344

```
> evalf(dPcontr)/1000;
```

0.2392895000

```
> evalf(Nrs)/1000;
```

2116.044104

```
> evalf(Nrscont)/1000;
```

2116.044103

Appendix C: Some DIANA input files

The command file for the non-linear DIANA calculations

```
*FILOS
INITIA
*INPUT
READ
*NONLIN
BEGIN EXECUT
 BEGIN LOAD
  LOADNR=1
  BEGIN STEPS
   BEGIN ITERAT
    ARCLEN
    GAMMA=0.25
    MAXSIZ=10
    NSTEPS=500
   END ITERAT
  END STEPS
 END LOAD
 ITERAT MAXITE=500
END EXECUT

BEGIN OUTPUT
 DISPLA TOTAL TRANSL
 DISPLA INCREM TRANSL
 FORCE REACTI TRANSL
 STRESS TOTAL CAUCHY GLOBAL
 STRESS TOTAL CAUCHY LOCAL
 STRAIN CRACK
 FORCE  EXTERN TRANSL
END OUTPUT
*END
```

The material properties in the data file

```
'MATERIALS'
  1 YOUNG     3.100000E+04
    POISON    2.000000E-01
    TOTCRK ROTATE
    TENCRV BRITTL
    TENSTR    1.400000E+00
    COMCRV CONSTA
    COMSTR    2.100000E+01
  2 YOUNG     2.100000E+05
    YIELD  VMISES
    YLDVAL    4.350000E+02
```

Command file for a phased calculation

```
*FILOS
INITIA
*INPUT
*PHASE
BEGIN ACTIVE
 ELEMEN 1 CIRCLE
END ACTIVE
*NONLIN
BEGIN EXECUT
 BEGIN LOAD
  LOADNR=2
  BEGIN STEPS
   EXPLIC SIZES 1 (1)
  END STEPS
 END LOAD
 ITERAT MAXITE=500
 ITERAT LINESE
END EXECUT


BEGIN OUTPUT FEMVIE BINARY
  file="ph1"
 DISPLA TOTAL TRANSL
 DISPLA INCREM TRANSL
 FORCE REACTI TRANSL
 STRESS TOTAL CAUCHY GLOBAL
 STRESS TOTAL CAUCHY LOCAL
 STRAIN CRACK
 FORCE  EXTERN TRANSL
END OUTPUT

*PHASE
BEGIN ACTIVE
  ELEMEN 1 CIRCLE 2 ELASTI
END ACTIVE
*NONLIN
BEGIN EXECUT
 BEGIN LOAD
  LOADNR=2
  BEGIN STEPS
   EXPLIC SIZES 1 (1)
  END STEPS
 END LOAD
 ITERAT MAXITE=500
 ITERAT LINESE
END EXECUT
BEGIN EXECUT
 BEGIN LOAD
  LOADNR=1
  BEGIN STEPS
```

```
  EXPLIC SIZES 0.5 (5000)
 END STEPS
 END LOAD
 ITERAT MAXITE=500
 ITERAT LINESE
END EXECUT

BEGIN OUTPUT TABULA
 BEGIN SELECT
  NODES 1106
 END SELECT
 displace
END OUTPUT

BEGIN OUTPUT FEMVIE BINARY
file="ph2"
 DISPLA TOTAL TRANSL
 DISPLA INCREM TRANSL
 FORCE REACTI TRANSL
 STRESS TOTAL CAUCHY GLOBAL
 STRESS TOTAL CAUCHY LOCAL
 STRAIN CRACK
 FORCE  EXTERN TRANSL
END OUTPUT
*END
```

Appendix D: Experiments based on the Ontario highway bridge design code

Design of Thin Concrete Deck Slabs by the Ontario Highway Bridge Design Code

Paul F. Csagoly

Principal Research Officer
Structural Research
Engineering Research and Development

May 1979

Ontario

Ministry of Transportation and Communications

Research and Development Division

Content

Introduction

The Ontario Ministry of Transportation and Communications (MTC) has been active in highway oriented structural research during the last decade. The work has touched upon various aspects of bridge engineering: one of the major programs dealt with determining the load carrying capacity of thin concrete bridge decks supported by either steel or concrete girders.

Sporadic research work by others indicated the presence of compressive membrane forces in continuous and/or laterally confined slabs, enhancing their vertical load carrying capacity. It was also observed that slabs having lost part of their thickness due to spalling or weakened by internal cracking were still capable of sustaining multiple of the original design load; a phenomenon that could not be explained by the flexural plate theory of Nadai and Westergaård, upon which the present AASHTO Specifications (Ref.17) and CSA Standards are based.

The MTC slab research program included the testing of various bridge model specimens at Queen's University (Kingston, Ontario), the assembly of a general mathematical model for failure, the measurement of membrane forces in confined concrete discs and a large number of prototype tests. The streamlined and computerized mathematical model permits a reasonably good estimate of ultimate load carrying capacity of partially confined slabs.

The Ontario Highway Bridge Design Code (OHBDC) permits the empirical design of slabs, if certain minimum boundary conditions are satisfied. The minimum isotropic four layer reinforcement is 0.3 percent, defined by serviceability limit states requirements regarding control of cracking. It has been found that this minimum reinforcement far exceeds that required for ultimate limit states considerations. This ratio is approximately half required by the present AASHTO load factor method and only one third of that resulting from any working stress design method.

The reduced amount of reinforcement with adequate concrete cover is also expected to improve the performance of slabs with regard to spalling; this is in addition to the obvious economy in construction.

Historical Background

The behaviour of plates under loads acting perpendicular to their planes has interested the early researchers at the time of the industrial revolution and it was the French mathematician Lagrange, who in 1811 succeeded in describing flexural plate responses by a fourth order partial differential equation:

$$\frac{\partial^4 Z}{\partial x^4} + 2\frac{\partial^4 Z}{\partial x^2 \partial y^2} + \frac{\partial^4 Z}{\partial y^4} = \frac{12(1-\mu^2)w}{Eh^3}$$

where: x and y: lateral coordinates

z: displacement perpendicular to the plate

μ: Poisson's ratio

w: distributed load

h: thickness of plate

The Lagrange equation, for all its beautiful symmetry and compactness, has a number of shortcomings regarding its use for computing responses in concrete bridge slabs:

1. it does not permit a closed format direct solution
2. has difficult boundary conditions
3. is not directly applicable to concentrated wheel loads and

4. fails to consider cracks inherent in bridge decks.

In trying to overcome these difficulties, the progress was slow. The combination of vertical shears and twisting moments at the boundary permitted the expression of reactions in the theorem of Kelvin and Tait introduced in 1867. Although the Fourier series (actually invented by d'Alembert) were available for 150 years, it occurred only in 1915 that E.T. Whittaker and G. N. Watson were able to successfully apply them for load representation. They proved that although the series describing concentrated loads are divergent, further successive integrations, by which shears, moments, rotations and displacements are obtained, yield usable, convergent series.

A. Nadai, by a deductive process involving functions of a complex variable, derived a solution of the Lagrange equation in a finite form, and published the results in his book "Die Elastischen Platten" in 1925. E. F. Kelley, published in 1926 a study of the influence of concentrated loads (Ref.1) in light of available test results and proposed formulae for computing bending moments. Finally, H.M. Westergaard, having resolved the problem of an infinite bending moment at the point of application of a concentrated load by introducing a rigid disk under the load, published his article (Ref.2) of historic consequence in 1930.

Slab design provisions of not only the AASHTO Specifications, but virtually those of the whole civilized world are now based on Westergaard's work, while the effects of cracks in the plate continuum and lateral restraint by beams, diaphragms and by the continuity of the slab have never been considered by any code writing authority other than MTC.

At the outset of the slab program, MTC has carried out a finite element flexural analysis of a square slab supported by four parallel girders. The outcome of this investigation, including close to 500 elements, has been left unreported as it only verified, within a remarkably small error of three percent, the present AASHTO method of design.

MTC became concerned about the behaviour of concrete bridge decks for two reasons. First, the permissible axle weights of commercial vehicles in Ontario had been increased from 18,000 lb to 20,000 lb in 1971 and a further increase to 22,000 lb within a short period of time was expected. Second, the then bare-deck policy of MTC in conjunction with inadequate concrete cover over the reinforcing bars resulted in considerable spalling occasionally exceeding 10 percent of deck area and two inches in depth. A loss of two inches in depth is theoretically equivalent to a decrease of flexural strength of a standard 7.5 in. thick deck by 33 percent if the deck was underreinforced and 55 percent if overreinforced.

The increase in axle weights and the apparent erosion of flexural strength did not, however, result in failures and therefore it could be convincingly argued that the load carrying capacity was underestimated by the current AASHTO method of design.

Model Tests at Queen's University

The 1971 American Concrete Institute annual convention, held in Denver, Colorado, included a symposium regarding the cracking, deflection and ultimate load of concrete slab systems. In general, the symposium concluded that the failure mode of slabs under concentrated loads is a combination of shear and flexure. It is referred to as punching failure, reflecting its nature of a frustum, whose upper surface coincides with that of the medium transmitting the loads to the slab, being pushed out.

In particular, the presence and benevolent effect of membrane forces were recognized. Y. Aoki (Ref.3) stated that "When the ultimate flexural strength based on yield line theory is evaluated taking arching into consideration, test results indicate that the collapse load in flexure becomes 2.1 times that calculated without considering the membrane force". B. Batchelor (Ref.4) announced that "One model tested under concentrated loads placed in a pattern corresponding to that of AASHTO specifications, failed in the combined beam-slab mode with a factor of safety of 6.5". J. Brotchie (Ref.5), who, by having measured the membrane forces on models separated flexural and arching effects for the first time, concluded: "The magnitude of strength increase and the improvement of behaviour at service and overloads are sufficient to warrant serious consideration of the utilization of arching action in design".

In 1972, MTC obtained its first load testing vehicle, whose features will be discussed later. The vehicle had been equipped with a hydraulic device capable of transmitting a patch load up to 125 Kips (555 kN) to a bridge deck. The vehicle was tested out on a bridge over the Falls River, that had been taken out of service some 20 years ago due to relocation of highway. A few reinforcing bars were exposed and strain-gauged, then the concrete was acid-etched and rebuilt. The tests indicated that for the given span-thickness ratio and percentage of reinforcing, only about one-sixth of the load was carried by direct flexure.

Encouraged by the test results of MTC and others, Queen's University, that has already been involved due to B. Batchelor's activities, was given a number of projects by MTC in order to clarify the issue in a systematic manner. Only two of these projects, being significant to the program, will be described in this paper. Both projects are related to beam-slab composite bridges, a deviation from the type of structures all previous investigations were concerned with.

The behaviour of I-beam bridge slabs was investigated by testing a total of nine 1/8th scale direct models of 24.4 m (80 ft) span four-beam bridges shown in Figure 1. The construction of the steel work, including the beams, diaphragms and shear connectors is illustrated in Figure 2. Deck slabs with orthotropic and with isotropic reinforcement, as well as plain concrete slabs, were tested. The orthotropic type modelled the reinforcement of conventional deck slabs. The influence of slab span-to-thickness ratio, load position, dead load stresses, reinforcement ratio, and concrete strength on the load-carrying capacity of the slabs were studied, together with the punching strength in a beam negative moment region.

The decks were subdivided into panels, which are defined as an area bounded by adjacent beams and diaphragms, indicated in Figure 3. The panels were tested, one at a time, to failure under single concentrated loads applied at their respective centres through a steel plate bearing on a neoprene pad. The contact area modelled the footprint of the tires of large earth-moving equipment. Of the total of 68 tests, all but one of the reinforced panels and some of the unreinforced ones failed by punching. The failure by punching usually left a neat elliptical hole, a little larger than the loaded area, in the top of the slab and a pushed-through frustum of a cone with an approximately circular base.

As the load was applied, longitudinal and diagonal cracks were observed on the underside of the slab, directly beneath the loaded area and they usually began to appear between 25 and 50 percent of the failure load. The crack pattern on the top was always elliptical in nature as illustrated in Figure 4. Although accelerated creep usually gave some warning, failure was always explosive, but cracking was confined to the panel tested.

There was considerable variation of the failure loads for slabs with orthotropic reinforcement; this was attributed to the variation of slab thickness of the small scale models. The evaluation of test data indicated that failure load is not significantly influenced by the location of the panel, by previous failures in adjacent panels, by the strength of concrete, by dead load stresses and whether the slab was under longitudinal compression or tension. Assuming a 16,000 lb design wheel load with an impact of 0.3, the minimum observed factor of safety was 16. By simulating a truck on four wheels of identical loads, it was shown that the beams of a conventionally designed bridge would fail prior to the concrete deck slab.

Isotropically reinforced slabs were tested in three and four beam models. Having maintained the distance between the outside beams as constant, the arrangement permitted two variations of the span-to-thickness ratio, 20.6 and 13.7, respectively. Figure 5 shows the average values of failure loads for various percentages of reinforcing steel in kN and in multiples of the AASHTO design wheel load. It can be seen that failure loads increase as span-to-thickness ratio decreases and as reinforcement ratio increases. It is of particular interest that the slab, supported by four beams but without any reinforcement, produced a multiple of 13.5. The conclusion of these tests was that a minimum isotropic reinforcement of 0.2 percent, prescribed by most codes for volumetric changes such as creep, shrinkage and temperature, is sufficient for ultimate limit states considerations.

The fatigue life of reinforced concrete slabs had never been investigated before, and it was felt that in view of reducing the reinforcement ratio, the problem required some attention. Making use of the four-beam steel work constructed for the static tests above described, five bridge models were built. The panel distribution and loading apparatus were also the same.

Altogether 37 individual fatigue tests were carried out on panels with orthotropic, isotropic and zero reinforcement. The applied cyclic load was in the form of a sinusoidal wave superimposed on a mean value, so programmed that the minimum load was of the order of .89 kN (200 lb) and the maximum load was a proportion of the estimated static strength of the panel. Frequency of application was between 1 and 5 Hz, well within 7 Hz limit (Ref.8) of the rate of loading having no effect on plain concrete.

A special concrete suitable for structural models, developed at Queen's University, was used for the slabs. Although the aggregate had been rather fine, the all-important ratio of tensile to compressive strength of this concrete was similar to that of prototype concrete. The reinforcement used in the model was a 13 gauge wire having a diameter of 2.32 mm (0.092 in); it was manufactured, indented and specially annealed by the Steel Company of Canada so that its yield stress conformed to

ASTM Standards for intermediate grade steel.

Crack patterns up to failure were much the same as those obtained in punching failures under static loads. Cracking was observed after a few cycles of repeated loading, the cracks widened and spread as the number of cycles increased but were always confined within the boundaries of the panel tested. The punched area after fatigue failure was often larger and less symmetrical than that resulting in failure under static loading and in some cases, fracture occurred in the bottom reinforcing steel within the loaded area.

Figure 6 indicates that the endurance limit of orthotropically reinforced slab panels is at least 50 percent of the static ultimate load. Slab panels with 0.2 percent isotropic reinforcement exhibited somewhat more scatter, but all test results could be lower bounded at 40 percent, thus reducing the multiple number from 16.0 to 6.4. Even with this reduction, the slabs are assured of infinite fatigue life since the maximum axle load that can be transmitted by the heaviest commercial vehicles presently on the highways (for a 23,000 lb. rated capacity) is 2.5 x 23.0 = 57.5 kips or 1.80 times the design axle load of 32.0 kips. It can be concluded therefore that fatigue life is of no concern regarding reinforced concrete bridge slabs and that the 40 percent endurance limit is compatible with the fatigue shear failure of concrete beams (Ref.8).

Mathematical and Physical Models

The facts that the Lagrange equation cannot be coupled with membrane force descriptions and that it deals with uncracked plates only, make it unsuitable to compute ultimate failure loads of prototype bridge deck slabs. The practicing design engineer would normally like to separate flexural and arching actions for his computations as shown in Figure 7, but in this case the interaction between the two actions is so intimate that separation is not warranted.

The idealized model of failure proposed by S. Kinnunen (Ref.9) has been proven to give a good estimate of the punching strength of simply supported slabs. B. Hewitt (Ref.10) expanded this model by incorporating a boundary restraining force F_b and boundary restraining moment M_b, both acting at the level of the tensile reinforcements as illustrated in Figure 8. Both F_b and M_b are products of the restraining factor F_R and the maximum respective boundary moment and force that can develop. Restraining factor F_R is an arbitrary parameter varying between 0.0 and 1.0, the latter for full (infinitely rigid) restraint conditions.

The criterion of failure is that punching occurs when the tangential strain at the top surface of the slab in the vicinity of the root of the shear crack reaches a critical value. By considering the equilibrium of the sector element shown in Figure 8 and this empirical failure criterion, the theoretical punching load P can be determined in an iterative process using a computer program (Ref.10) developed for this purpose.

Although, the restraining factor of a prototype is difficult to establish, the computer program permitted the variation of parameters within certain limits. Figure 9 illustrates the results of one such exercise, where the effect of the restraining factor on the punching load was studied. It can be observed that the punching load is a rather sensitive function of F_R, increasing by about 200 percent from zero to full restraint. Figure 10 indicates the decrease of punching load of a typical deck slab with 0.2 percent isotropic reinforcement.

This mathematical model has certain geometrical limitations. Its primary value is that by parametric studies, the most significant aspects can be identified and to an extent, quantified. These unquestionably are the span-to-thickness ratio and the quality of confinement; all other parameters have been found to be of limited significance.

Prior to MTC's slab research program, the most important work was carried out by J. Brotchie and M. Holley (Ref.5). They tested 45 model slabs, some unreinforced, 15 in. (381 mm) squares in plan, with thicknesses of 0.75, 1.50 and 3.00 in (19, 38 and 76 mm) giving span-to-thickness ratios of 20, 10 and 5. The reinforcement ratios were 0.0, 0.5, 1.0, 2.0 and 3.0 percent.

They used uniformly distributed loads, so their results are not directly applicable to slabs exposed to concentrated wheel loads. The value of their work lies in the fact, that they were able to measure membrane forces, by load cells - six to each side, thus establishing the existance and nature of arching action due to lateral confinement. Figure 11 illustrates a typical load deflection curve for an underreinforced slab with edge restraint showing three phases of behaviour:

A. Commencing with a purely elastic flexural response continued by the development of the lateral membrane force after cracking; the maximum membrane force obtained at a deflection approximately half the slab thickness.

B. After the deformed slab reached a neutral position with respect to the membrane force, the latter starts to contribute to the deformation and diminishes gradually.

C. The large deformation of the slab activates the reinforcing net and develops a tensile membrane force.

Figure 12 illustrates the development of the complementary restraining force measured. It is interesting to note that the slab, after having passed through its neutral position, will be forced downward by the combined effects of the applied load and the membrane force developed, explaining the explosive nature of failure of non-reinforced and slightly reinforced slabs. It is also worthwhile to observe that in the practical range of maximum axle weights, as permitted by commercially available equipment hardware and tires, the response of the slab is either fully elastic (meaning that the stress in reinforcement would not exceed about 4.0 ski or 27.0 MPa) or is just developing the compressive membrane force, as the deflection is in the 0.25 in (6 mm) range, or about 1/30th of the slab thickness.

Figures 13 and 14 are further underlining the three-phased nature of laterally restrained concrete deck slabs. In their conclusions, the authors point out, that the results reported are valid only for short term loads, what wheel loads certainly are.

MTC's physical model tests are reported in Reference 11. The experiment included the testing, by a centrally located concentrated load, 27 circular specimens, each 22.5 in. (572 mm) in diameter. Variables were slab thickness: 1.25 in (32 mm), 1.50 in. (38 mm) and 1.75 in (44 mm) and reinforcement ratio: 0.2, 0.3 and 1.0 percent, providing for nine combinations with three specimens each. The specimens were to model an 8.0 ft. (2.44 m) prototype span, resulting in a geometric scale factor of 1:4.27 and in a force scale factor of 18.23, which is the square of the former.

As opposed to the rectangular models used by previous investigators (Ref.5), the circular shape was selected here to reflect the observation that regardless the geometry of the slab boundary and supporting system, the pattern of a punching failure is always circular, or an ellipse not much deviating from a circle. The mathematical model applied is also circular in plan, therefore providing a direct comparison between theoretical results and experimental data.

The circular shape also offers a practical advantage of measuring the membrane forces by strain gauged steel rings instead of expensive individual load cells. The ring, in close and firm contact with the slab specimen at the level of bottom reinforcement, provides a predetermined restraint (between F_R = 0.50 to 0.75 in this case) and the tangential strains in the ring measured by the gauges can be transformed into radial membrane forces by applying the equations of Lammè. There were three rings, one for each specimen thickness, in order to provide the prescribed range of restraint factor F_R.

The testing apparatus is given in Figure 15, including the supporting frame, the restraining ring and the specimen proper. The specimens were cast in a polished steel tray, assuring a circumferential accuracy close to one thousands of an inch. Figure 16 illustrates the delicate setup, consisting of pairs of 30° segmental wedges, that were placed and tapped between the specimen and the constraining ring to provide firm and uniform line contact during testing. The load was concentrically applied through a 2.5 in. (63 mm) diameter neoprene pad.

All specimens failed in punching shear as predicted. Initially, two perpendicular cracks formed on the underside of the specimen, intersecting at the point of load application. Subsequently, an additional pattern of radial cracking appeared and failure occurred when a large circular crack formed, defining the boundary of the frustum being pushed out. Figure 17 depicts the cross section, cut by saw, of a typical specimen failed in punching shear.

The measured restraining force is plotted against the applied load for four selected specimens in Figure 18. The better than linear development of the restraining force is quite similar to that observed by others (Ref.5), as indicated in Figure 12. The difference is that in this case, the tests were terminated prior to the membrane force reaching its maximum in order to prevent damage occurring to the testing apparatus at failure. The initial restraining force indicated in Figure 18 is due to the preloading that was unavoidable when the wedges were tapped into their secure positions.

Theoretical results and experimental data regarding failure loads are compared in Figure 18. If they were identical, the dots would coincide with the 45° line drawn. It can be seen that with the exception of two tests, the 45° line serves as a lower bound to all data, confirming that the mathematical model provides safe, conservative predictions for the ultimate load carrying capacity of bridge deck slabs within the range tested.

Encouraged by this outcome, the computer program was then to investigate a number of combinations of span-to-thickness ratio, reinforcement percentage and restraint, corresponding to the specimens tested. The results of this investigation are given in Table 1, emphasizing the dramatic effect of restraint on the failure load of underreinforced slabs and giving a feeling of magnitude of actual load carrying capacities.

Prototype Tests

Simultaneously with the modelling work at Queen's University and at home by MTC, a testing vehicle, a tractor/semi-trailer combination, illustrated in Figure 20, has been constructed. As an afterthought, the trailer has been fitted out with a hydraulic punching device, shown in Figure 21, capable of transmitting a load of 125 kips (555 kN). The system includes a hydraulic jack, a load cell, two 10 in (254 mm) square neoprene loading pads at 3 in (76 mm) apart, controlled by a set of four valves. Central deflection of the slab is measured by an LVDT attached to a 12 ft. (3.6 m) long aluminum bar. The output from the load cell and the deflectometer drive the pen of an X-Y recorder carried by the vehicle, and is visible to the valve operator. A typical load/displacement curve, using cyclic loading, is shown in Figure 22.

The original purpose of the punching apparatus had been to proof test a large number of bridges, whose concrete decks exhibited an advanced state of deterioration. Such a state is usually indicated by extensive cracking and the percolation of water through the cracks, as depicted in Figure 23. The continuous seepage of water results in stalactites and an unmistakeable dark greyness of the concrete due to saturation.

The proof-testing project included 40 bridges with well over 200 individual tests (Ref.12). The maximum applied test load was limited to 100 kips (445 kN), although the system permitted 125 Kips (555 kN). If the deflection obtained was greater than anticipated, the test was repeated in a cyclic fashion. When the upper tips of the resulting hysteresis curves diverged, the test was discontinued for fear of destroying the slab and the maintenance forces were advised regarding the deteriorated state of the structure. These latter were only a very few.

There were two failures, both occurring on the same bridge, approximately at 65 kips (288 kN) during the first stroke of testing and without warning. One of the failures is illustrated in Figure 24. The circumstances of the failures were investigated and it was noted that in many places the concrete was reduced to sand and gravel due to deterioration and leeching and both locations were on the cantilevered part of the slab

1 kip ≅ 4,5 kN

where membrane forces cannot develop. The bridge has since been replaced.

The large volume of prototype test results has also permitted an investigation regarding the actual restraint factor F_R in existing bridges. The investigation consisted of running the computer program using measured parametric data and varying the restraint factor until a match between the observed and calculated deflection was reached. The figures listed in Tables 2 to 4 seem to indicate that a minimum value of $F_R = .50$ is present for all composite structures, while in non-composite bridges the lower bound value is about $F_R = .25$. This observation, in conjunction with Table 1 provides, a better assessment of the actual load carrying capacity of existing bridges.

In order to verify the predictions derived from various model analyses, MTC decided to construct a number of panels with reduced percentage of reinforcement in the Conestogo bridge (Ref.13), a structure designated for trying out a number of engineering innovations. There were three variables:

a. slab thickness; 7.0, 7.5 and 8.0 in. (178, 190 and 203 mm)

b. reinforcement: 0.2, 0.3, 0.6 and 1.0 percent

c. concrete cover: 2.0, 2.5 and 3.0 in (51, 63 and 76 mm)

providing a total of 36 panel combinations. All the panels were successfully tested for a 96 kips (422 kN) load by the punching device. Stresses in reinforcing bars were monitored in most of the panels and were found acceptable for all cases. It was observed, however, that all panels with 0.2 percent reinforcement, i.e. #4 bars at 16 in. (407 mm) centres - depicted in Figure 25, exhibited excessive cracking that did not disappear after the removal of the load.

At the same time, panels with 0.3 percent reinforcement - regardless of the other parameters involved, showed only hairline cracking of limited extent that became invisible after the load was removed. Since, in the practical range of commercial vehicle capacity for axle loads, these cracks did not open up, the 0.3 percent was empirically accepted as satisfactory for serviceability limit states and all further structures were built to that criterion.

In addition to resisting punching loads, the concrete deck slab is engaged as a transverse flexural component in distributing live loads to the supporting beams. As such, peak negative moments are expected to develop in the slab where supported in accordance with the theory of flexure. In order to clarify the issue, a four-girder bridge was tested using the punching device. In addition to central deformation, deflections were also measured at a number of points along a transverse line passing through the point of load applications.

The bridge deck, loaded to 100 kips (445 kN), thus provided a transverse deflection diagram illustrated in Figure 26. Transverse curvatures were calculated by a double derivation, and using sectional and material properties, transverse moments and stresses were established. The calculations indicate that the maximum tensile stress in the top of the deck would, under no circumstances, exceed 200 psi (1.4 mPa) - a fact also borne out by hundreds of other bridge decks without longitudinal cracks. One important conclusion of this test was that increasing the concrete cover to 3 in. (76 mm) over the top reinforcement would result in no detrimental effects.

In contrast, a new concrete bridge deck supported by and composite with two trapezoidal steel girders, was found to exhibit a 55 ft (16.8 m) long longitudinal crack coinciding with one of the internal steel webs (Ref.14). This bridge had been built with 0.3 percent reinforcement, was extensively tested and became a concern because of the crack.

These type of bridges are constructed with temporary diaphragms between the boxes to provide dimensional stability while the slab concrete is being placed. After the concrete set, the diaphragms are usually removed for architectural reasons. Further computations revealed that the torsional stiffness of the closed boxes cause extremely high transverse bending stresses when differential vertical displacements occur between the boxes due to live loads. In order to prevent this from happening, diaphragms will not be removed in the future.

The basic experimental data (Ref.6) were derived from steel beam models with diaphragms. Due to construction requirements, these diaphragms are always present in steel bridges. As in prestressed concrete beam bridges the construction of the diaphragms is rather cumbersome, time-consuming and expensive, MTC investigated a bridge, by testing, regarding the effect of eliminating all diaphragms except those at the supports (Ref.15). The bridge consists of three spans, four girders continuous for live load, a composite concrete slab: it is perhaps the most common in present day construction.

The bridge was extensively instrumented and tested, for both punching shear and overall vehicle weight effects. It has been concluded that in the tested range, concrete slabs with 0.3 percent reinforcement, supported by pre-cast-prestressed AASHTO girders do not require the assistance of intermediate disphragms to develop the necessary membrane forces.

Provisions of the Ontario Bridge Code

While in general, designing a bridge to the provisions of the Ontario Bridge Code (OHBDC) will be more time consuming, requiring a better understanding of structural behaviour and more attention to details, the design of reinforced concrete slabs supported by beams will be simplified if the slabs satisfy certain conditions. These are in accordance with Clause 7.8.5.2;

"(a) The span length of a slab panel perpendicular to the direction of traffic shall not exceed 3.7 m (12.1 ft.), and the slab shall extend at least 1.0 m (3.3 ft.) beyond the centreline of the external longitudinal supports of a panel. In the case of an external panel a curb integral with the slab may be used instead of the 1.0 m overhang, provided that the combined cross-sectional area of slab and curb, beyond the centreline of the external girder, is not less than the cross-sectional area of one metre length of deck slab.

(b) Span length to thickness ratio of the slab shall not exceed 15 (span is defined as the distance between edges of flanges plus one half the stringer or girder flange width).

(c) Slab thickness shall not be less than 190 mm (7.5 in), and spacing of the isotropic reinforcement bars in each face shall not exceed 300 mm (12 in).

(d) All cross frames and diaphragms shall extend throughout the cross section of the bridge between external girders, and the maximum spacing of such cross frames or diaphragms shall be as follows:

Steel I and Box Girders: 7.5 m (24.6 ft.)

Reinforced and prestressed concrete girders: diaphragms shall be provided at abutments and piers.

(e) Spacing of shear connectors in steel/concrete composite systems shall not exceed 0.6 m (24 in).

(f) Edge stiffening shall be provided for all slabs having main reinforcement parallel to traffic."

In addition to the basic 0.3 percent reinforcement, the Code requires additional top (negative) steel for cantilever moments. Considering other, non-quoted provisions, a balanced design - i.e. external and internal girders subjected to same load effects - will result in distance of approximately 0.7 m (2' - 4") between the curb and centreline of external girder. It is expected that the basic reinforcement will be satisfactory for all designs with curb only. In case of wider sidewalks, additional steel maybe necessary, but the Code permits considering the thickened parts of the slab and parapet walls as edge beams for load distribution.

The basic equation of the Code to be met at ultimate limit states for punching shear is:

$$.65\ R \geq 1.20\ D + 1.40\ (1 + i)L$$

where R = failure load

D = dead load effect - about 0.20L

i = impact : 0.45

L - live load effect

For the values stated : R ≥ 3.49L and with L = 100 kN (22.5 kips) 1kip ≙ 4,44kN

R ≥ 350 kN (78.5 kips) or an axle load of 700 kN (157.0 kips). This value can be compared with the maximum practical single axle load of 255 kN (57.5 kips) and the maximum practical tandem axle load of 490 kN (110.0 kips) described earlier.

Reinforcing steel percentage is calculated on the basis of effective area of the concrete slab, i.e. from the interface of the two bottom isotropic layers of steel to the top of the concrete. For a 190 mm (7½ in) slab, 0.3 percent is equal to a

#4 bar @ 305 mm (12 in.) and 0.2 percent a #5 bar @ 407 mm (16 in) centres.

Conclusions and Recommendations

1. A mathematical model, incorporating arching effects in concrete slabs, by which the ultimate load carrying capacity can be predicted, has been assembled and verified by both laboratory model and prototype tests.

2. If the bridge deck meets certain geometrical and structural conditions, 0.3 percent isotropic reinforcement satisfies both serviceability and ultimate limit states criteria of the Ontario Bridge Code.

3. Considering that no design is required in using the empirical process described, the obvious economy in construction and the expected improvement of the deck performance due to 3 in (76 mm) cover over the top reinforcement, the adoption of the 0.3 percent reinforcement is recommended.

List of Figures

References

1. "Effective Width of Concrete Bridge Slabs Supporting Concentrated Loads" by E. F. Kelley, Public Works, March 1926
2. "Computation of Stresses in Bridge Slabs due to Wheel Loads" by H. M. Westergaard, Public Works, March 1930
3. "Shearing Strength and Flexural Cracking and Capacity of Two-way Slabs Subjected to Concentrated Loads" by Y. Aoki and H. Seki - ACI Publication SP-30, 1971
4. "Compressive Membrane Enhancement in Two-way Bridge Slabs" by P. Y. Tong and B. deV. Batchelor, ACI SP-30, 1971
5. "Membrane Action in Slabs" by J. F. Brotchie and M. H. Holley, ACI SP-30, 1971
6. "Investigation of the Ultimate Strength of Deck Slabs of Composite Steel/Concrete Bridges" by D. deV. Batchelor, B.E. Hewitt, P. Csagoly and M. Holowka - Transportation Research Record 664, 1978.
7. "Investigation of the Fatigue Strength of Deck Slabs of Composite Steel/Concrete Bridges" by B. deV. Batchelor, B. E. Hewitt and P. Csagoly, TRR 664, 1978.
8. "Fatigue of Concrete" by G. M. Norby, ACI Proceedings, Vol.55, 1958
9. "Punching of Concrete Slabs without Shear Reinforcement" by S. Kinnunen and H. Nylander, Transactions of The Royal Institute of Technology, Stockholm, No.158, 1960
10. "An Investigation of the Punching Strength of Restrained Slabs with Particular Reference to the Deck Slabs of Composite I-beam Bridges" by B. E. Hewitt, Ph.D. thesis, Queen's University, Kingston, Ontario, 1972.

Tables

2,4m

SLAB SPAN	PROTOTYPE IDENTIFICATION THICKNESS	SPAN/THICKNESS RATIO	STEEL%	AVERAGE FAILURE	VARIOUS RESTRAINT VALUES Fr=0 (kips)	Fr=0.25 kips	Fr=0.50 kips	Fr=0.75 kips	Fr=1.0 kips
8' - 0"	5.34"	18.0	0.2	94kips	11	43	73	99	121
			0.3	97kips	16	47	75	100	121
			1.0	103kips	38	52	86	110	134
8' - 0"	6.40"	15.0	0.2	150kips	18	66	108	146	
			0.3	140kips	27	72	112	149	180
			0.8	155kips	55	91	127	162	196
			1.0	155kips	62	97	132	168	202
8' - 0"	7.47"	12.8	0.2	173kips	27	95	153	205	250
			0.3	201kips	40	103	159	210	255
			0.8	182kips	86	138	186	235	281
			1.0	191kips	99	148	195	243	291

TABLE 1. PROJECTED PROTOTYPE CAPACITIES.

Table 2. Steel beam and concrete slab (non-composite).

Bridge Number	Stringer Spacing (m)	Stiffener Spacing (m)	Slab Thickness (mm)	Main Rebars (mm)	Distribution Rebars (mm)	Experimental Deflection (mm)	Concrete Strength (MPa)	Restraint Factor (F_r)
S1	1.83	3.81	180	#5 @ 305 (T) #5 @ 150 (B)	#5 @ 305 (T) #5 @ 150 (B)	3.56 3.81	52.5 62.7	0.25 0.23
S2	1.74	4.78	180	#5 @ 150 (T) #5 @ 150 (B)	#5 @ 455 (T) #5 @ 915 (B)	2.29 5.08 4.57	54.7 54.7 40.8	0.33 0.20 0.21
S14	1.75	7.62 to 4.72	180	#5 @ 150 (T + B)	#5 @ 455 (T + B)	2.29 2.79	53.7 43.5	0.33 0.31
S17	2.84	9.14	215	#5 @ 125 (T + B)	#4 @ 510 (T + B)	1.52	41.5	0.71
S32	3.45	3.56	180	#5 @ 150 (T + B)	#5 @ 150 (T + B)	5.08 4.82	32.5 36.4	0.63 0.61
S34	1.83	6.10 to 7.01	180	#5 @ 150 (T + B)	#4 @ 380 (B)	3.56	52.5	0.24
S35	1.52 to 1.84	6.10 to 7.21	180	#5 @ 150 (T + B)	#5 @ 535 (T) #5 @ 455 (B)	2.79 1.78	26.8 44.3	0.34 0.55
S37	3.51	3.12	215	#6 @ 150 (T + B)	#6 @ 150 (T + B)	3.30	19.3	1.00
S39	1.52	3.05	180	#5 @ 150 (T + B)	#4 @ 380 (T + B)	3.56 2.54	27.49 38.52	0.21 0.25

1 ft. = 0.3048 m   1 in. = 25.4 mm   1 psi = 6.89×10^{3} MPa   1 psi = 6.89 kPa

Table 3. Steel beam and concrete slab (composite).

Bridge Number	Stringer Spacing (m)	Stiffener Spacing (m)	Slab Thickness (mm)	Main Rebars (mm)	Distribution Rebars (mm)	Experimental Deflection (mm)	Concrete Strength (MPa)	Restraint Factor (F_r)
S23	2.74	5.79 to 8.23	205	#6 @ 230 (T + B)	#4 @ 380 (T) #4 @ 430 (B)	0.71 0.84 1.17	27.6 (design)	1.0 1.0 1.0
S38	2.13	5.49	205	#6 @ 250 (T + B)	#4 @ 305 (T + B)	1.60 1.50 1.02	29.6 27 6 (est) 27.6 (est)	0.75 0.83 1.00
S18	1.93	5.72	180	#5 @ 150 (T + B)	#5 @ 305 (T + B)	1.78	18.9	1 00
S37	3.51	3.15	215	#6 @ 150 (T + B)	#6 @ 150 (T + B)	3.05 2.80	48 6 27 6 (est)	0 80 1.00
B1	1.93	4.46	195	#5 @ 150 (T + B)	#5 @ 380 (T + B)	1.65	27.6	0.96
B2	2.59	7.51	195	#5 @ 150 (T + B)	#5 @ 305 (T + B)	1.78	37 3	0 75
B3	1.83	4.34	190	#6 @ 230 (T + B)	#4 @ 230 (T + B)	1 35	28.5	1.00
B4	1.83	4.57	180	#6 @ 230 (T + B)	#4 @ 230 (T + B)	1.65	25.1	0 98
B5	3.17	6.74	215	#5 @ 150 (T + B)	#5 @ 305 (T + B)	1.78	38.00	0 94

1 ft. = 0.3048 m 1 in. = 25.4 mm 1 psi = 6.89×10^3 MPa 1 psi = 6.89 kPa

Table 4. Concrete beam and concrete slab (monolithic).

Bridge Number	Stringer Spacing (m)	Stiffener Spacing (m)	Slab Thickness (mm)	Main Rebars (mm)	Distribution Rebars (mm)	Experimental Deflection (mm)	Concrete Strength (MPa)	Restraint Factor (F_r)
S3	3.15	7.01 & 10.36	200	#5 @ 150 (T + B)	unknown	1.40	42.9	1.0
S5	7.77	2.13	215	#5 @ 280 (T) #5 @ 140 (B)	#4 @ 535	0.58 0.97 0.99 0.71	67.9 60.1 66.0 60.1	0.75 0.50 0 48 0.71
S6	3.20	10.36	255	#5 @ 190 (T + B)	#4 @ 305	0.46 0.48 0.37	76.1 74.2 56.6	0.75 0.75 0.75
S10	2.95	3.74	230	#5 @ 150 (T + B)	#5 @ 455 (T + B)	0.71 0.71 0.38	61.1 71.1 55.9	0.75 0.63 1.00
S15	3.04	5.49 & 7.32	180	#4 @ 125 (T + B)	#4 @ 610 (T + B)	1.27	42.6	1.00
S22	1.83	4.80	200	#4 @ 150 (T + B)	#4 @ 455 (T + B)	1.52	68.3	0.40
S32	3.30	-	200	#5 @ 150 (T + B)	#4 @ 610 (T) #4 @ 510 (B)	2.29 1.45	36.4	0.82 1.00
S42	1.93		200	#5 @ 280 (T) #5 @ 140 (B)	#4 @ 510 (B)	0.28 0.25 0.28	27.6 (assumed)	1.00 (all)

1 ft. = 0.3048 m 1 in. = 25.4 mm 1 psi = 6.89 x 10³ MPa 1 psi = 6.89 kPa

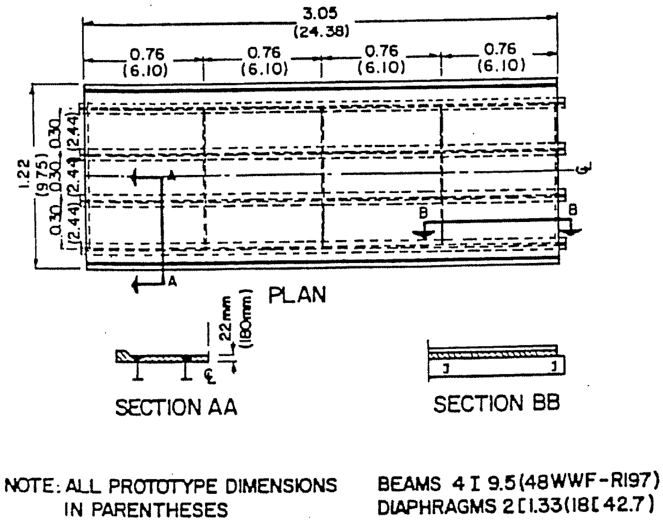

Figure 1, Details of Prototype Four-Girder Bridges

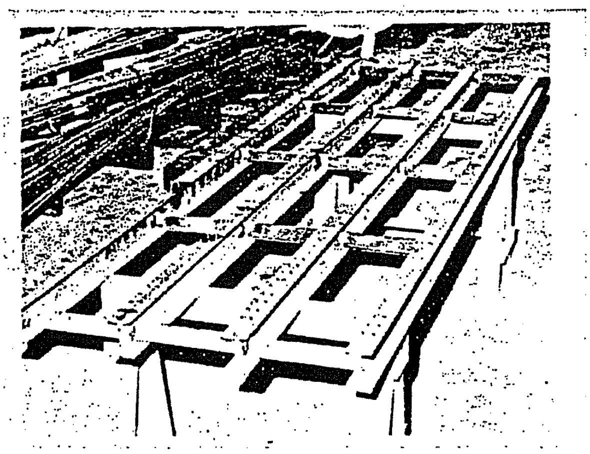

Figure 2, View of Four-Beam Model

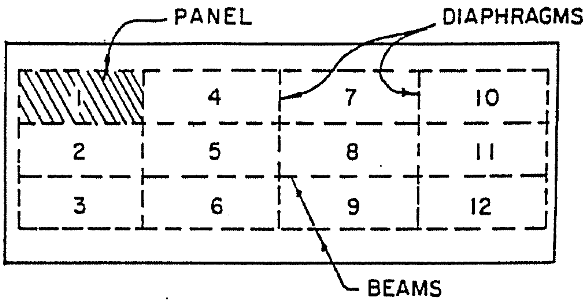

Figure 3, Designation of Bridge Panels

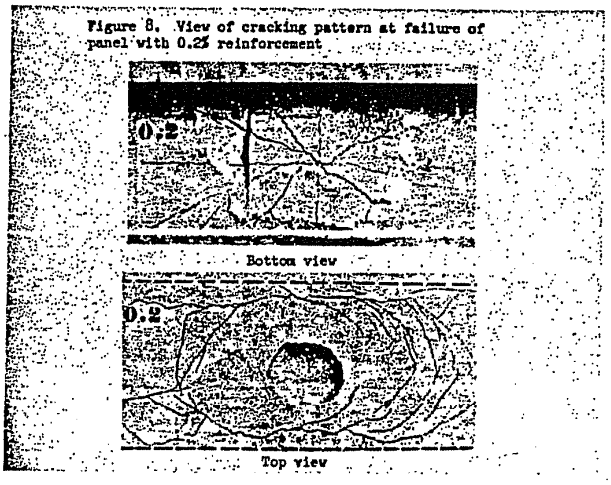

Figure 4, View of Cracking Pattern at Failure of a Panel

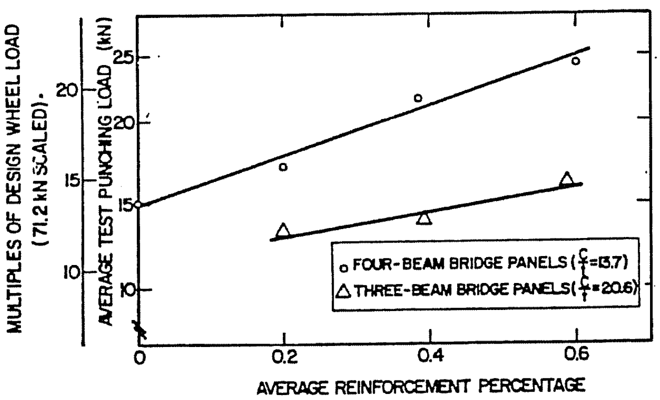

Figure 5, Load v. Isotropic Reinforcement Percentage

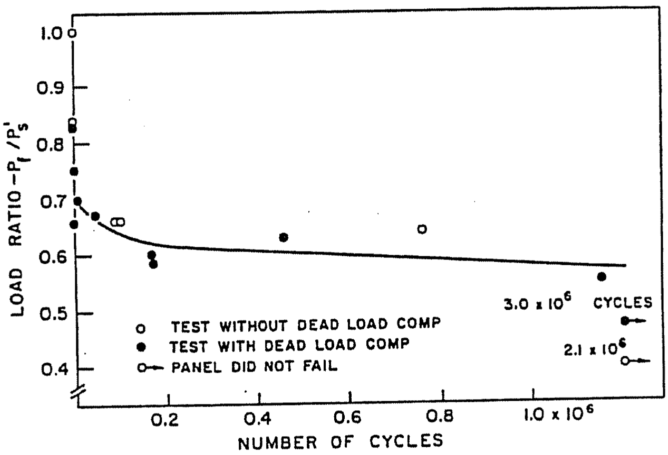

Figure 6, Fatigue Failure of Orthotropically Reinforced Slabs

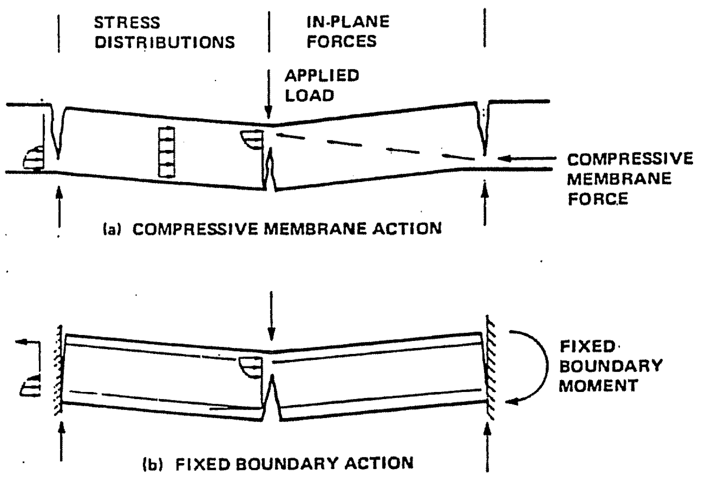

Figure 7, Arching Action in Deck Slabs

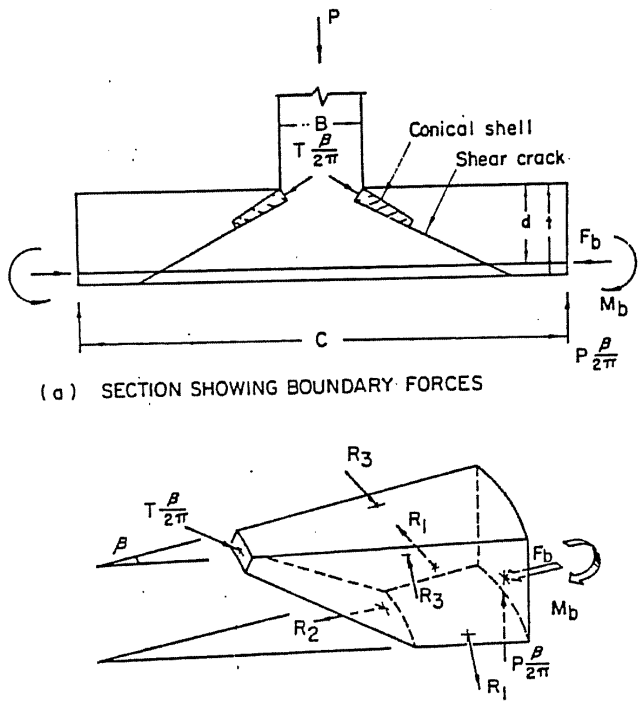

Figure 8, Mechanical Model of a Slab with Boundary Restraints

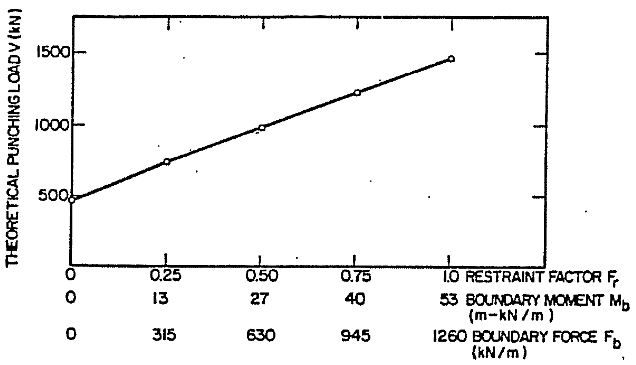

Figure 9, Variation of Theoretical Punching Load with Restraint Factor

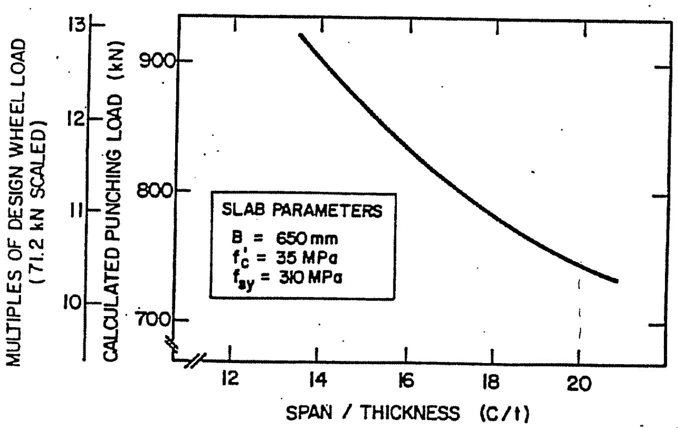

Figure 10, Variation of Theoretical Punching Load with Span-to-Thickness

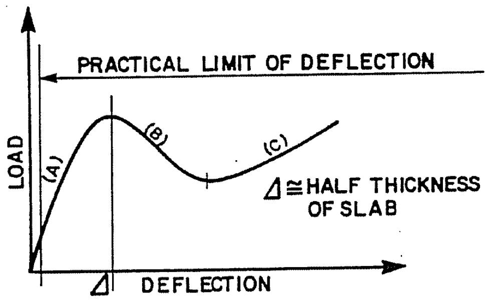

Figure 11 Deflection - Load Curve

Figure 11, Typical Load-Deflection Curve for Underreinforced Slab

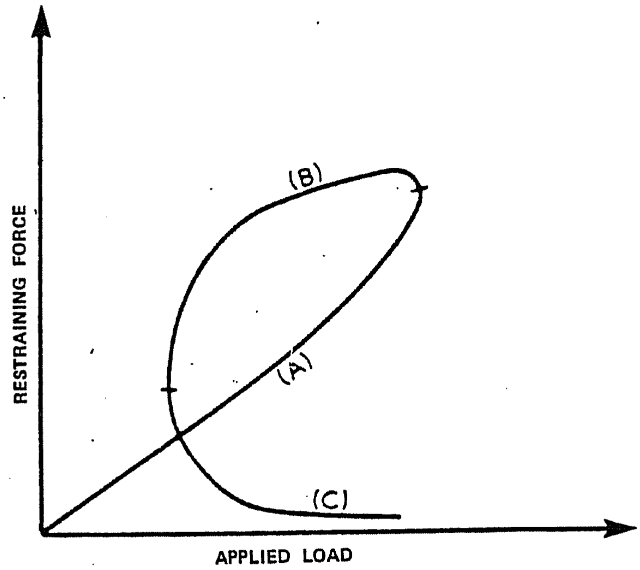

Figure 12, Typical Load-Restraining Force Curve

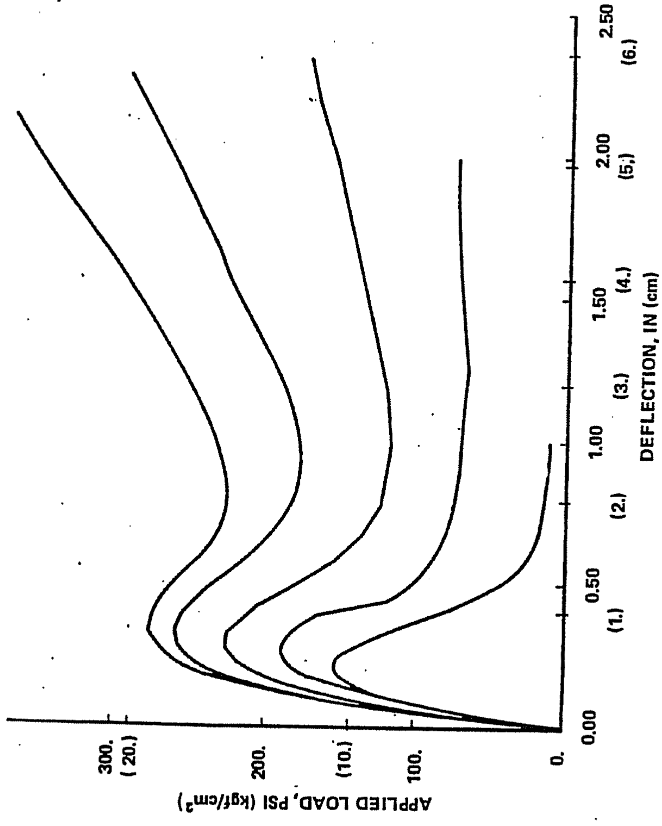

Figure 13, Load-Deflection Curves for Span-to-Depth Ratio of 10

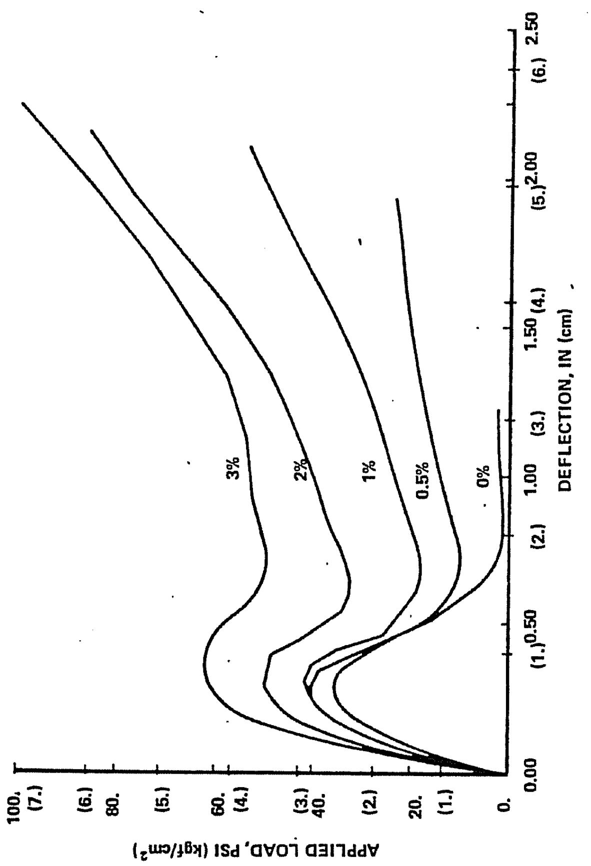

Figure 14, Load-Deflection Curves for Span-to-Depth Ratio of 20

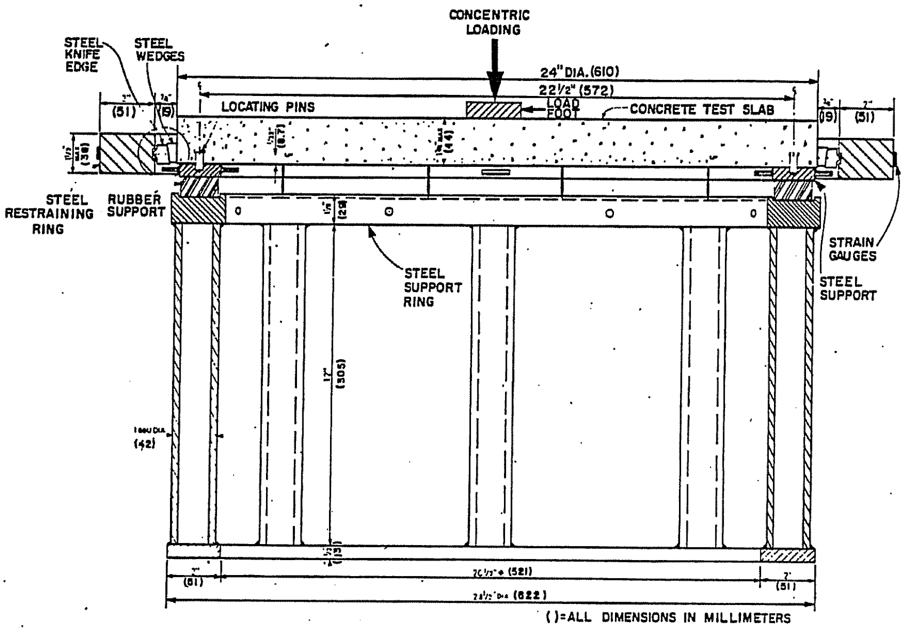

Figure 15, Section Through Testing Apparatus

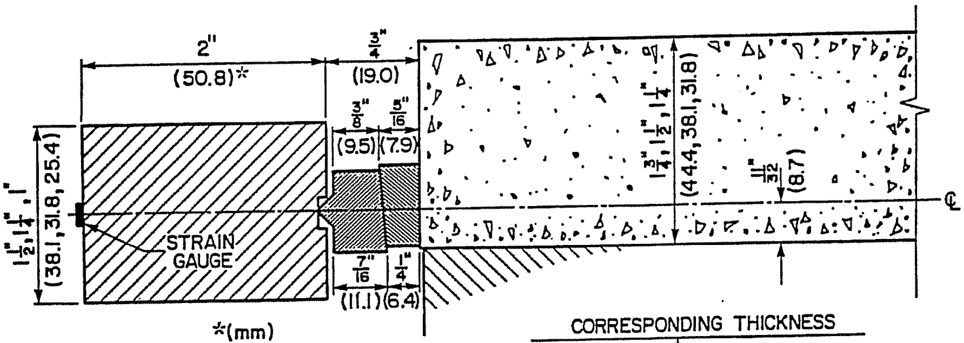

CORRESPONDING THICKNESS

STEEL RINGS	CONCRETE SLABS
1 1/2" (38.1mm)	1 3/4" (44.4mm)
1 1/4" (31.8mm)	1 1/2" (38.1mm)
1" (25.4mm)	1 1/4" (31.8mm)

FIGURE 16 METHOD OF PROVIDING AN AXIAL RESTRAINING FORCE

Figure 16, Method of Providing an Axial Restraining Force

Figure 17, Cross Section of Specimen Failed in Punching Shear

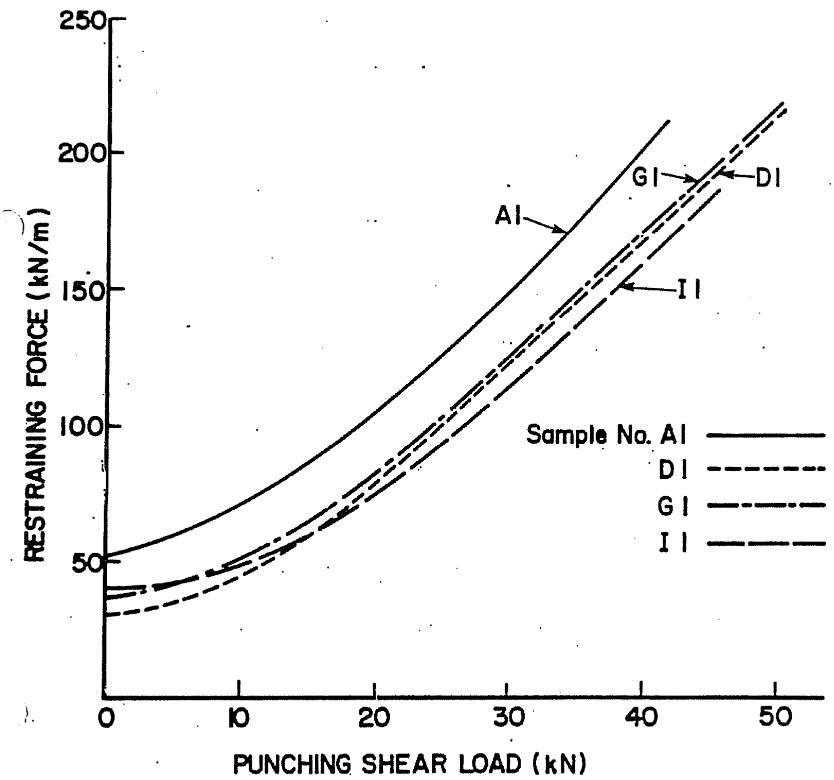

Figure 18, Membrane Force as Function of Applied Load

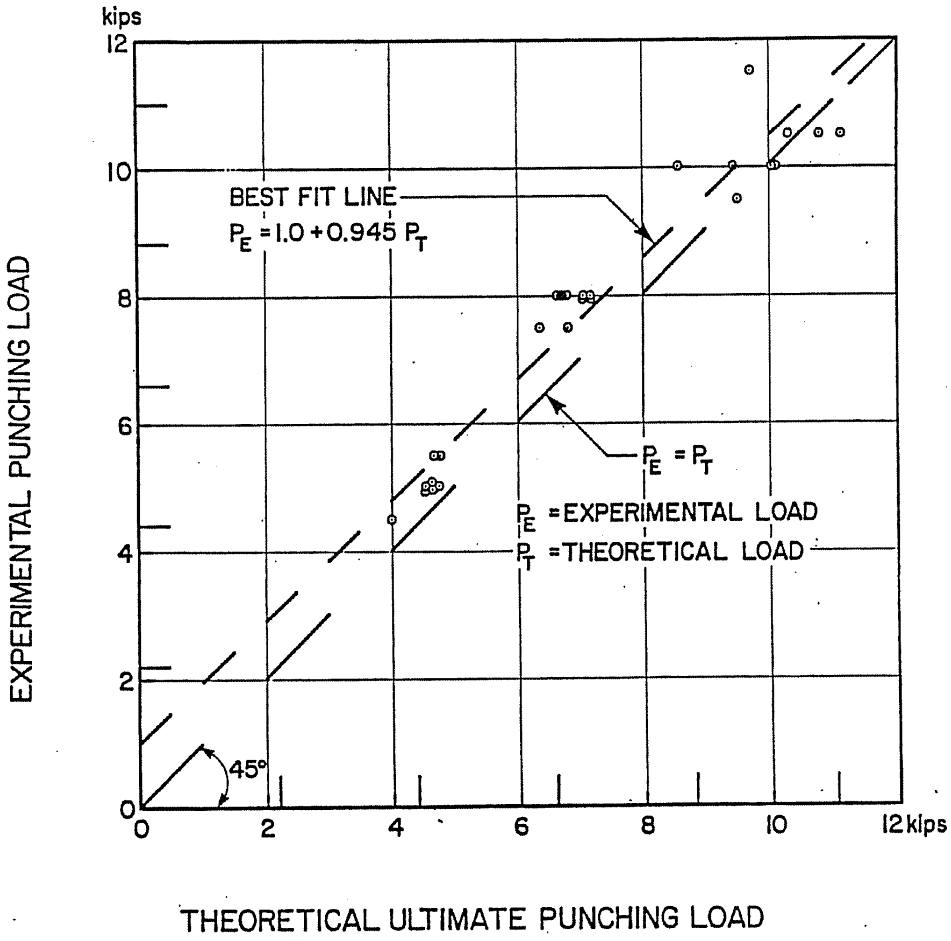

Figure 19, Comparison Between Theoretical and Experimental Results

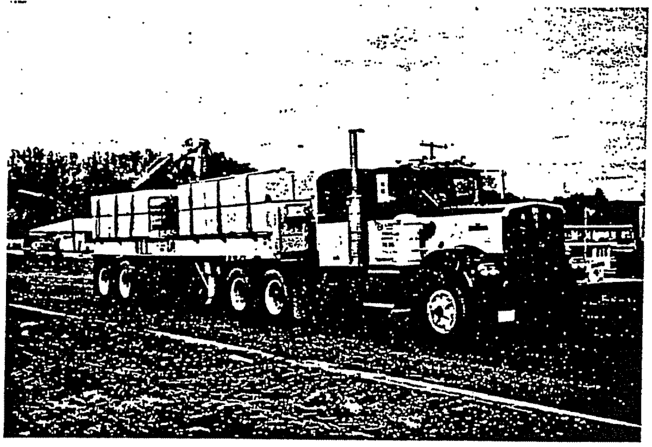

Figure 20, MTC Bridge Load Testing Vehicle

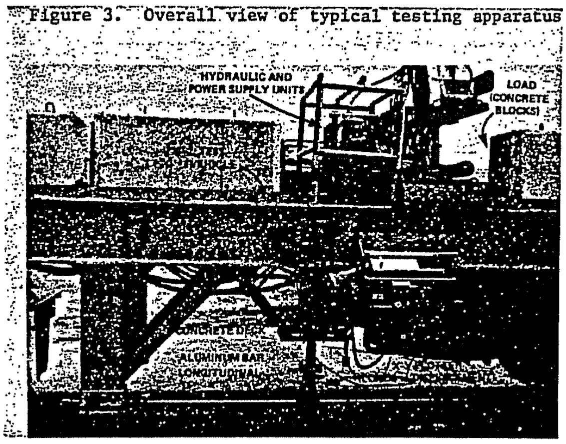

Figure 21, Overall View of Punching Shear Testing Apparatus

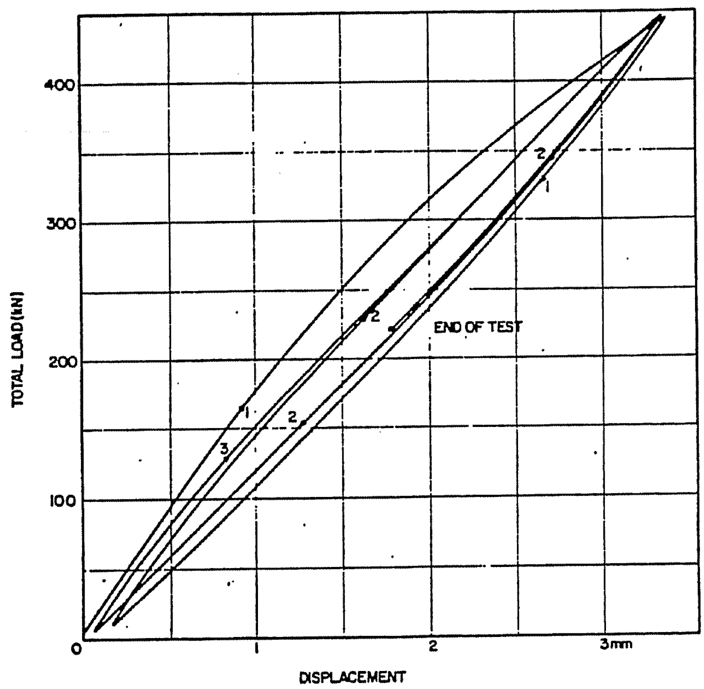

Figure 22, Plot of Typical Load/Deflection Curve

Figure 23, Typical Slab in Advanced State of Deterioration

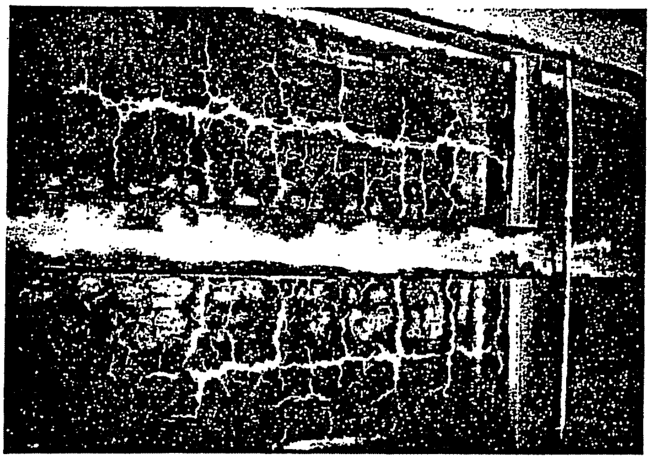

Figure 24, Punching Failure of a Bridge Deck

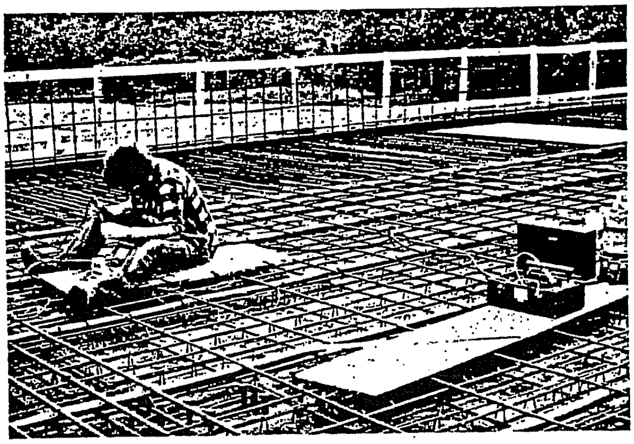

Figure 25, 0.2 Percent Reinforcement Being Installed

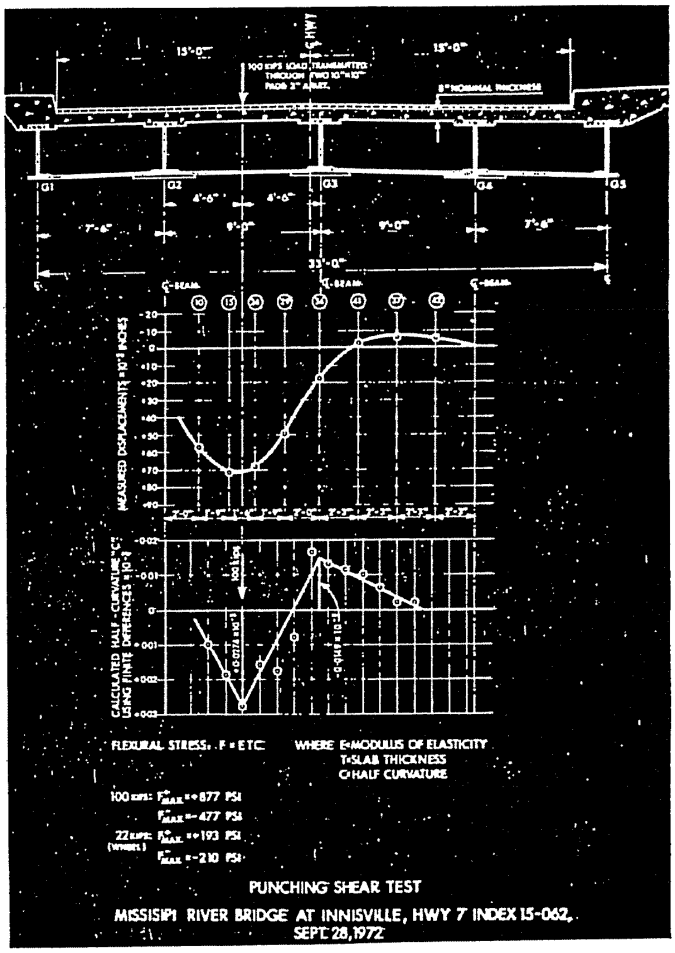

Figure 26, Results of the Innisville Bridge Test

Appendix E: New Zealand code

6.1 Introduction

6.1.1 General

(a) Objective

The objective of evaluation of an existing bridge or culvert is to obtain parameters which define its load carrying capacity. Two parameters are required - one for main members and one for the deck.

The overall procedure is summarised in 6.1.5. The process shall take account of the actual condition of the structure and the characteristics of the traffic and other loads. If at some future date, any of the conditions change significantly, the structure shall be re-evaluated accordingly.

(b) Rating and Posting

Evaluation may be carried out at two load levels (see definitions in 6.1.2):

(i) Rating Evaluation

Rating parameters define the bridge capacity using overload load factors or stress levels, i.e., those appropriate for overweight vehicles.

(ii) Posting Evaluation

Posting parameters define the bridge capacity using live load factors or stress levels, i.e., those appropriate for conforming vehicles.

Because much of the procedure is identical for these two types of evaluation, the criteria are presented together, and where appropriate, the different procedures are set out side by side on the page.

(c) Culverts

Culverts shall be treated on the same basis as bridges, except that further evaluation of a culvert is not required, provided the following apply:

(i) it has a span less than 2 m, and

(ii) it has more than 1 m of fill over it, and

(iii) it is undamaged, and

(iv) there are no unusual circumstances.

For most culverts, evaluation of the top slab as a deck will be sufficient.

6.1.2 Definitions

Rating:	The proportion of the Rating Load which the bridge can withstand under overload criteria. It is expressed as a percentage, defined as the Class for main members, and an alphabetic symbol defined as the Grade for decks.
Rating Load:	A load consisting of one lane of conforming vehicles (taken as 0.85 HN), plus one lane containing an overweight vehicle loaded to the maximum which would be allowed to cross a Class 100 Grade A bridge unsupervised, as set out in the *Overweight Permit Manual*(1) (taken as 0.85 HO), including impact. See 6.4.3.
Overweight Vehicle:	A vehicle which exceeds the load limits set out in the *Heavy Motor Vehicle Regulations*(2), and therefore requires an overweight permit.
Overload Capacity:	The section capacity, in terms of the net unfactored service load, of a critical member or group of members at load factors or stress limits appropriate to overweight vehicles. See 6.4.2.
Posting:	The proportion of the Posting Load which the bridge can withstand under live load criteria. It is expressed as a percentage for main members, and a specific axle load for decks.
Posting Load:	A load consisting of conforming vehicles in each of two lanes, taken to be 0.85 HN, including impact. See 6.4.3.
Conforming Vehicle:	A vehicle loaded to the limits set out in the *Heavy Motor Vehicle Regulations*(2).
Live Load Capacity:	The section capacity, in terms of the net unfactored service load, of a critical member or group of members at load factors or stress limits appropriate to conforming vehicles. See 6.4.2.

6.1.3 Rating Requirements

(a) These requirements apply to all bridges on roads controlled by authorities participating in the Transit New Zealand policy for overweight permits as set out in the *Overweight Permit Manual*(1). This requires an inventory of structural capacity for overload to be maintained for each bridge. This is expressed as the Rating, defined in 6.1.2. By comparing a specific overweight vehicle with the Rating Load, and use of the Bridge Rating, an estimate of the effect of the vehicle on the bridge can be made, as described in the *Overweight Permit Manual*(1).

In the case of State Highways, and some of the major alternative routes, the inventory is in the form of basic moment and shear, or other capacities of bridge members, stored in the Highway Permits computer system(3). This enables the effects of a specific overweight vehicle on any bridge to be determined more accurately than by use of the Rating alone.

(b) The procedures set out in Section 6 are intended to be used for existing bridges which require evaluation. New bridges designed to HN-HO-72 and fully complying with the design requirements of this document also require rating, and the methods could be used for this. However, unless rating information is readily available, or there are unusual circumstances, all new bridges shall be evaluated on their design capacities. Since the rating load is 0.85 times the design load, the Class is 100/0.85 = (say) 120%, and the grade is A. Capacities entered into the Highway Permits system should be the design values of HO or HO + HN moment, shear or other parameters as appropriate, with impact and eccentricity.

6.1.4 Posting Requirements

If a bridge has insufficient capacity to sustain loads at normal live load factors or stress levels, up to the maximum allowed by the *Heavy Motor Vehicle Regulations*[2], it is required to be posted with a notice showing its allowable load, or Posting, as defined in 6.1.2.

6.1.5 Evaluation Procedure

The steps necessary for a full evaluation, either for rating or posting, are shown in Table 6.1. Details of each step will be found in the clauses referenced.

Table 6.1: Evaluation Procedure

<table>
<tr><td>Step 1</td><td colspan="4">Carry out site inspection, (6.2).</td></tr>
<tr><td>Step 2</td><td colspan="4">Determine appropriate material strengths, (6.3).</td></tr>
<tr><td>Step 3</td><td colspan="4">Identify critical section(s) of the main supporting members, and the critical effect(s) on them, (6.4.1).</td></tr>
<tr><td>Step 4</td><td colspan="4">Determine the overload capacity and/or the Live Load Capacity, at each critical main member section, (6.4.2).</td></tr>
<tr><td>Step 5</td><td colspan="2">If rating is being done manually:

Analyse the structure for effects of rating or posting load at each critical section, (6.4.3).</td><td colspan="2">If data is to be entered into the Highway Permits system:

Follow the requirements for main member element data in the Highway Permits Assurance Manual(3), (6.4.6)</td></tr>
<tr><td>Step 6</td><td colspan="2">Determine rating or posting percentage, (6.4.5)</td><td colspan="2"></td></tr>
<tr><td>Step 7</td><td colspan="3">Concrete deck:

Determine if the empirical method is applicable, (6.5.2(a)).</td><td>Timber deck:

-</td></tr>
<tr><td>Step 8</td><td>If empirical method is applicable:

Determine ultimate wheel load, (6.5.2(b)).</td><td colspan="2">If empirical method is not applicable:

Determine section capacity per unit width at critical locations in slab, (6.5.3(a)).</td><td>Determine section capacity of the nominal width of deck considered to carry one axle, (6.5.4(a)).</td></tr>
<tr><td>Step 9</td><td>-</td><td colspan="2">Analyse the deck for rating or posting loads, (6.5.3(b)).</td><td>Determine moments due to rating or posting axle loads, (6.5.4(b)).</td></tr>
<tr><td rowspan="2">Step 10</td><td colspan="4">Determine Deck Capacity Factor and/or allowable axle load.</td></tr>
<tr><td>(6.5.2(c))</td><td colspan="2">(6.5.3(c))</td><td>(6.5.4(c))</td></tr>
<tr><td>Step 11</td><td colspan="4">If data is to be entered into Highway Permits System, follow the requirements for deck element data in Highways Permits Assurance Manual(3).</td></tr>
</table>

6.2 Inspection

6.2.1 General

Appropriate inspection shall be carried out as a part of the evaluation of the load carrying capacity of any bridge, to determine member condition, and to verify dimensions. Where necessary, the extent of corrosion or decay shall be determined by physical measurement.

The following significant characteristics of the roadway and traffic shall be assessed:

- position of lane markings;
- roughness of deck and approaches;
- mean speed of heavy traffic;
- heavy traffic type, and proportion of the total vehicle count.

Some guidelines on inspection are contained in *Bridge Inspection Guide*[(4)].

6.2.2 Impact Factors

Appropriate impact factors shall be determined for the various bridge members. Each value shall be:

either (i) the design value from 3.1.5, or in the case of timber elements, from 4.4.2.

or (ii) a value derived from site measurements.

A measured value shall be used if the design value is considered to be unrealistic.

Dynamic measurements shall be made under heavy loads which are representative of actual traffic, in terms of both mass and speed, at either rating load level or posting load level or both. A sufficient number of vehicles shall be included to give confidence in the statistical values chosen. The impact values derived shall be those which are exceeded by less than 5% of vehicles in either category.

6.3 Material Strengths

Material strengths for calculation of section capacity shall be determined as described below. The strengths used shall be characteristic values, as defined in the relevant material code, or determined as in 6.3.6. Where testing is undertaken, a TELARC registered laboratory or other appropriate agency shall be used.

6.3.1 Concrete

Concrete compressive strength shall be determined by one of the following methods:

(a) From drawings, specification or other construction records.

(b) From the following nominal historical values:

Construction Date	Specified Strength, MPa
Up to 1932	14
1933 to 1940	17
1941 and later	21

(c) From cores cut from the bridge.

Cores shall be taken from areas of low stress, in the members being analysed, and so as to avoid reinforcing and prestressing steel. Cutting and testing shall be in accordance with NZS 3112, Part 2(5).

Where core tests are carried out, the statistical analysis described in 6.3.6 shall be applied to determine the compressive strength value to be used in calculations.

6.3.2 Steel Reinforcement

The characteristic yield strength of reinforcement shall be determined by one of the following methods. It should be noted that if the steel is of unusually high strength, sections may in fact be over-reinforced, and the restriction referred to in 6.4.4(a) shall apply.

(a) From drawings, specification or other construction records.

(b) From the following nominal historical values:

Construction Date	Characteristic Yield Strength, MPa
Up to 1932	210
1933 to 1966	250
1967 and later	275

(c) From tensile tests of bar samples of appropriate diameter removed from the bridge members being analysed. Testing shall be in accordance with BS EN 10002-1(6).

(d) From non-destructive tests of bars of appropriate diameter in-situ, after removal of cover concrete. The method used shall have been authenticated by correlation with tests in accordance with BS EN 10002-1(6).

Test locations shall be on the members being analysed, chosen so as to be unaffected by bends or welded splices in bars.

Where testing is performed as in (c) or (d), the statistical analysis described in 6.3.6 shall be applied to determine the characteristic value to be used in calculations. A separate analysis shall be performed for each bar diameter.

6.3.3 Prestressing Steel

The characteristic yield strength or the 0.2% proof stress of prestressing steel shall be determined by one of the following methods:

(a) From drawings, specification or other construction records.

(b) From the lowest alternative value specified in BS 5896[7] for the wire or strand diameter.

6.3.4 Structural Steel

The characteristic yield strength of structural steel shall be determined by one of the following methods:

(a) From drawings, specification or other construction records.

(b) From the following nominal historical values:

Construction Date	Characteristic Yield Strength, MPa
Up to 1940	210
1941 and later	230

(c) From tensile tests of coupons removed from the members being analysed, in areas of low stress. Testing shall be in accordance with BS EN 10002-1[6].

(d) From non-destructive tests of the steel in-situ.

Where testing is performed as in (c) or (d), the statistical analysis described in 6.3.6 shall be applied to determine the characteristic value to be used in calculations.

6.3.5 Timber

Characteristic stresses shall be in accordance with NZS 3603[8], or where applicable, AS 1720.2[9] and AS 2878[10]. Where the species of timber is unknown, it may be determined by removing 10 mm diameter core samples from the bridge and submitting them for expert analysis.

Characteristic stresses shall be based either on the lowest grading of any member in the bridge, or on the actual grading of each timber member, according to the visual grading rules of NZS 3631[11] or, where applicable, AS 2082[12] or AS 2858[13]. The moisture content shall be determined from core samples cut from the bridge.

Characteristic stress/strength modification factors shall comply with the applicable standard, NZS 3603[8] or AS 1720.1[9], except as modified by 4.4.2.

Determination of design stresses for timber is discussed in *Strength and Durability of Timber Bridges*(14).

6.3.6 Analysis of Test Results

In order to obtain characteristic strength values for calculation purposes, results of steel and concrete tests shall be analysed statistically. Each test result shall be the mean of tests on at least two samples taken from one location in the structure, or the mean of two (or more, as required by specific test procedures) non-destructive tests from one location on a bar or member. For analysis, a group of test results shall all originate from similar members or from identical bar diameters as appropriate. Tests shall be taken at sufficient locations to ensure that results are representative of the whole structure, or the entire group of similar members, as appropriate.

An acceptable method of analysis is to determine a value $\overline{X}$ - ks, where:

$\overline{X}$ is the mean of the group of test results
k is a one-sided tolerance limit factor
s is the standard deviation of the test results

k shall be determined on the basis that at least a proportion, P, of the population will be greater than the value calculated, with a confidence, α.

Values of k for various values of P, α and n, the number of test results, are given in Table 6.2.

It is recommended that for structural and reinforcing steel, P and α should both be 0.95, and that for concrete, P and α should both be 0.90.

Table 6.2: One-sided Tolerance Limit Factors for a Normal Distribution

Values of k for α = 0.90

n	P = 0.900	0.950	0.975	0.990	0.999
2	10.253	13.090	15.586	18.500	24.582
3	4.258	5.311	6.244	7.340	9.651
4	3.188	3.957	4.637	5.438	7.129
5	2.744	3.401	3.983	4.668	6.113
6	2.494	3.093	3.621	4.243	5.556
7	2.333	2.893	3.389	3.972	5.201
8	2.219	2.754	3.227	3.783	4.955
9	2.133	2.650	3.106	3.641	4.771
10	2.066	2.568	3.011	3.532	4.628
11	2.012	2.503	2.936	3.444	4.515
12	1.966	2.448	2.872	3.371	4.420
13	1.928	2.403	2.820	3.310	4.341
14	1.895	2.363	2.774	3.257	4.274
15	1.866	2.329	2.735	3.212	4.215
16	1.842	2.299	2.700	3.172	4.164
17	1.819	2.272	2.670	3.137	4.118
18	1.800	2.249	2.643	3.106	4.078
19	1.781	2.228	2.618	3.078	4.041
20	1.765	2.208	2.597	3.052	4.009
21	1.750	2.190	2.575	3.028	3.979
22	1.736	2.174	2.557	3.007	3.952
23	1.724	2.159	2.540	2.987	3.927
24	1.712	2.145	2.525	2.969	3.904
25	1.702	2.132	2.510	2.952	3.882
30	1.657	2.080	2.450	2.884	3.794
35	1.623	2.041	2.406	2.833	3.730
40	1.598	2.010	2.371	2.793	3.679
45	1.577	1.986	2.344	2.762	3.638
50	1.560	1.965	2.320	2.735	3.604
60	1.532	1.933	2.284	2.694	3.552
70	1.511	1.909	2.257	2.663	3.513
80	1.495	1.890	2.235	2.638	3.482
90	1.481	1.874	2.217	2.618	3.456
100	1.470	1.861	2.203	2.601	3.435
120	1.452	1.841	2.179	2.574	3.402
145	1.436	1.821	2.158	2.550	3.371
300	1.386	1.765	2.094	2.477	3.280
500	1.362	1.736	2.062	2.442	3.235
∞	1.282	1.645	1.960	2.326	3.090

Values of k for α = 0.95

n	P = 0.900	0.950	0.975	0.990	0.999
2	20.581	26.260	31.257	37.094	49.276
3	6.155	7.656	8.986	10.553	13.857
4	4.162	5.144	6.015	7.042	9.214
5	3.413	4.210	4.916	5.749	7.509
6	3.008	3.711	4.332	5.065	6.614
7	2.756	3.401	3.971	4.643	6.064
8	2.582	3.188	3.724	4.355	5.689
9	2.454	3.032	3.543	4.144	5.414
10	2.355	2.911	3.403	3.981	5.204
11	2.275	2.815	3.291	3.852	5.036
12	2.210	2.736	3.201	3.747	4.900
13	2.155	2.670	3.125	3.659	4.787
14	2.108	2.614	3.060	3.585	4.690
15	2.068	2.566	3.005	3.520	4.607
16	2.032	2.523	2.956	3.463	4.534
17	2.002	2.486	2.913	3.414	4.471
18	1.974	2.453	2.875	3.370	4.415
19	1.949	2.423	2.840	3.331	4.364
20	1.926	2.396	2.809	3.295	4.319
21	1.905	2.371	2.781	3.262	4.276
22	1.887	2.350	2.756	3.233	4.238
23	1.869	2.329	2.732	3.206	4.204
24	1.853	2.309	2.711	3.181	4.171
25	1.838	2.292	2.691	3.158	4.143
30	1.778	2.220	2.608	3.064	4.022
35	1.732	2.166	2.548	2.994	3.934
40	1.697	2.126	2.501	2.941	3.866
45	1.669	2.092	2.463	2.897	3.811
50	1.646	2.065	2.432	2.863	3.766
60	1.609	2.022	2.384	2.807	3.695
70	1.581	1.990	2.348	2.766	3.643
80	1.560	1.965	2.319	2.733	3.601
90	1.542	1.944	2.295	2.706	3.567
100	1.527	1.927	2.276	2.684	3.539
120	1.503	1.899	2.245	2.649	3.495
145	1.481	1.874	2.217	2.617	3.455
300	1.417	1.800	2.133	2.522	3.335
500	1.385	1.763	2.092	2.475	3.277
∞	1.282	1.645	1.960	2.326	3.090

6.4 Main Member Capacity and Evaluation

6.4.1 General

The bridge Overload and/or Live Load Capacity shall be determined in terms of the net unfactored service load at the critical section of any member or group of identical members which could be critical under any live loading. The capacity of a member may be in any terms - i.e., moment, shear, torsion, direct force, bearing, or an interaction relationship between any of these.

Assumptions which may be made about the behaviour of specific structures in defined circumstances are set out in 6.4.4.

6.4.2 Section Capacity

The gross section capacity shall be calculated using the criteria specified in 4.2 to 4.6 for design, except that load factors shall be taken from Tables 6.3 and 6.4. The measured effects of corrosion or other deterioration shall be taken into account if appropriate.

From the gross section capacity shall be subtracted the dead load effect, and any other effect considered to be significant, all factored as necessary to give the overload capacity or the live load capacity as required.

Other effects to be considered shall be those included in the following load groups of Tables 3.1 and 3.2:

For Rating	For Posting
Group 4	Group 1A or 2A

(a) For members for which the Ultimate Limit State is critical:

For Rating:

$$R_o = \frac{\phi R_i - \gamma_D(DL) - \Sigma(\gamma(Other\ Effects)}{\gamma_o}$$

For Posting:

$$R_L = \frac{\phi R_i - \gamma_D(DL) - \Sigma(\gamma(Other\ Effects)}{\gamma_L}$$

Where:

R_o	=	Overload Capacity
R_L	=	Live Load Capacity
R_i	=	Section strength, using material strength determined from 6.3
ϕ	=	Strength reduction factor from Table 6.5
DL	=	Dead load effect
γ_o	=	Overload load factor from Table 6.3
γ_L	=	Live load factor from Table 6.3
γ_D	=	Dead load factor from Table 6.4
γ	=	Load factor(s) on other effects, taken from Table 3.2, being the product of the factors inside and outside the brackets.

(b) For prestressed concrete members for which the Serviceability Limit State is critical:

For Rating

$$R_o = \begin{pmatrix} \text{Gross capacity} \\ \text{at stress } f_o \end{pmatrix} - (DL) - \begin{pmatrix} \text{Other} \\ \text{Effects} \end{pmatrix}$$

For Posting

$$R_L = \begin{pmatrix} \text{Gross capacity} \\ \text{at stress } f_L \end{pmatrix} - (DL) - \begin{pmatrix} \text{Other} \\ \text{Effects} \end{pmatrix}$$

or for members constructed in stages, where section properties vary between stages.

$$R_o = \left[f_o - \sum\left(\frac{DL_n}{Z_n}\right) - \sum\left(\frac{\text{Other Effects}}{Z_o}\right)\right] Z_F \qquad R_L = \left[f_L - \sum\left(\frac{DL_n}{Z_n}\right) - \sum\left(\frac{\text{Other Effects}}{Z_o}\right)\right] Z_F$$

Where :
- f_o = Allowable stress appropriate to overweight vehicles
- f_L = Allowable stress appropriate to conforming vehicles
- DL_n = DL effect for construction stage n
- Z_n = Section modulus applicable to stage n
- Z_o = Section modulus applicable to other effects
- Z_F = Section modulus in final condition

Allowable stress shall be taken from Table 3.1, that is Group 4 for Rating, and Group 1A for Posting.

Table 6.3 : Overload and Live Load Factors *

Rating for overloads:	γ_o	1.49
Posting for conforming loads:	γ_L	1.90

* In no case shall the load factor on the total of all gravity load effects be less than 1.25.

Table 6.4 : Dead Load Factors, γ_D *

Wearing surface, nominal thickness	1.40
In situ concrete, nominal sizes Wearing surface, measured thickness	1.20
In situ concrete, measured dimensions and verified density Factory precast concrete, verified density. Structural steel	1.10

* In no case shall the load factor on the total of all gravity load effects be less than 1.25.

Table 6.5: Strength Reduction Factors, ϕ

Superstructure Condition	Critical Section Properties based on:	
	Construction drawings and assessed sound material	**Measured dimensions or verified as-built drawings, and measured sound material**
Elastic Analysis Method		
Good or Fair	$1.00\phi_D$	$1.00\phi_D$
Deteriorated	$0.80\phi_D$	$0.90\phi_D$
Seriously Deteriorated	$0.70\phi_D$	$0.80\phi_D$

Where ϕ_D is the applicable strength reduction factor given by the materials design standard, or for timber, given by 4.4.2.

6.4.3 Live Loading and Analysis

The bridge shall be considered to be loaded with elements of live loading at their most adverse eccentricity on the roadway, as defined in 3.2.3(a), except that if the bridge has a carriageway width of less than 6.0m, and is marked out for two lanes, it shall be assessed on the basis of both lanes being loaded. Impact shall be included, as described in 6.2.2.

(a) A one-lane bridge shall be loaded as follows:

For Rating	For Posting
0.85 HO	0.85 HN

A bridge shall be considered as one-lane if its width between kerbs or guardrails is less than 6 m, except that a motorway ramp with one marked lane plus shoulders shall be considered as one-lane even if the width is more than 6m.

(b) A bridge with two or more lanes shall normally be loaded as follows:

For Rating	For Posting
0.85 HO in the most adverse lane, together with 0.85 HN in one other lane	0.85 HN in each of the two most adverse lanes

If the case of one lane loaded is more critical, this configuration shall be used.

A bridge with multiple lanes shall be considered loaded in more than two lanes if this is more realistic due to heavy traffic flow.

The bridge shall be analysed assuming elastic behaviour to determine the effects of the above loads at the critical locations for which capacities have been determined. Analysis shall take into consideration the relative stiffnesses of the various members, and their end conditions. Stiffness values for reinforced concrete members shall allow for the effects of cracking.

6.4.4 Assumptions for Specific Structural Situations

(a) Over-reinforced Concrete Sections

The intent of Clause 8.4.2 of NZS 3101[15] shall be complied with. The capacity of a reinforced concrete section shall not be taken as more than that derived using the area of tension steel which would correspond to a distance from the extreme compression fibre to the neutral axis of 0.75 C_b.

C_b is the distance from extreme compression fibre to neutral axis at balanced strain conditions, as defined in 8.4.1.2 of NZS 3101[15].

(b) Concrete Kerbs Cast onto a Composite Deck

Where a kerb has been cast directly onto the deck over its full length, and has at least a nominal amount of reinforcing steel connecting it to the deck, and is within the effective flange width of the beam, the moment capacity of the outer beam may be calculated assuming that the kerb is an integral part of it, with the following provisos:

- The area of concrete in the kerb shall be assumed to be 50% of its actual area, to allow for shear lag effects, unless tests indicate otherwise.
- The neutral axis shall not be taken to be above the level of the deck surface.

(c) Concrete Handrails

No reliance shall be placed on the contribution to longitudinal bending capacity of beams by concrete handrails.

(d) Steel Beams with Non-Composite Concrete Deck

No account shall be taken of such a non-composite deck in determining the bending capacity of the beams, except insofar as it may stiffen the beam top flanges, and thus increase their buckling load. Friction shall not be considered to contribute to composite action, nor to the stiffening of top flanges.

(e) Steel Beams with Timber Deck

Effective lateral support of the beam flanges by the deck shall only be assumed if the timber deck fastenings are adequate in number and condition.

(f) Continuous or Framed-in Beams

For beams with full moment continuity between spans, of normal proportions and showing no signs of distress, the following simplified procedure may be followed. The overall moment capacity of each span may be converted to that of an equivalent simple span by subtracting (algebraically) the midspan positive moment capacity from the mean of the two negative moment capacities at its supports. This will give the overall ordinate of the moment of resistance diagram, and both dead and live load moments may then be calculated as though it were a simple span. This procedure shall not be followed for a short span whose length is less than 60% of an adjacent long span, nor for live load effect on a span adjacent to a free cantilever span. The possibility of uplift at an adjacent support shall be considered.

(g) Spans Built Into Abutments

Reinforced concrete T-beam spans built monolithically with their abutments may be considered for treatment as in (f), with the following provisos:

(i) if negative moment yield at abutments can be shown to occur at a load greater than 85% of that at which midspan positive moment yield occurs, the working load capacity may be based on the full yield capacity of the section at all locations;

(ii) if negative moment yield at abutments occurs at a lesser load than 85% of that at which midspan positive moment yield occurs,

Either: the net unfactored service load capacity may be based on the full yield capacity at the abutments, with a reduced yield capacity at midspan, corresponding to the actual moment when abutment yield occurs,

or: the net unfactored service load capacity may be calculated assuming zero abutment moment capacity.

In any case, where negative moment capacity is to be relied on, the ability of the abutments to resist the overall negative moments, without excessive displacement, either by foundation reaction or by earth pressure, or both, shall be assured.

(h) Horizontal Support Restraint

Where the bearings and supports of a beam possess sufficient strength and stiffness horizontally, the horizontal support reaction to live loading may be taken into account where appropriate.

6.4.5 Evaluation

For each critical location in the bridge, the evaluation percentage shall be calculated as described below. In both calculations, the denominator shall include the effects of eccentricity of load and of impact. R_o and R_L are the section capacities calculated as 6.4.2.

If data is to be entered into the Highway Permits system, the CLASS calculation is not necessary. See 6.4.6.

For Rating

$$CLASS = \left[\frac{R_o x100}{Rating\ \ load\ \ effect}\right]_{\min} \%$$

The minimum value for any member in the bridge except the deck, shall be recorded in a structural inventory as the CLASS for manual calculations during processing of overweight permits in accordance with the *Overweight Permit Manual*(1). For this purpose, any value of CLASS more than 120% shall be recorded as 120%.

For Posting

$$GROSS = \left[\frac{R_L x100}{Posting\ \ load\ \ effect}\right]_{\min} \%$$

The minimum value for any member in the bridge except the deck, shall be rounded to the nearest 10%. If this value is less than 100%, it shall be recorded after the word GROSS in Panel 2 of the Heavy Motor Vehicle Bridge Limit Sign, shown in Diagram 4 of the 4th Schedule of the *Heavy Motor Vehicle Regulations*(2).

If the speed is restricted by inserting a value in Panel 3 of the sign, the impact factor used in the calculation may be reduced as follows:

Speed	Impact Factor
30 km/h	(I - 1) x 0.67 + 1
10 km/h	(I - 1) x 0.33 + 1

Where I is the Impact Factor appropriate for unrestricted heavy traffic.

6.4.6 Highway Permits Data

In the particular case of State Highway bridges, and some bypass routes, the basic Rating data described above is stored in the Highway Permits system database. A description of the form in which the data is required, and the calculations which the program performs, is contained in *Highway Permits Assurance Manual*(3).

6.5 Deck Capacity and Evaluation

6.5.1 General

The following three procedures are given in this clause:

- Reinforced concrete decks by empirical method, based on assumed membrane action.

- Reinforced concrete decks by elastic plate bending analysis
- Timber decks.

Generally, a reinforced concrete deck panel which is supported on four sides should be evaluated by the empirical method if it meets the criteria listed in 6.5.2(a). All other reinforced concrete deck panels should be evaluated by the elastic plate bending analysis method. In addition, reinforced concrete deck slabs shall be evaluated for their punching shear capacity for wheel loads, taking into account deterioration of the bridge deck using the factors in Table 6.5.

It shall be assumed that vehicle wheels can be transversely positioned anywhere between the kerbs or guardrails, but not closer to them than the restriction imposed by the 3m wide load lane of HN-HO-72 loading (Figure 3.1).

6.5.2 Reinforced Concrete Decks: Empirical Evaluation Method

(a) Criteria for Determining Applicability of the Empirical Method

The empirical method takes account of membrane action in the slab, and is based on test results. Evaluation of both composite and non-composite reinforced concrete deck slab panels may be determined by this method provided the following conditions are satisfied:

- the supporting beams or girders shall be steel or concrete,
- cross frames or diaphragms shall be continuous between external beams or girders, and the maximum spacing of such cross frames or diaphragms shall be as follows:

  Steel I beams and Box Girders of steel or concrete: 8.0 m
  Reinforced and prestressed concrete beams: at supports
- the ratio of span length (L_s) to minimum slab thickness shall not exceed 20. In skew slabs where the reinforcing has been placed parallel with the skew, the skew span, $L_s / Cos\ Y$ shall be used, where Y = angle of skew.
- the span length (L_s) or $L_s / Cos\ Y$ shall not exceed 4.5 m.
- the concrete compressive strength shall not be less than 20 MPa.
- the slab thickness, or for slabs of variable thickness the minimum slab thickness, shall be not less than 150 mm.
- there shall be an overhang beyond the centreline of the outside beam of at least 0.80 m measured perpendicular to the beam. The overhang shall be of the minimum slab thickness used to determine the span to thickness ratio above. This condition may be considered satisfied if there is an integral continuous concrete kerb or barrier which provides a combined cross sectional area of slab and kerb or barrier not less than the cross sectional area of 0.80 m of deck slab.

(b) Deck Strength in Terms of Wheel Load

500x200

For rating (HO wheel contact area Alternative (b) of Figure 3.1 assumed), the unfactored ultimate resistance, R_i, of a composite or non-composite deck slab shall be obtained from Figures 6.1 to 6.5.

900x600

For posting (HN wheel contact area assumed), the value from the charts shall be multiplied by 0.6.

The value of reinforcement percentage, q, used to determine R_i shall be the average of the lower layer reinforcement percentages at the mid span of the slab, in the two directions in which the reinforcement is placed. Values of R_i for slab depths or concrete strengths intermediate between those on the charts shall be obtained by interpolation. The dead load and other load effects are ignored in this method.

The strength reduction factor, ϕ_D, for design by the empirical method is 0.5. The strength reduction factor, ϕ, used for evaluation shall be taken from Table 6.6, by multiplying ϕ_D by the appropriate factor. In this table, deck deterioration is quantified by the Crack-to-Reinforcing Ratio, CRR, defined as follows:

$$CRR = \frac{\textit{Total length of visible cracks}}{\textit{Total length of bottom reinforcement in both directions}} \times 100$$

The above lengths shall be measured in a 1.2 m square area on the bottom of the slab, central between supports.

Table 6.6: Strength Reduction Factors, ϕ for Slabs Evaluated by the Empirical Method

Superstructure Condition	Slab Section Properties based on:	
	Construction drawings and assessed sound material	Measured dimensions or verified as-built drawings, and measured sound material
Good or Fair (CRR ≤ 40%)	$0.90\,\phi_D$	$1.00\,\phi_D$
Deteriorated (CRR = 70%)	$0.60\,\phi_D$	$0.70\,\phi_D$
Seriously Deteriorated (CRR = 100%)	$0.30\,\phi_D$	$0.40\,\phi_D$

(c) **Evaluation**

For each type of slab panel in the bridge, the parameters shall be calculated as follows. Rating and posting wheel loads shall be taken from Tables 6.7 and 6.8. Impact factor, I, shall be as described in 6.2.2. γ_o and γ_L shall be taken from Table 6.3.

$I = 1.3$
$\gamma_o = 1.49$.
Overload factor

For Rating

Deck Capacity Factor (DCF)

$$= \left[\frac{\textit{Overload wheel load capacity}}{\textit{Rating load effect}} \right]_{\min}$$

$$= \left[\frac{\phi R_i}{\gamma_o x 95\ x\ I} \right]_{\min}$$

For Posting

Allowable Axle Load (kg)

$$= \left[\frac{\textit{Liveload wheel load capacity}}{\textit{Posting load effect}} x\ 8200 \right]_{\min}$$

$$= \left[\frac{\phi x (0.6 R_i)}{\gamma_L x 40\ x\ I} x\ 8200 \right]_{\min}$$

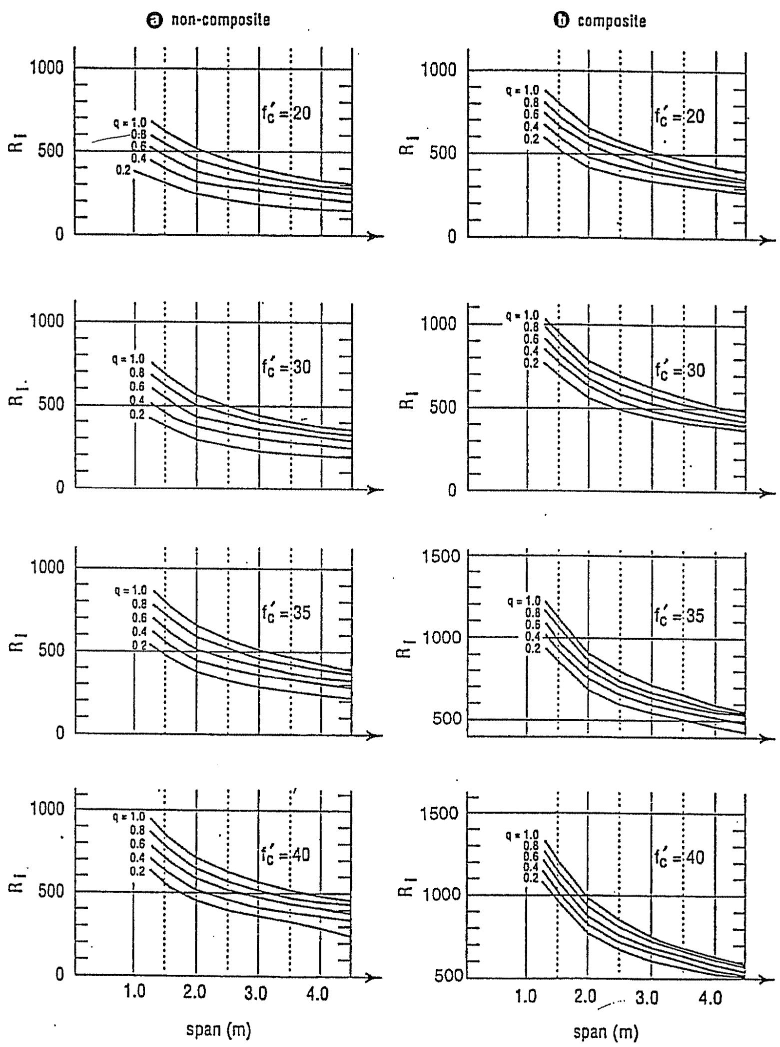

Figure 6.1 : *R_i(kN)* of 150 mm Thick Concrete Deck

6 - 22 BRIDGE MANUAL
SECTION 6: EVALUATION OF BRIDGES AND CULVERTS
September 2004

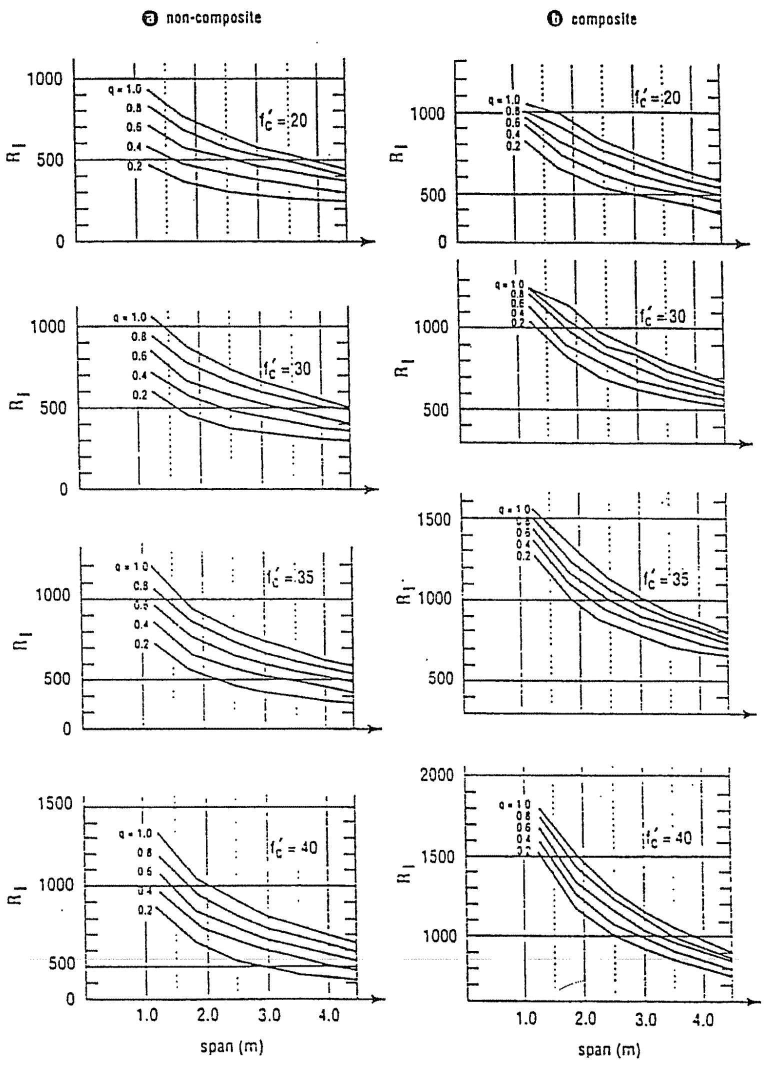

Figure 6.2 : $R_i(kN)$ of 175 mm Thick Concrete Deck

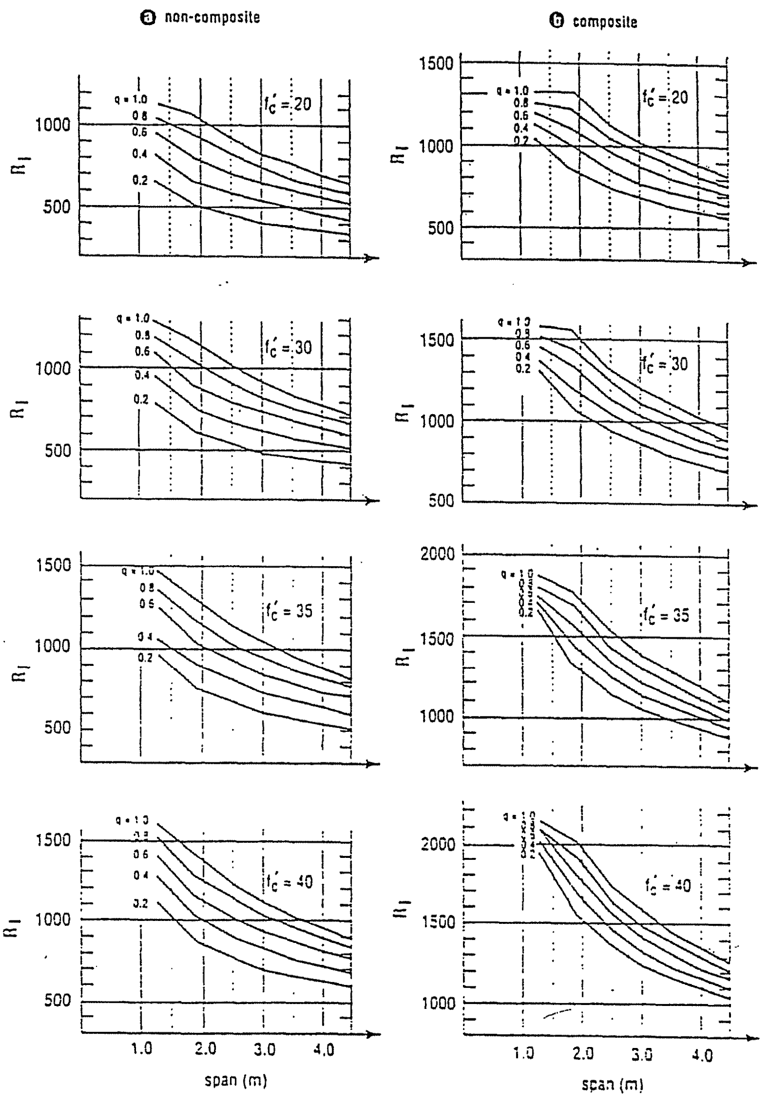

Figure 6.3 : $R_i(kN)$ of 200 mm Thick Concrete Deck

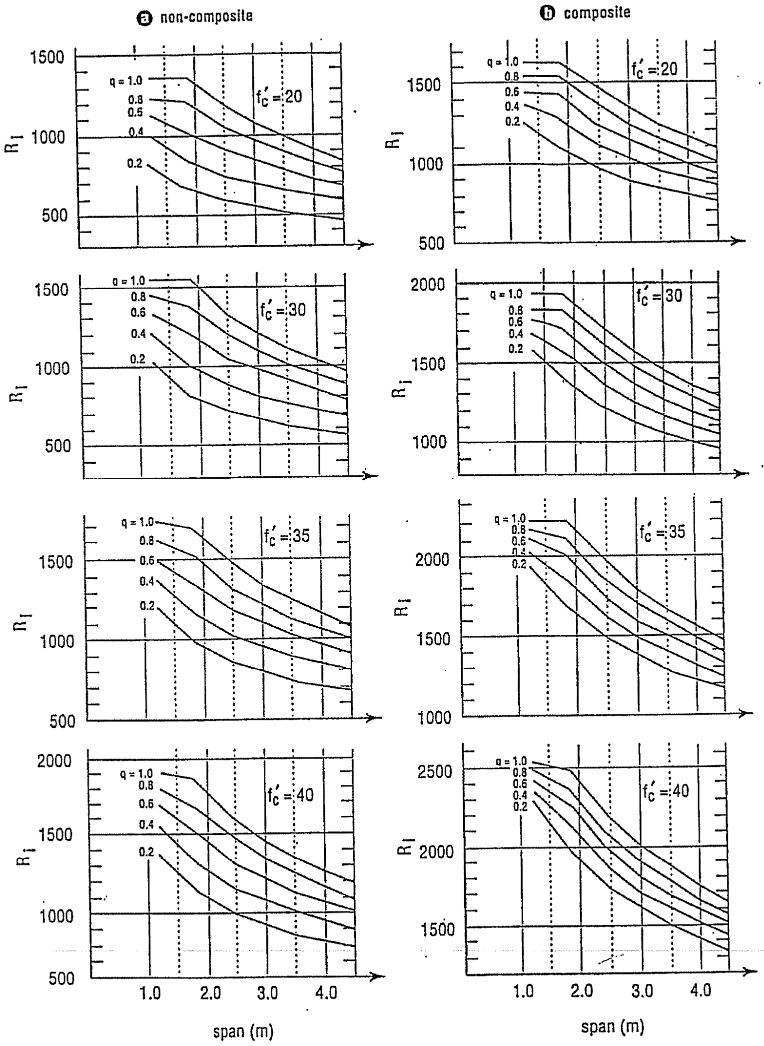

Figure 6.4 : *R_i(kN)* of 225 mm Thick Concrete Deck

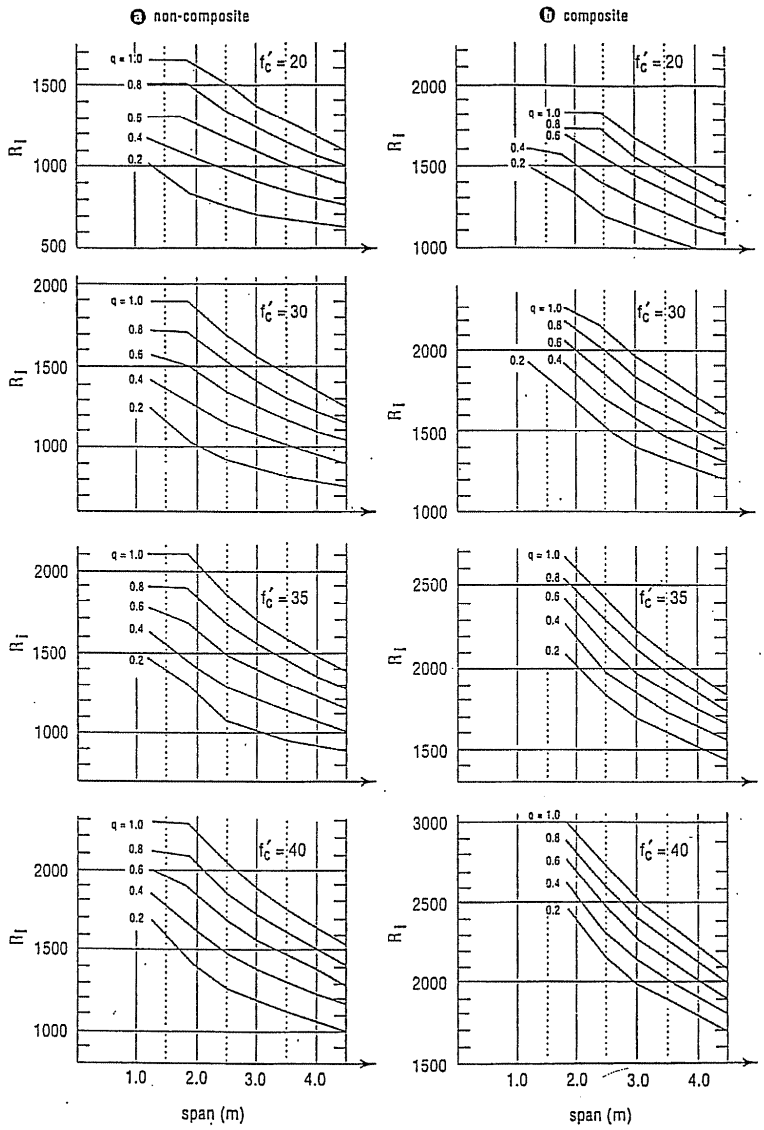

Figure 6.5 : ***R_i(kN)*** **of 250 mm Thick Concrete Deck**

6.5.3 Reinforced Concrete Decks: Plate Bending Analysis

(a) Section Capacity at Critical Locations

The deck slab live load or overload flexural capacity shall be determined using serviceability limit state criteria, in moment per unit width at critical locations in the slab. A simplification may be made in the case of a slab which is considered to act as a one-way slab, that is, if it has an aspect ratio of at least 4. Provided it has a positive moment capacity in the long span direction at least 50% of that in the short span direction, all moment capacities in the long span direction may be ignored.

(b) Live Loading and Analysis

For Rating

The deck shall be considered to be loaded with the most adverse of the axles or axle groups listed in the *Overweight Permit Manual*(1), at a Vehicle Axle Index of 1.3. For deck spans up to 3 m, these may be reduced to the three alternatives described in Table 6.7.

For Posting

The deck shall be considered to be loaded with the most adverse of the axles or axle sets described in the *Heavy Motor Vehicle Regulations*(2), Second Schedule, Tables 1, 2 and 3, as amended by Amendment No 5. For deck spans up to 3 m, these may be reduced to two alternatives described in Table 6.8.

Table 6.7 : Deck Rating Loads

Axle Type	Axle Load, *kN*	Wheel Track and Contact Area
Twin-tyred Single tyred, large tyres 2/8-tyred oscillating axles, spaced 1.0 m	105 190* 133	As for HN axle As for HO axle, alternative (b) As for HO axle, alternative (a)

Table 6.8 : Deck Posting Loads

Axle Type	Axle Load, *kN*	Wheel Track and Contact Area
Twin-tyred Four-tyred oscillating	80* 93	As for HN axle 4/250 x 150 mm areas equally spaced within 2500 mm overall width

* Wheel loads from these axles are used for evaluation by the empirical method in 6.5.2(c).